Doctoral theses at NTNU, 2023:431

Einar Albert Rødtang

Ice and Ice Forces in Small Steep Rivers

Doctoral thesis

NTNU
Norwegian University of Science and Technology
Thesis for the Degree of Philosophiae Doctor
Faculty of Engineering
Department of Civil and Environmental Engineering

NTNU
Norwegian University of Science and Technology

Einar Albert Rødtang

Ice and Ice Forces in Small Steep Rivers

Thesis for the Degree of Philosophiae Doctor

Trondheim, December 2023

Norwegian University of Science and Technology
Faculty of Engineering
Department of Civil and Environmental Engineering

NTNU
Norwegian University of
Science and Technology

NTNU
Norwegian University of Science and Technology

Thesis for the Degree of Philosophiae Doctor

Faculty of Engineering
Department of Civil and Environmental Engineering

ISBN 978-82-326-7564-7 (printed ver.)
ISBN 978-82-326-7563-0 (electronic ver.)
ISSN 1503-8181 (printed ver.)
ISSN 2703-8084 (online ver.)

Doctoral theses at NTNU, 2023:431

Printed by NTNU Grafisk senter

Preface

The present thesis is submitted to the Norwegian University of Science and Technology (NTNU) for partial fulfilment of the requirements for the degree of Philosophiae Doctor (Ph.D.).
The work was carried out at the Department of Civil and Environmental Engineering, NTNU, in Trondheim, under the supervision of Professor Knut Alfredsen, NTNU. Professor Knut Høyland, NTNU and Professor Leif Lia, NTNU were co-supervisors.
The research in this thesis was financed as a 3-year strategic PhD scholarship at the department of Civil and Environmental Engineering, NTNU.
In accordance with the requirements of the Faculty of Engineering at NTNU, the present thesis comprises and introduction to the research that has resulted in three scientific papers.

Abstract

Given the right circumstances ice can wreak havoc on riverine infrastructure. Ice runs pushing ice floes against bridge piers is frequently the governing design condition for bridges in cold regions. The physics of these interactions are complex and forces are hard to predict. Current standards and calculation methods for calculating these quasi-static ice forces disagree both on order of magnitude and underlying mechanics. While there reigns general agreement that ice thickness and ice strength are critical parameters, great difficulties remain for the accurate and reliable estimation of these parameters (Paper I). In small-steep rivers in particular these estimates are difficult. Anchor ice dams complicate things by encouraging the growth of highly complex and variable ice structures. Paper III provides a novel approach for quickly and accurately estimating ice thicknesses in generally inaccessible steep rivers using an unmanned aerial vehicle (UAV), structure for motion and automated GIS processing. Paper II provides new insights into how ice strength varies in steep rivers. Through statistical analysis it shows a novel and effective way of predicting anchor ice dam locations, proportion of river impacted by anchor ice dams as well as providing new data on how anchor ice dam strengths are distributed. As a whole, this thesis provides the river ice engineer with new and balanced guidance on how to go about predicting ice forces in small steep river.

Sammendrag

Is kan under visse omstendigheter påføre store skader på infrastruktur i elver. Istrykk på bropilarer er ofte dimensjonerende for bruer i kalde strøk. Fysikken bak disse interaksjonene er komplekse og kreftene vanskelige å forutsi. Nåværende design-koder og kalkulasjons metoder for disse kvasi-statiske iskreftene er uengie om både størrelses orden og underliggende mekanikk. Det regjerer en generel konsensus at is-tykkelse og is-styrke er kritiske parametre, men store vanskeligheter gjenstår før nøyaktige og påligelige estimater av disse er mulig (Paper I). Spesielt i små bratte elver så er disse estimatene vanskelige. Bunn-is dammer kompliserer ting ved å oppmuntre vekst av høyst komplekse og variable is strukturer. Paper III beskriver en ny tilnærming for raskt og effektiv estimering av is-tykkelse i generelt utilgjengelige bratte elver ved bruk av fjernstyrt drone, structure from motion (SfM) og automatisert GIS prosessering. Paper II gir ny innsikt i hvordan is-styrke varierer i bratte elver. Gjennom statistisk analyse så viser den en ny og effektiv måte å forutsi bunn-is dam lokasjoner, brøk av elven påvirket av bunn-is dam formasjon, i tillegg til å gi nye data om hvordan bunn-is dam styrke er distribuert i disse elvene. Som en helhet så tilbyr denne avhandlingen elve-is ingeniøren med en ny og balansert veiledning på hvordan man best kan forutsi is-krefter i små bratte elver.

List of publications

The present thesis is based on three scientific papers, which will be referred to by their roman numbers in the following:

Paper I: Review of river ice force calculation methods
E. Rødtang, K. Alfredsen, K. Høyland and L. Lia, Cold Regions Science and Technology, 2023. DOI: 10.1016/j.coldregions.2023.103809
(E. Rødtang is the first author and primarily responsible for writing, analysis and data collection)

Paper II: In-situ ice strength distribution of anchor ice dams
E. Rødtang, J. John, K. Alfredsen and K. Høyland, Cold Regions Science and Technology, vol. 215, no. September 2022, pp. 1-17. DOI: 10.1016/j.coldregions.2023.103982
(E. Rødtang is the first author and primarily responsible for writing, analysis and data collection)

Paper III: Drone surveying of volumetric ice growth in a steep river
E. Rødtang, K. Alfredsen and A. Juárez, Frontiers in Remote Sensing, vol. 2, no. December, 2023. DOI: 10.3389/frsen.2021.767073
(E. Rødtang is the first author and primarily responsible for writing, analysis and data collection)

Contents

Chapter 1

Introduction

Norway alone has thousands of rivers and more than 17000 bridges (NTB, 2018). Most of these bridges cross small steep rivers. Most rivers are by physical necessity small. Yet bridge codes, and indeed most research, consider almost exclusively the case of a bridge crossing a large river of modest slope. Size and slope are frequently interdependent: large rivers tend to have a more modest slope than smaller rivers. When predicting ice forces on bridges, and other infrastructure, this disconnection is particularly grievous. Steep and modestly sloped rivers produce different kinds of ice, see different large scale ice structures (e.g. anchor ice dams, step-pool structures) and the ice obtains different velocities during ice runs. This thesis aims to describe some of these differences and underlying phenomena and hence deduce a better way than the present state of the art for predicting quasi-static forces (I.e. forces where inertia forces are negligible) on riverine infrastructure in small steep rivers.

Fundamentally, three things are required to estimate future ice forces. Ice thickness, ice strength and a robust theoretical framework. As such this thesis will describe the principal features of each. Figure 1.1 shows how the papers that constitute this thesis interrelate to this end.

The underlying motivation for this thesis can be summed up thusly: Ice forces frequently govern the design dimensions of bridges in cold climates. Over designing bridges is a waste of resources and under dimensioning bridges is a hazardous undertaking. In steep rivers in particular codes give predicted forces that differ by an order of magnitude between each other (Rødtang et al., 2023). Better strategies for predicting these forces are therefore necessary.

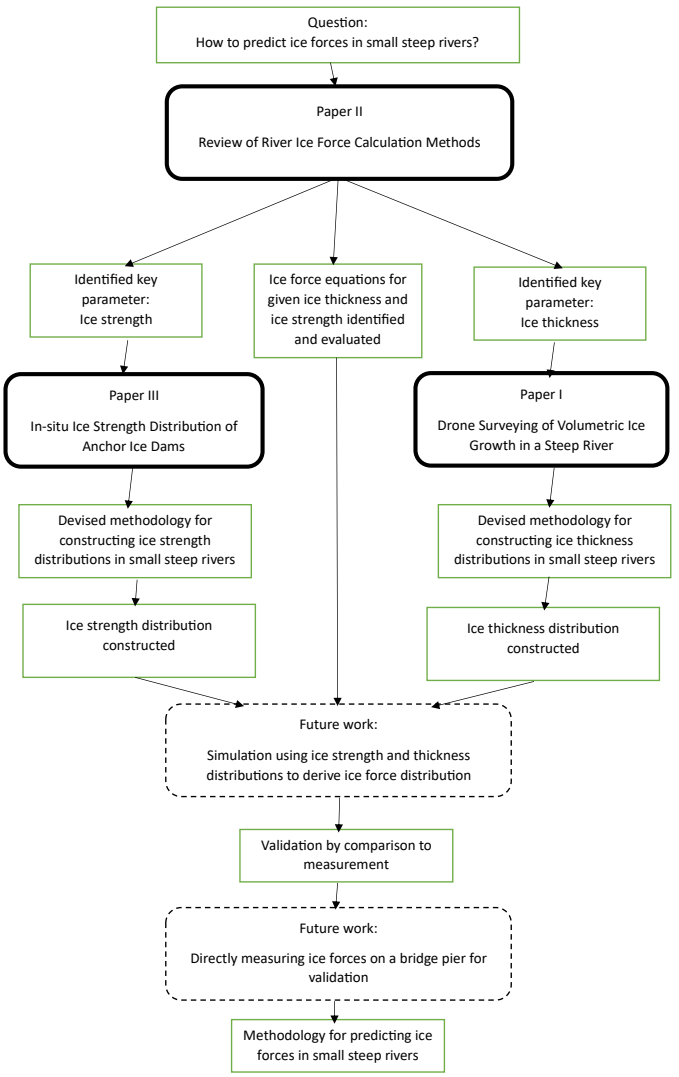

Figure 1.1: Overview of how the papers that compose this thesis interrelate

Chapter 2

Background

2.1 Ice growth

Figure 2.1: Anchor ice and border ice formation in Sokna 2020/12/16

Any treatment of ice forces in steep rivers is incomplete without a rudimentary consideration of ice growth processes and mechanisms. As air temperature drops, so does the river temperature. In a steep river turbulence will ensure that the temperature of the river is essentially constant across the water column, with slightly cooler water at the air-water interface and slightly warmer water at the riverbed-water interface wherever you have groundwater influx. As the air temperature remains negative the water eventually supercools and hence ice will nucleate on particulates in the river (Ghobrial & Loewen, 2021). The formation of these ice particles - called frazil - releases energy warming up the surrounding water, thus slowing down the freeze-up and keeping the water

temperature close to 0 °C. Ice floes, these small (0 - 5 mm) (Osterkamp & Gosink, 1983) frazil particles will therefore accumulate on the surface, at first just as loosely agglomerated slush. This slush however traps relatively still water and allows the frazil particles to grow further, allowing the exposed part of the slush to freeze and form frazil pans of defined structure and mechanical integrity. When these pans rub against each other they form raised edges. These pans or "pancakes" are unconstrained and therefore drift down the river (Shen et al., 2004). Meanwhile, at the riverbank the water is relatively still and the water depth shallow. Hence landfast ice will nucleate there and grow as a thin sheet towards the centre of the river, preferentially in slower moving sections of the river. At this point the thickness of the ice is governed by the slope of the water line, water - ice friction and temperature (Pariset et al., 1966). As the ice from both banks approach each other the pancake ice flowing down the river along the surface gets stopped by this bank ice and hence the ice cover grows upstream as more pancake ice is arrested and eventually freezes stuck to the rest of the pancake ice. Through the ice cover heat will diffuse and ice growth is primarily driven by columnar ice growth downwards at a diminishing rate (The thicker the ice the more insulating it is). Depending on the flow velocity, ice cover cohesion, ice strength, ice thickness and water level changes, this incipient ice cover can collapse, breaking apart and shoving together at a new mechanical equilibrium (Wazney et al., 2018). This forms much thicker ice of highly irregular surface geometry. In modestly sloped rivers these processes describe most of the ice formation. In steep rivers however anchor ice formation is relatively more important. Turbulence causes frazil to get thoroughly mixed in the water column and hence impact the river bed. As frazil impacts the riverbed, it adheres and grows. This type of ice is called anchor ice, the green below the water in Figure 2.1 is an example of anchor ice. Anchor ice forms preferentially at wide sloping segments of the river (See Paper II). As anchor ice grows from the bottom of the river at variable rates anchor ice dams form. This causes the river to take on a step-pool structure (Dubé et al., 2014). In other words anchor ice dams dam up water behind them forming a pool of water. At the ice dam there is a sudden drop of water level and another pool dammed up by the next anchor ice dam. The fraction of ice in a river that is anchor ice varies, but in the Sokna river during the 2020 - 2021 field season the author estimates 20% anchor ice by volume. The most important aspect of anchor ice however is how it changes the hydraulic regime of the river. A level ice cover (a relatively flat ice cover thickening by pseudo-columnar ice growth) will form in the pools upstream of anchor ice dams as usual, however this ice is generally supported on 3 sides, each bank and the anchor ice crest. As the anchor ice dam perforates or breaches the pool will be drained. Whatever level ice has formed at that point will either collapse fully or partially or remain and trap insulating air beneath itself thus inhibiting ice growth at the new water level. Depending on the details around how the ice dam breaches and the discharge time history a highly complex ice cover can arise upstream of the anchor ice

dam, one composed of several layers of air, level ice, collapsed ice and anchor ice (Turcotte et al., 2011).

2.2 Ice runs

Figure 2.2: Ice runs frequently stop and form ice jams. The picture show an ice jam in the river Stjørdalselva in central Norway. Picture taken march 2021.

An ice run can at its simplest be defined as "a large amount of ice being transported by a river". Ice runs are frequently the events that constrain the design of bridge piers. A several ton block of ice moving down a river at a speed of up to several meters per second (Nafziger et al., 2016) will impart significant forces upon whatever stands in its way. Ice runs come in two primary varieties; thermal and mechanical. Thermal ice runs are the least dramatic and usually only impart modest forces on structures. A thermal ice run is triggered by ice melting in place, therefore losing strength and and eventually breaking loose and floating down the river. These ice runs are less sudden than the mechanical ice runs, and the loss in strength and ice thickness due to melting means lower forces when the ice does impact structures. Mechanical ice runs are relatively more violent and sudden. They are triggered by sudden changes in discharge breaking apart the ice, enabling it to flow downstream. The discharge increase may be triggered by snow melt or rain. In practice combinations of thermal and mechanical ice runs can also happen where the ice cover has been weakened by a period of melt, which enables a sudden discharge increase to trigger an ice run. While some empirical and heuristic methods exist (Madaeni et al., 2020) predicting ice runs remains difficult. Metrologists and hydrologists have become quite adept at predicting discharge. However understanding, mapping and predicting how much discharge will trigger an ice run for a particular ice cover, remains difficult. In steep rivers in particular the exact time history of temperature and discharge strongly affects how prone an ice cover is to an ice

run (Beltaos, 2008). Figure 2.2 shows an ice jam caused by a mechanical ice run and situated downstream of a small steep river.

2.3 Ice-structure interaction

Quasi static ice structure interactions can be classified in various ways, according to fracture mechanism, limiting mechanism (force, stress or momentum) or structure geometry. The terms quasi static ice structure interactions is used to distinguish these interactions from purely static interactions, I.e. no fracture occurring and purely inertial interactions. Details of these delineations and corresponding equations are detailed in Paper I. Here a brief overview will suffice. The two most important fracture mechanisms are crushing and bending, because these generally result in the highest forces and significantly lower forces respectively. It is often a design objective to ensure that bending failure occurs in preference to crushing. This is generally achieved by using a sloping design. Other fracture mechanisms, such as splitting, cleavage, shear, buckling and combination failures do occur but in general receive less attention. Note that while bending failure is driven by the sloping structure inducing a vertical force that sets up a bending moment that causes fracture relatively close to the structure, buckling is primarily driven by a compressive force induced by a vertical structure, the compressive force then causes an instability resulting in fracture further away from the structure. Crushing is characterised by complete disintegration of the ice close to the structure by many small cracks. Disintegrated ice is extruded up and down close to the structure. Bending failure on the other hand is characterised by the structure deflecting the ice sheet up (or down) and the ice sheet failing in bending some distance away from the structure (Ashton, n.d.). Figure 2.3 shows ice floes wedged up against one of the 800 mm diameter bridge piers of Sokna bridge following an ice run.

2.4 Mapping ice thickness

Ice thickness is one of the principal predictors of quasi-static ice forces. Therefore collecting and analysing ice thickness data is of great importance. How to collect ice thickness data in steep rivers however is a non-trivial problem. Steep rivers have a high variability that single point measurements are unable to capture. Furthermore, ice properties can change drastically throughout the thickness of the ice cover. Air and water filled voids are also common. In such a circumstance "Ice-cover thickness" is an ambiguous term. Do you include just the top snow/columnar ice layer without voids? Or maybe the thickest continuous ice layer is better? All layers subtracting voids is an option. Whether or not to include lower anchor ice layers is also a difficult question. In practice measuring and defining all layers of ice at a point in a steep river can be difficult and for very deep layers practically infeasible. Ice microstructure changes

Figure 2.3: Ice floes stranded against Sokna Bridge. 29/01/2020.

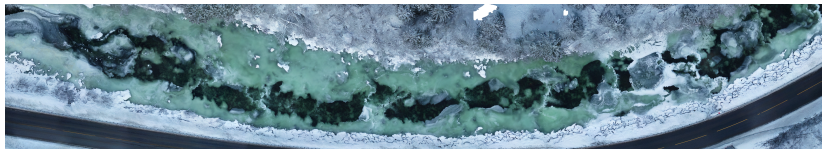

Figure 2.4: Orthomosaic composed of drone imagery. Shows anchor ice formation in Sokna 2021/01/05

continuously from peak thickness "steel" ice to loosely agglomerated anchor ice of negligible strength. These difficulties make it tempting to hand-wave a definition of ice thickness. However depending on your choice of definition a point might have an ice thickness of 10 cm or 200 cm, which will make an order of magnitude difference in predicted ice forces. During an ice run ice floes can stack and sometimes this "stacked" thickness governs forces anyway. There is no ideal definition. However, no matter which definition is used it is important to clearly state assumptions.

Traditionally ice thicknesses are recorded by walking out on the ice, drilling a hole and using some kind of measuring stick to measure the thickness. For more rigorous measurement campaigns transects or grids of holes are used instead. Steep rivers have low strength suspended ice covers, drops and rapid currents. Therefore it is rarely practical to do systematic grid measurements or even transect measurements. Paper III describes an improved method for measuring steep river ice thicknesses and derive corresponding distributions. By taking drone imagery when the river is partially frozen, as shown Figure 2.4 a finer understanding of ice thickness distributions can be obtained.

2.5 Ice strength

In any consideration of ice-structure interaction ice strength is a critical parameter. The strength of a sample is the maximum stress that a sample can sustain before fracture. Strength is often seen as a material property, however its value depends on test conditions as well as failure condition. A distinction is made between ductile and brittle failure. Ductile failure occurs when a material undergoes significant deformation and stretching before ultimately breaking, while brittle failure happens suddenly and without significant plastic deformation. Primarily ductile materials, such as many plastics, exhibit extensive necking and localized deformation, allowing them to absorb energy before failure. Primarily brittle materials, like ceramics or glass, lack this ability and tend to fracture with minimal deformation, often resulting in sudden and catastrophic failure. A variety of strengths have been defined in relation to different test conditions. Some of the most useful ones include compressive, tensile, shear and flexural strength. Combined, experiment specific strengths are also common. Great care and intellectual rigour is necessary when using ice

strength values from different sources, "compressive strengths" from two different sources say may at first glance appear comparable. However if confinement conditions are different these strengths may not be directly comparable. Fully specifying measurement conditions is important for meaningful comparisons. The Sanderson pressure-area curve illustrates this point well (Palmer et al., 2009). The Sanderson pressure-area curve shows that in general ice pressures on structures reduce with area. Hence if naive ice pressure data from structures is used to derive ice strength as a material property it is likely to be wrong.

Ice strength is variable and has been found to vary with a wide range of parameters including temperature, sample orientation, porosity, grain size, grain type, ice type, loading rate, sample size, sample homogeneity, impurity concentrations, impurity distribution and test rig stiffness. Most strength tests aim to induce uniform stress fields in the sample under test, however in practice this is difficult to achieve with most samples having excessive heterogeneity for this to be possible. Things are not helped by large grain sizes necessitating correspondingly large sample sizes and hence the test rig stiffness influencing measured strengths (Ashton, n.d.).

Ice strength measurements are either conducted on lab grown ice samples, samples collected from the field and transported to the lab or conducted in-situ in the field. Lab based tests are easier to control, however samples from the field are often of more immediate practical usefulness. Testing samples taken from the field introduces questions of the the effect of ageing, thermal shocks, improper storage and other transport related effects. In-situ (in the field) test techniques have been developed - and extensive use has been made of one of these (The borehole-jack) in this thesis - however controlling and recording the conditions of these tests is problematic and interpretation can therefore be difficult. For a more extensive discussion of the borehole-jack see Paper II and the section 3.2.

Chapter 3

Methods

3.1 Study site

The work of this thesis primarily centres around the river Sokna, shown in Figure 3.1. Sokna is a small steep river flowing through a mountainous area in central Norway. Sokna flows into the Gaula river in the towns of Støren, approximately 40 km south of the city of Trondheim. This river was chosen as the focus for several reasons. Primary reasons was that during winter Sokna consistently freezes over in a step-pool structure and forms a large number of anchor ice dams. Furthermore proximity to Trondheim and the road that goes along the river drastically simplifies access, making up to several fieldwork days per week throughout the winter season practicable. Finally availability of high quality digital terrain models and previous research carried out in Sokna such as (Stickler et al., 2010) and (Heggen & Alfredsen, 2013) made Sokna an excellent of river to focus on for this PhD work.

The Sokna river is 52 km long, has an average gradient of 20.6 m/km and a normal runoff of 23.0 $l/s*km^2$. The Sokna catchment has an area of 564 km^2 , whereof 54% is forest, 19% is bare mountain, 17% marshland and the rest miscellaneous other. During winter the average temperature is -3.0 ℃ , the temperature dipping below -20 ℃ however not uncommon ('The Norwegian Water Resources and Energy Directorate', n.d.).

3.2 The borehole jack (BHJ)

The borehole jack is a metal cylinder that is inserted into a pre drilled hole in the ice. Once inserted a piston gets pushed out from the BHJ into the ice parallel to the ice surface. The piston has a maximum stroke length of 30 mm. For a schematic of this setup see Figure 3.2. This piston moves at an approximately constant rate and fractures the ice. The BHJ is fitted with two load cells that together measure the force the piston imparts on the ice. Usually in the case of brittle compressive failure the force increases in a pseudo-linear manner and

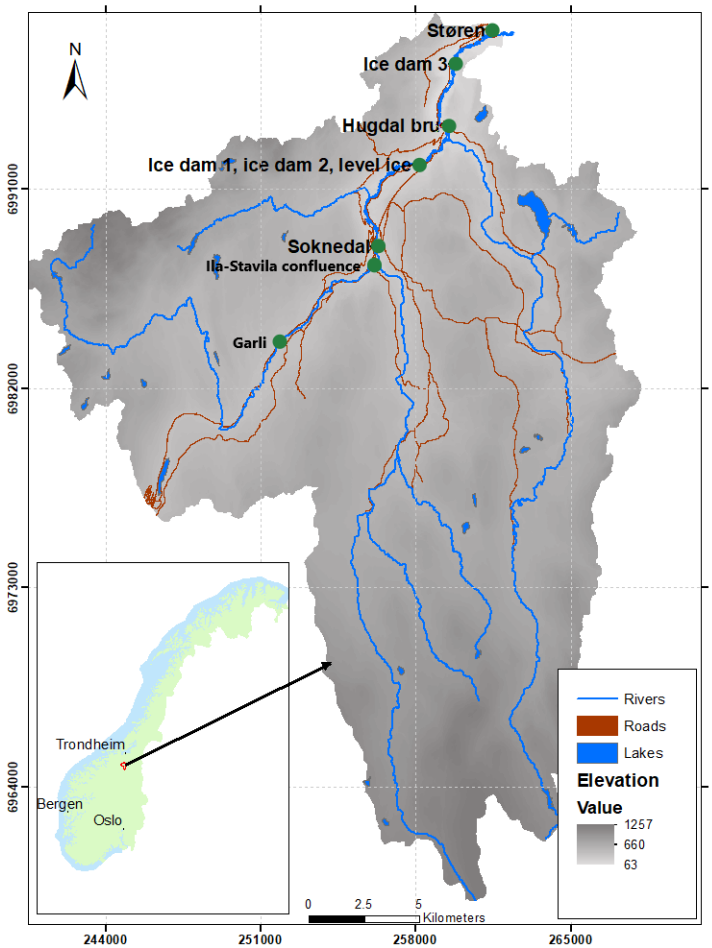

Figure 3.1: Map of the Sokna catchment including some key locations

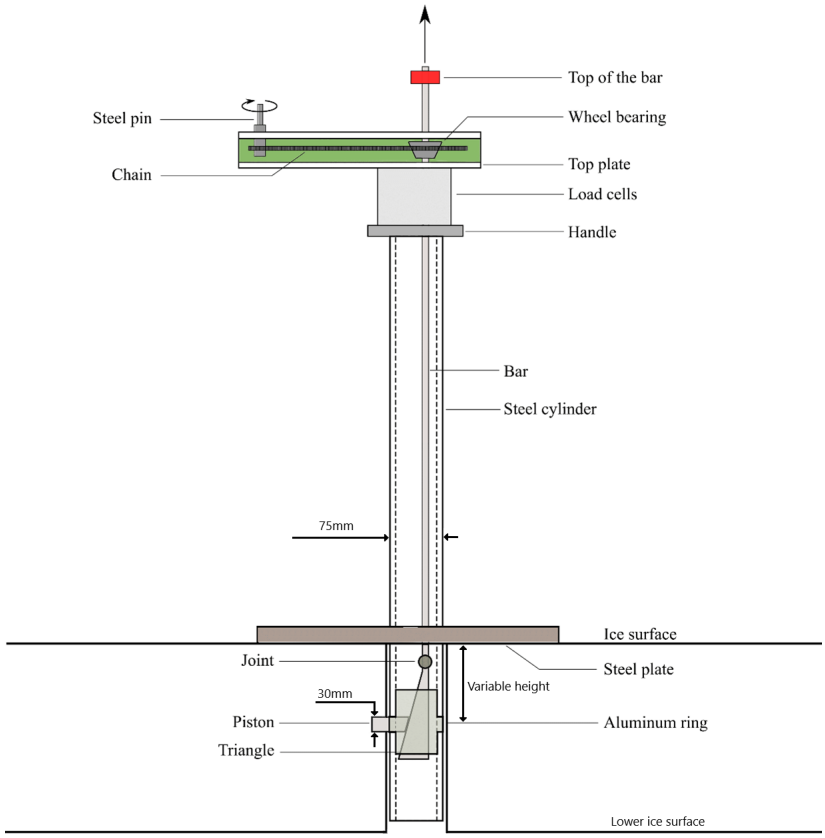

Figure 3.2: Schematic of the borehole-jack (BHJ) used in this study (Kallelid, 2018)

then experiences a sharp drop as the ice fails. Fractured ice is then extruded out from the contact zone which gives an irregular force measurement (Schulson & Duval., 2009). This would be the standard outcome when simple columnar ice is measured, when measuring the varied ice of a small steep river much more variability can be expected.

It is important to stress that the pressure measured by the BHJ is not the same as the unconfined compressive strength of the ice. According to Shkhinek et al. (2010) the BHJ pressure is 2 - 5 times higher than the unconfined compressive strength of ice. Lack of standardization in BHJ jack designs and variation measurements conditions furthermore makes the direct comparison of BHJ data from different studies difficult (Shkhinek et al., 2010).

The BHJs sensitivity to temperature in particular was an issue for the integrity of BHJ data collected in the field. Hence the BHJ was calibrated to various temperatures at 5 intervals (0 , -5 , -10 , -15 and -20). Calibration was carried out by pushing the BHJ piston into a loadcell in the NTNU ice lab cold room set to the appropriate temperatures. Care was taken to ensure that the temperature of the BHJ and the cold room were in equilibrium. 10 runs were conducted for each temperature and a calibration coefficient for each temperature was derived by comparing the force measured by the loadcell and BHJ. This was averaged over each run as well as by averaging over the relevant force range (1 kN - 15 kN). Field air temperature measurements and interpolation could then be used to correct measurements taken in the field. This calibration was repeated at various points throughout the field seasons when drift in the performance of the BHJ was noticed due to changes in lubrication, grit, wear and tear.

3.3 The load panel

At the beginning of this PhD a great deal of effort, consternation and gripe was spent designing, constructing and mounting a load panel on one of the Sokna bridge piers. A schematic of this is shown in Figure 3.3. The intent behind this 150 kg+ contraption, was to directly measure the forces imparted by an ice run upon a bridge pier. Ice forces have been measured like this once or twice before, the Norströmsgrund lighthouse (Nord et al., 2016) and the Rätan hydropower dam (Hellgren et al., 2020) in particular are worth mentioning. The largest set of bridge ice forces come from the Confederation bridge measurement campaign, these however were obtained using accelerometers instead of loadpanels (Shrestha & Brown, 2018). The Sokna bridge campaign would have given the first measurements of its kind. Unfortunately no directly usable measurements were for various reasons obtained. These reasons include, battery failure, SD card failure, ice run snapping cables and a seasons without applicable mechanical ice runs. At the time of writing the load panel is still mounted on Sokna bridge and may produce successful measurements in the future.

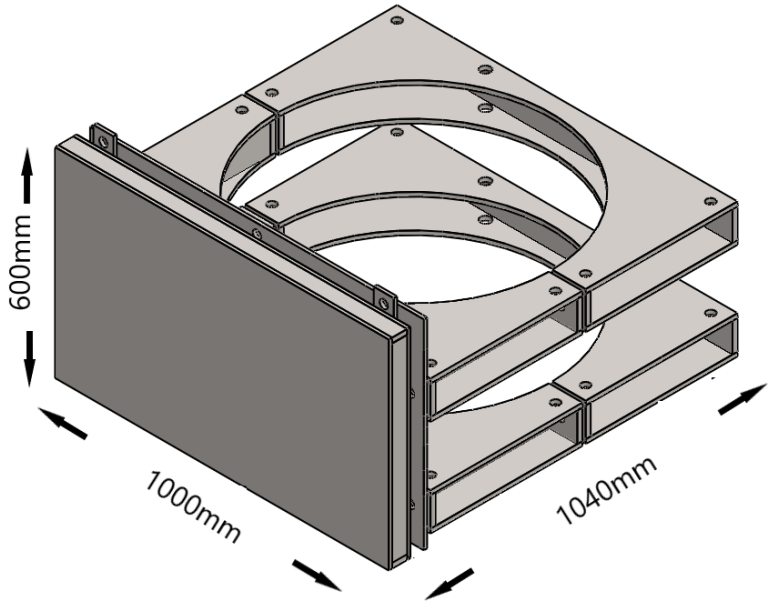

Figure 3.3: Model of the Sokna bridge load panel

3.4 UAV photography and structure from motion

A DJI Phantom 4 RTK drone was used to to collect photographs of ice conditions in the Sokna river. The Sokna images were stitched together into 3D models of the ice cover using the structure from motion software Agisoft Metashape Professional. Photographs were taken at different times and hence ice volumes could be estimated using QGIS and a custom python script.

3.5 Cold lab work and thin sections

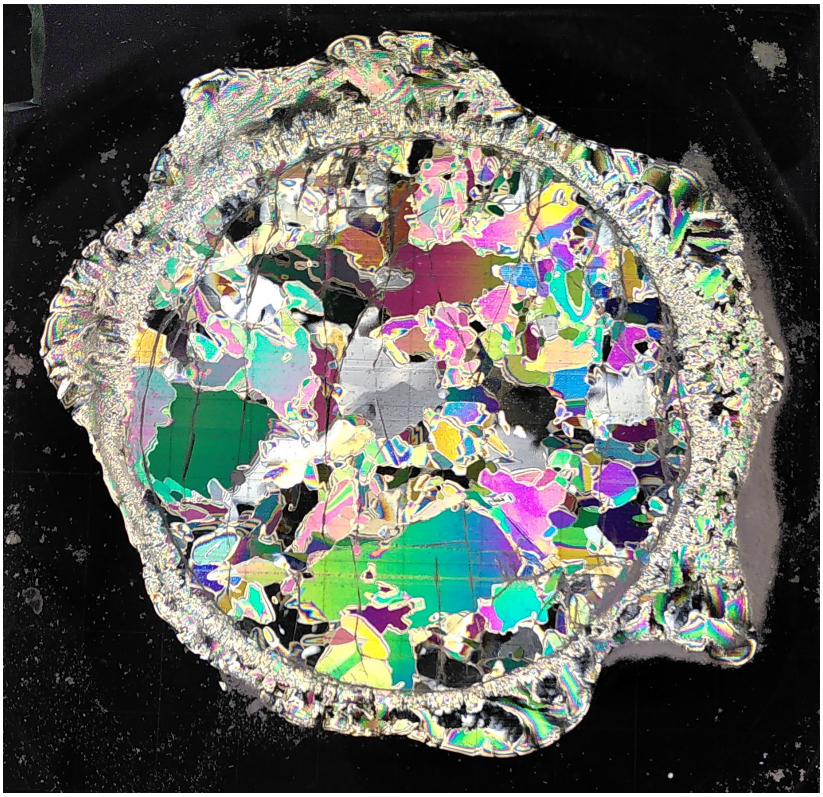

Figure 3.4: Example of ice core thin section photograph with relatively large grains

Collected ice cores were preserved in the ice lab at NTNU at a temperature of -20 ℃. This enabled processing of ice cores retrieved in the field without further deterioration. During one field season 27 ice cores were retrieved from

Sokna river and processed in the ice lab. Where practicable ice cores had a corresponding BHJ measurements taken in holes drilled adjacent to the ice core hole. Processing generally involved thin section photography and density measurements of the ice. The thin section photography was both some of the most beautiful and difficult to analyse data collected during this PhD. See Figure 3.4 for and example. Thin section photography takes advantage of peculiar property of ice: The crystal structure of ice acts as a filter to polarized light, hence if ice is shaved thin enough to not have overlapping grains each grain will show up as a different colour when photographed under polarized light (Gow, 1986). Thin enough was usually 1 - 2 mm thick depending on the size of the grains. Thin section photographs hence allow detailed characterization of the grain structure of ice. To generate the thin sections, ice cores were cut with a bandsaw into smaller cylinders. These were then adhered to glass plates using distilled water. The glass plate was then attached to a Leica microtom using vacuum and the microtom was used to shave the ice down to 1 - 2 mm thickness.

Two methods of density measurements were used, buoyancy based and volumetric. For volumetric density measurements a cut of an ice core is assumed to be a perfect cylinder and the ratio between the weight of this cylinder and its volume is taken as the density. For the buoyancy based measurement the cut of the ice core is weighted in air and submerged in paraffin. Thus enabling the computation of a density of a volume that disregards open voids.

3.6 The rudimentaries of cold weather fieldwork AKA things go wrong

Some who read this thesis will at some point find themselves doing cold weather fieldwork. It is a rewarding undertaking and I recommend it. River ice fieldwork is however - by its nature - prone to going wrong. Sharing some lessons - some hard earned - that I learned throughout my own fieldwork is in order.

3.6.1 Pay attention to the beauty

There is much worth looking at in and around frozen rivers. Paying attention to it is what makes the whole undertaking worth it.

You may find yourself seeing any number of wonderful phenomena and varied wildlife. While on the river I saw eagles, otters, salmon, moose, an - admittedly dead - badger and tracks and droppings from a mysterious predator. However, of all the animals I saw the White Throated Dipper (Fossekall in Norwegian) impressed me the most. Even in the most frigid depths of winter it would fly from open lead to open lead and dive looking for food. It baffles me how such a creature can survive. Even the humblest of White Throated Dippers will see more of the frozen river and more intuitively understand it than you

Figure 3.5: Snowbeards found within Sokna, the pictures do not do them justice.

or I ever will. The White Throated Dipper deserves its status as Norway's national bird and ought to be considered the patron saint of river ice researchers everywhere. The wildlife aside. Throughout my time as a river ice researcher. I saw ice in forms most endless and fascinating. I saw phenomena too rare, ephemeral and niche to ever get the research their innate beauty demands. Never forget to simply pause, look and marvel at what you see. On one occasion I spent the lions share of a day of fieldwork investigating ice beards. You will not have heard of ice beards before, mostly because I didn't know whether they had another name, so I named them such. Ice beards is frost that has accumulated under an over hang in the shape of a beard. They form in ice caverns attached to anchor ice dams, where an open lead provides a steady supply of humidity. Mere touch or a gust of wind is enough for them to disintegrate. Do ice beards matter when predicting ice forces on structures? No. No they do not. They are far too rare and light to be of any consequence in that matter whatsoever. But they are interesting and worth looking at. Just look at Figure 3.5 they are beautiful.

3.6.2 Bring spare woollen socks

On one occasion I was skiing down Sokna recording anchor ice dam locations. I step through the ice and my foot gets soaked. Unpleasant at the best of times. However, when the air temperature is below -20 and the car is halfway up the river it is quite a bit more of a pressing issue than usual. For the record, the correct way of wearing socks is a thin inner sock and a thick woollen outer sock. The two sock solution will protect you from blisters (Knapik & Hamlet, 1996). The woollen socks will keep you warm, even when wet. Very useful after falling through the ice, the aftermath of which can be seen in Figure 3.6. Just take care not to cut off circulation, all the socks in the world wont keep you warm if you are wearing an undersized boot. Ideally you will be wearing Sorrel or similar quality boots a size or two larger than your usual.

Figure 3.6: The picture shows the aftermath after I fell through the ice. I was not alone and had spare socks, so it was ok.

3.6.3 Get a partner in crime

Self explanatory. When things go wrong having someone that has your back is invaluable. And even when things aren't, not being alone will massively increase your productivity and make the whole undertaking a fair bit more pleasant and less insurmountable. Never work on the ice alone. Besides, you might - like myself - not know how to drive, a useful skill in this line of work as it turns out.

3.6.4 Batteries and the cold don't mix well

The performance of most batteries deteriorate significantly at very cold temperatures. Your fieldwork, whatever its objective, may include any number of batteries. Think hard about all of them. About how to keep them warm, how to charge them, how many spares to bring and what to do when they just don't work. During my fieldwork experience I have had my cellphone battery drain from full to flat in minutes due to the cold. I have had to cut fieldwork short due to the battery in an electric car performing poorly in the cold. Cars have refused to start due to cold batteries. Fieldcomputers shutting down in the middle of recording data. On one occasion the batteries of the expensive Phantom DJI 4 drone suddenly failed while the drone was over the river and consequently it unceremoniously smashed into the river. And, most traumatic of all, I have had the batteries powering the load panel meant to record ice run forces fail just before the ice run hit. Never trust batteries.

3.6.5 Eat, drink and get enough rest

Figure 3.7: A weary fieldworker clearly in need of rest and a hot drink

This is trite, oft given and equally often ignored advice. Fieldworkers quickly learn that in order to stay warm you need woollen layers, however many the weather demands. Sometimes however fieldworkers grow chilly, even when competently and suitably dressed for the weather. In the cold the body expends a lot of energy producing heat, if you haven't eaten you won't have enough energy to burn fast enough to stay warm. Fatty calorific food works best here. Fieldworkers in my experience usually eat enough but drink too little. You cannot combust calories without enough water in your system. With all the physical labour and heat you will be producing you will need to eat and drink more than usual. Bring energy bars and a thermos of water at the minimum (plastic

bottles of water, even left in the car, won't do they freeze). Finally sleep enough, take breaks and don't overdo it. When tired is when you will make your most serious mistakes.

3.6.6 Ice is slippery

Figure 3.8: The institute car inexorably sliding towards its doom

Ice is slippery in general of course, but this is especially important when working on anchor ice dams. Getting chains for your boots will keep you alive and massively increase your productivity. Just don't get that awful cheap stuff you see peddled in the local grocery store. You want chains that enable you to run on ice with confidence. If they don't let you do that, get something better. Once you are confident in your ability to walk on ice, make sure that your vehicle can too. On one particularly memorable instance we had to barter our way to some sand to retrieve our car from nearly having slid into the river Figure 3.8.

3.6.7 Keep your blades sharp

A wide range of river ice measurements involve drilling and otherwise cutting ice. The difference between a properly sharp ice augur and blunt one adds up to hours and hours of extra work. So get more spare blades than you think you need, learn how to sharpen them or make friends with someone who does. Remember that blades will dull much faster when drilling in a small steep river than when drilling on say a lake. This is because you are much more likely to accidentally hit rock and other miscellanea when drilling in a small steep river.

3.6.8 Have a checklist

There is no feeling quite like realising after having spent 2 hours driving and setting up your equipment that you forgot something critical back at the office and you now have to meekly pack back up again and head back home without having collected any data all. A well thought out checklist is the magic bullet that could save you from that sort of - for myself at least - alarmingly common heartache.

3.6.9 Its OK to give up

Sometimes the weather takes a turn for the worse, the discharge in the river is higher than expected, equipment fails, you are too tired to continue or the fieldwork plan developed in the comfort of your office simply turns out to be, for any number of reasons, unfeasible when faced with the cold light of day. Learning when to throw in the towel is an essential part of fieldwork. Often your energy is better spent resting or trying something new.

3.6.10 Seek help

PhDs are by their nature though. They are made to be. And while much can and should be said on how to make them healthier experiences in general, from the budding PhD students point of view the best advice is simple: Seek help. Seek help early - and late - and often. And above all else seek help when you are stuck, when you are not working, when you don't quite know what to do. It is all to easy to only ask for help when you don't really need it. Don't wait to call for a supervisors meeting until you have something to show off, their primary purpose is not for you to brag, but for you to get unstuck. And don't restrict your quest for help to supervisors either. Talk to your fellow PhDs about your troubles, seek out technicians, random academics and really anyone who might give you their time of day. And most importantly, remember that NTNU - and a lot of other universities too for that matter - offer free psychology services for their PhD students. It helped me and I recommend it for when the going gets tough.

Chapter 4

Main contributions

This thesis provides 3 main contributions to the field of river ice research. Firstly it provides a novel method for estimating river ice thicknesses and volumes in small steep rivers. By using UAV photography, structure from motion processing and physical reasoning spatially distributed ice thickness estimates can now be obtained in small steep rivers with minimal manual labour. Second contribution is to provide an in-depth review of previous research on ice structure interactions and evaluate their applicability to bridge piers in small steep rivers. Hence providing a natural point of reference for river ice engineers and researchers interested in ice-structure interactions in small steep rivers. The third contribution is to provide the first dataset on spatial distribution of ice strength in small steep rivers. Furthermore the analysis of this dataset provides novel insights into how ice strength varies throughout small steep rivers.

Together these contributions provides the foundation for a practical approach to estimating possible ice forces in small steep rivers. Paper I shows that despite disagreements on the finer point of ice force prediction there is broad agreement that the two by far most important parameters for predicting ice forces are ice thickness and ice strength. Measuring and predicting these parameters in small steep rivers however is not a trivial matter. Traditionally the ice thickness of a stable ice cover has been measured by drilling holes and manually measuring the thickness. For large rivers this works fairly well since ice thickness changes relatively slowly and predictably along the length and width of the river. Hence fewer manual measurements are required to get a good representation of the ice thickness distribution of a river. For small steep rivers ice thickness changes drastically and discontinuously over very short distances, furthermore the high variability of step-pool structures can make these ice covers treacherous and difficult to access safely for manual measurement. To solve this problem Paper III suggests a methodology for remote estimation of ice thickness distribution in small steep rivers by using drone imagery, structure from motion software and manual measurement calibration. This methodology improves the feasible granularity of ice thickness measurements in small steep rivers. While much previous work has been done measuring strength of marine

ice and lab based measurements of fresh water ice, before Paper II no recorded literature to the authors knowledge of ice strength distribution in small steep rivers. While retrieving ice cores and crushing them is a standard method for ice strength measurements, Paper II uses an in-situ approach using a borehole-jack thus enabling a relatively rapid collection of the distribution of ice strength data in a small steep river. The data collected in Paper II being the only ice strength data for small steep rivers makes it essential research for estimating ice forces in small steep rivers. Hence Paper I, Paper III and Paper II together form a cohesive research project furthering our understanding of ice forces in small steep rivers.

As part of this PhD work a load panel was constructed to directly measure ice forces on a bridge pier in Støren. Unfortunately, due to various mishaps such as battery problems, corrupt SD cards and absence of ice runs no good ice run data was recorded.

4.1 Summary of Paper I - "Review of River Ice Force Calculation Methods"

This paper constitutes a review and evaluation of current analytical methods for determining quasi-static ice forces on bridge piers in rivers. Both peer-reviewed and grey literature is evaluated. The aim was to evaluate the applicability of these methods for the calculation of forces on bridge piers in small steep rivers. Limit stress equations have been considered, while thorough consideration of limit force and limit momentum equations were beyond the scope of this review. Disagreement between investigators and scope for further inquiries were highlighted. The paper shows that the predicted ice forces from different calculation methods frequently differ by more than an order of magnitude. It also shows broad agreement that ice forces increase linearly with ice thickness for vertical structures and with ice thickness squared for sloping structures. Similarly the paper shows broad agreement that ice forces increase linearly with ice strength, except for wider structures where clearing forces can be significant, with the caveat that the definition of ice strength varies substantially between authors. Finally the paper provides a roadmap for necessary future research on river ice forces in small steep rivers. As a whole the paper serves as a useful first point of reference for researchers and engineers interested in ice forces on bridge piers in rivers.

4.2 Summary of Paper II - "In-situ Ice Strength Distribution of Anchor Ice Dams" Paper

Ice runs and ice jams can cause significant damage to infrastructure and other human interests. Accurate modelling and prediction of these events rely on

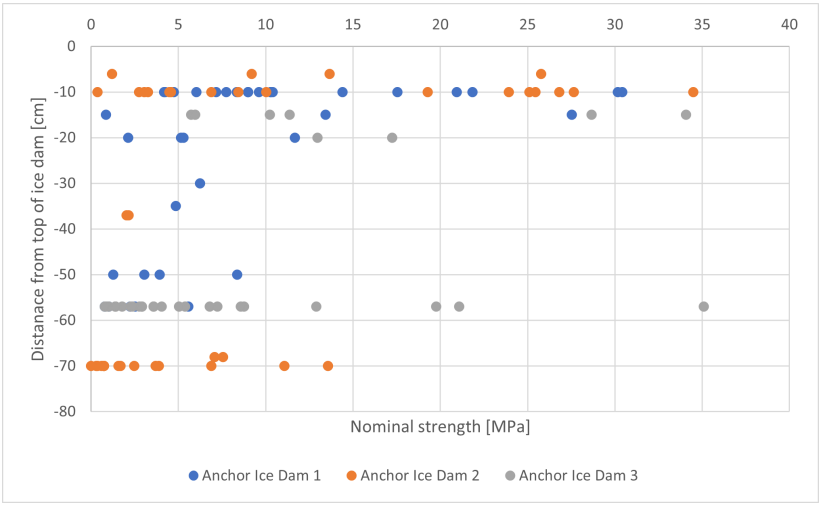

Figure 4.1: Calibrated ice strengths measured at different depths in three different ice dams

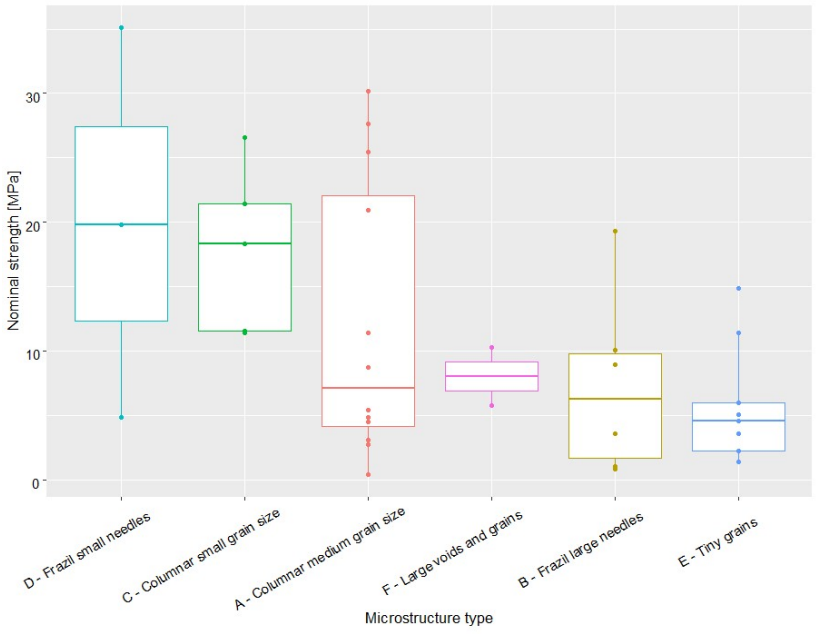

Figure 4.2: Thin section microstructure vs closest calibrated BHJ measurement.

data and assumptions about river ice properties. This paper seeks to address the lack of data on ice strength distributions and associated properties in small steep rivers and to obtain a better understanding of these. To this end during the 2020 – 2021 winter field season a large ice data collection campaign was carried out in the Sokna river in central Norway. The following types of data were collected for anchor ice dams and level ice sections: Borehole Jack (BHJ) in-situ ice strength, ice thickness, density, thin section imagery and associated depth measurements. Figure 4.1 shows how in-situ anchor ice dam strengths vary with depth. While Figure 4.2 shows how the same ice strength varies with observed ice microstructure. A total of 27 ice cores and 68 thin sections successfully collected and processed. Furthermore, a survey was carried out recording GPS coordinates of anchor ice dams in the river. Meteorological and hydrological data was also collated, and large boulder location data was obtained through analysis of aerial photography. Analysis of these data gave ice strength distributions and indicated some trends about how ice strength varies within a small steep river. Analysis of ice dam location data gave a binomial generalized linear model for modelling ice dam locations (Equation (4.1)).

$$P(Icedam) = 1.577 + 0.596s - 0.461\frac{ds}{dx} - 0.205b + 0.054w - 0.046sw + bw \quad (4.1)$$

This model describes how river width (w), slope (s) and to a lesser degree large boulder density (b) affect ice dam location. Sinuosity was shown to have no effect on ice dam location. This work highlights the significant variation of microstructure and large-scale structure of ice in small steep rivers.

4.3 Summary of Paper III - "Drone Surveying of Volumetric Ice Growth in a Steep River" Paper

Steep rivers exhibit complex freeze-up behaviour combining formation of columnar ice with successions of anchor ice dams to build a complete ice cover, resulting in an ice cover with complex geometry. Representative ice thickness data is essential for accurate hydraulic modelling, assessing the potential for ice induced floods, understanding environmental conditions during winter and estimation of ice-run forces. Traditional single point measurements are therefore unrepresentative and gathering sufficiently distributed measurements for representativeness is labour intensive and at times impossible with hard to access ice. Structure from Motion (SfM) software and low-cost drones have enabled river ice mapping without the need to directly access the ice, thereby reducing both the workload and the potential danger in accessing the ice. In this paper we show how drone-based photography can be used to efficiently survey river ice and how these photographic surveys can be processed into digital elevation models (DEMs) using Structure from Motion. We also show how DEMs of the riverbed, riverbanks and ice conditions can be used to deduce ice volume

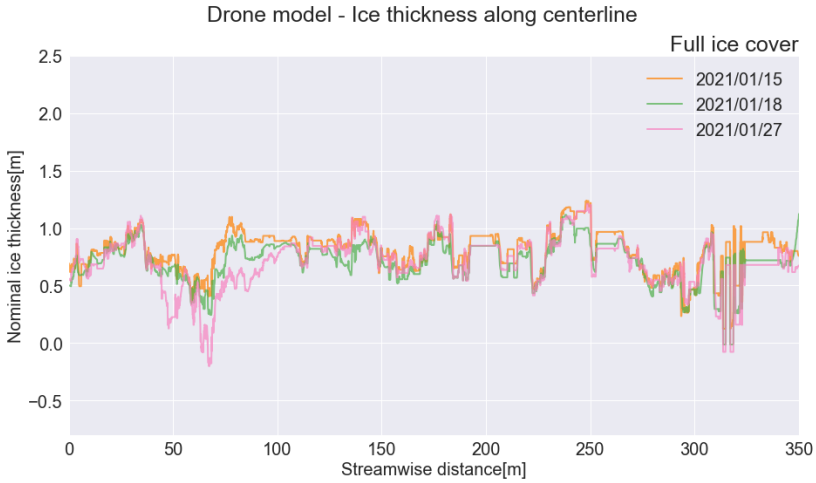

Figure 4.3: Ice thicknesses along the centerline of a segment of the Sokna river derived from the described drone methodology

and ice thickness distributions. One example of such an ice thickness distribution is shown in Figure 4.3. A QGIS plugin has been implemented to automate these tasks. These techniques are demonstrated with a survey of a stretch of the river Sokna in Trøndelag, Norway. The survey was carried out during the winter 2020-2021 at various stages of freeze-up using a simple quadcopter with camera Figure 4.4 shows an example of a drone picture later used to develop an orthomosaic of the river. Ground Control Points were measured with an RTK-GPS and used to determine the accuracy of the measurements.

Figure 4.4: Drone picture of Sokna taken 5th January 2021

Chapter 5

Discussion

5.1 The best equations for predicting ice forces in small steep rivers, and their problems

Recommended equations depend upon the intended application. However, under no circumstances should an ice force equation be used uncritically and without proper understanding of the equation's limitations. Where the purpose of the calculation is design, the most conservative equation should be used, unless the validity of less conservative equations can be justified.

However, some equations should not be used for small steep rivers at all: The Korzhavin crushing equations is not strictly applicable to small rivers and is therefore not recommended for this purpose (Korzhavin, 1971). The simple 2D bending equation is not applicable to narrow structures and is therefore not recommended for use in small rivers (Ashton, n.d.). The Ralston 3D result lacks empirical basis and is therefore not recommended (Ralston, 1980). Furthermore, analytical expressions for several of its parameters are not available.

Most of the equations considered may be used, but only in specific circumstances. Where bending failure is known to occur, and substantial data exists the ISO elastic-brittle sloping structure solution should be used. Because the ISO elastic-brittle sloping structure solution is recent and developed through the consensus of international experts it should in general be favoured where possible. Where there is a lack of data the large number of parameters that need to be specified the ISO elastic-brittle sloping structure solution must be used with caution. The approach in this case should be to perform sensitivities with ranges of the parameters which may not be known and then the results of this analysis should be weighted up against experience and engineering judgement (ISO 19906, 2019).

Where minimal resources or ice engineering experience are available simpler approaches can be justified. Both the Afanasev's elastic plate model and Edwards and Croasdales empirical model are applicable to small conical structures (Korzhavin, 1971)(Ashton, n.d.). Edwards and Croasdales equation rely

upon a wider range of ice thicknesses and should therefore be preferred. However, for thick ice both expressions should be treated with suspicion.

The Russian practice SNiP 2.06.04-84 is underpinned by substantial geographically distributed data and can therefore be safely applied in Russia. However, lack of data and translation means that SNiP cannot easily be applied outside Russia. Furthermore, SNiP may err on the side of being overly conservative (SNiP, 2004).

The CSA S6:19 standard can safely be applied where reliable ice strength data exists. If reliable ice strength data does not exist, the standard is not especially useful since the ice force scales linearly with the ice strength, and the ice strength can vary between 0.4 MPa and 1.5 MPa (standards association, 2019).

The ISO crushing equation can be safely applied in region where the C factor has been shown to be acceptable. Although it must be pointed out that the ISO C factors are nominally developed from offshore data and as such their applicability to rivers without modification is debatable for various reasons: Ice runs only happen a few times, if any, in a river per year, as such exposure rates on riverine structures are quite different from exposure rates on offshore structures. ISO specifically highlights that data for narrow structures in thick ice is lacking (ISO 19906, 2019).

The Finnish standard is very simplistic. This approach can only be used where the ice strength used has been shown to be sufficiently conservative. Primarily useful in regions with relatively modest ice forces(Eurocode, 2017).

The Swedish ice rubble equation should only be used for relatively narrow spans, the equation breaks down for wide spans (Vägverket, 1987).

The Korzhavin design pressure formula and the Ashton quick force calculation equations in practice give similar results, but Ashton is easier to use. Either are useful for first pass estimation of ice forces (Korzhavin, 1971)(Ashton, n.d.).

5.2 Accuracy of ice thickness measurement by drone methodology

A small unmanned aerial vehicle was used in combination with Structure from Motion photogrammetry to build digital elevation models of river ice during the winter season in a small stream. The use of the UAV allowed mapping the extent and estimating the volume of ice during the winter, also during conditions were traditional mapping strategies requiring access to the ice surface (Turcotte et al., 2017) would be impossible. An important feature of this method is the ability to map anchor ice dams (Turcotte et al., 2011) , which is controlling the ice formation and hydraulic conditions in small streams like Sokna (Stickler et al., 2010).

The RTK drone proved to produce accurate ice cover DEM data and compared to ground control points measured with RTK GPS the errors were within

a few centimeters. The RMS errors (That is, the root mean square distance between the GPS control points and the DEM derived from drone imagery using photogrammetry) from this study (here they round to the same as the mean errors) are of a similar magnitude to those quoted by Alfredsen et al. (2018), who while comparing drone photogrammetry derived DEM of and ice cover with ground control points found RMS errors in the range 0.06 m – 0.106 m. When Stott et al. (2020) mapped a small ice-free river in Scotland using comparable equipment to this study they also achieved similar RMS errors (0.066 m – 0.072 m).

Depending on lighting conditions, clarity, and depth of the water, the no-ice DEM may either represent the water surface or the riverbed. The lower the water level in the raw data for the no-ice DEM the harder this type of error is to identify by inspection as the error is small. Conversely, the deeper the water, the easier the error is to identify by inspection, but the error, however, can be much more severe. These types of errors can in principle be removed by manually eliminating the problematic areas from the analysis, however this is prone to human error and bias. The no-ice DEM should therefore ideally either be obtained through visual photography by a drone at discharges corresponding to water depth of less than 1 m (Maddock & Lynch, 2020) or optimally be obtained through lidar scanning at an appropriate wavelength for penetrating the water (Mandlburger et al., 2020). The latter method was used by Alfredsen and Juarez (2020) to integrate ice jam remnants in the river bathymetry, and hence numerically assess the impact of ice on flow patterns.

Steep rivers also have an extra source of error compared to low-gradient rivers; they have higher turbulence (Mandlburger et al., 2020), and highly turbulent water will often be captured in the DEM as solid. Furthermore, small steep rivers have rapid local changes in the water surface therefore two pictures of the same area taken in close succession may disagree on whether the water surface or the riverbed should be included in the DEM. Small steep rivers do have some advantages over big low gradient rivers: in a small river a higher percentage of the volume under the upper surface of the ice cover is ice, therefore the models' upper bound is closer to the real value than if the same method had been applied to a big river. This makes it easier to justify using the estimates derived from the drone method for engineering purposes. If used for engineering purposes, the data should be treated as an upper bound and care should be taken not to add excessive safety factors on top of that. It should also be kept in mind that manual methods for ice thickness measurement that work well on big rivers are often inapplicable to small steep rivers. The short spans and high ice-bank adhesion in small rivers also make air-filled voids common and freeboard-based calculations unfeasible.

The DEMs were cut to the riverbank, as this reduces it to the area of interest, hence removing any potential issues associated with the accuracy at the edge of the DEM, such as tall trees blocking line of sight. Vegetation overhang was a significant source of error in the first pass model. Depending on snow fall

and foliage, overhanging trees will show up in the DEM as different elevations unrelated to the underlying ice thickness. These errors were however drastically reduced in the final model by inspecting the orthomosaic and cutting away any overhanging vegetation in the no-ice DEM. It is possible that some errors due to overhanging vegetation persists in later DEMs, as snow can cause vegetation to shift to new places. For DEMs of modest extent, manual inspection and removal of vegetation is likely less labour intensive and less error prone than automatic classification of the point cloud. For larger DEMs and larger data sets, automatic surface classification should be considered (Husson et al., 2016).

The difference between manual ice thickness measurements and the drone model ice thickness estimates being reasonably well described by a normal or modified normal distribution suggests that it is possible to calibrate the drone model with manual measurements. I.e., use a few manual measurements to determine the mean error, then subtract that from the drone model. The drone model would then represent a best estimate of the ice thickness, rather than a conservative estimate.

5.3 Unifying models

Figure 5.1: Stranded ice floes under Sokna bridge, early 2020. The distribution of the dimensions of these ice floes are described in Rødtang et al. (2023)

As part of this PhD a statistical model for describing anchor ice dam incidence in small steep rivers was developed. An areal model of ice thickness of an anchor ice dam as well as collected in-situ anchor ice dam strength measurements were also created. While on their own these are interesting, one further step

is necessary for them to be truly useful. The models must be unified into a coherent whole. The key missing step would be to connect a description of the static ice cover to a description of the ice floe size distribution during an ice run. Further work is necessary, both theoretical and empirical before a robust model connecting static ice cover of small steep rivers to ice floe size distribution can be made. Figure 5.1 shows stranded ice floes under Sokna bridge, the dimensions of these were recorded, more such measurements should be made.

Ice forces on bridge piers during an ice run is an inherently stochastic process. As such the ideal approach for computing ice forces would involve monte carlo simulation. Ice thickness and ice strength distributions constructed during this PhD work would be useful for that. The simulation would be improved however if a good model for the connection between ice thickness and ice strength in small steep rivers could be constructed. Assuming independence could work as a first order approximation, however data from Paper II suggests that there are definite variations of ice strength with depth.

5.4 Equivalent force potential

An alternative to considering ice thickness and strength independently is to instead consider the integral of their product as shown in Equation (5.1).

$$F_{potential} = k \int_0^{h_{total}} \sigma(h) dh \tag{5.1}$$

Parameter h is ice thickness measured from the top of the ice, h_{total} is the total ice thickness, σ is BHJ ice strength and k is a constant such that $F_{potential}$ equals the maximum force exerted upon a structure by an ice floe with $\int_0^{h_{total}} \sigma(h) dh$ experiencing complete crushing. k can be determined by direct measurement, or estimated with equations described Paper I. Note that due to the scale effect k depends on h_{total}.

This quantity times a structure dependent constant would give an upper bound on how much force the ice from a particular point in the river could apply to the structure. The real force would be less because during an ice run the ice would break apart partially or fully before reaching the structure. With the borehole jack (BHJ) this becomes a measurable quantity that avoids some of the pitfalls of defining thickness and strength independently. In practice the equivalent force potential is estimated by doing BHJ measurements at representative depths then extrapolating. Paper II shows an example of such a measurement, its equivalent distribution and predicted forces.

Many force prediction equations take σh as input. Many of these are described in Paper I. Most of these will be favourably improved by replacing this with $\int_0^{h_{total}} \sigma(h) dh$ where possible.

Chapter 6

Conclusion

Paper I provides an in-depth overview of equations derived thus far for the calculating ice forces on piers in rivers. It highlights how most methods rely on offshore, saline ice data or data from large rivers. Furthermore it compares and contrasts the relative merits of various approaches on how they apply to small steep rivers in particular and outlines what further research is necessary to improve their applicability to small steep rivers. The paper shows that there is broad consensus that ice forces increase with ice strength and ice thickness. This implies that once a model for ice thickness and ice strength distributions has through a measurement program been obtained, a model for ice force return periods can be derived through Monte Carlo analysis, provided a robust theoretical framework is applied.

In small steep rivers however it is not necessarily true that ice forces increase with ice thickness since ice strength and void fraction regularly cause thicker ice to be weaker than thin competent ice. This is especially true where the river has a significant proportion of anchor ice and a high frequency step pool structure. In such rivers it hence becomes critical to characterize not just the average ice thickness and strength but also its spatial variability. Traditional manual point measurements of ice thickness are therefore insufficient, a 3D approach is necessary. As described in Paper III the spatial distribution of river ice thickness can be approximated using drone photography and structure from motion analysis. By including discharge, LIDAR bathymetry data and freeze-up imagery a useful upper bound estimates on ice thickness distributions can be made. This 3D model can then be calibrated using traditional point measurements to provide a best estimate spatial model of ice thickness.

Spatial ice thickness distribution alone however is, as mentioned, not sufficient to estimate ice forces. Ice strength measurements are necessary. Traditionally river ice strength measurements have been conducted by retrieving ice core samples from the river and then later apply a crushing test in the lab. This approach has some definite draw backs: samples can deteriorate before reaching the lab, lab tests do not provide realistic confinement conditions and the method is labour intensive. Furthermore the strength of weaker ice structures

and large void fraction ice is difficult to measure with this method. Paper II provides an alternative in-situ method for measuring ice strength distribution in small steep rivers. Borehole-jack (BHJ) measurements provide a method for rapidly obtaining distributed anchor ice and level ice strengths. Furthermore this paper provides the first quantitative description and mathematical model of ice strength variability within and between anchor ice dams in a river.

The combination of a theoretical framework (Paper I), a method for ice thickness measurement (Paper III) and a method for ice strength measurement (Paper II) is in conclusion a step in the right direction for predicting ice forces on piers in small steep rivers.

Key conclusions:

- The principal problem facing river ice research at present is a lack of large cohesive datasets and rigorous statistical thinking.
- A wide range of contradictory methods for calculating quasi-static ice forces have been developed. The principal points of agreement are that forces increase linearly with ice thickness for vertical structures and with ice thickness squared for sloping structures. Furthermore there is broad agreement that forces scale linearly with ice strength, except for wider structures where clearing forces can be significant. Ice strength and thickness are together generally acknowledged to be the most important parameters when predicting quasi-static ice forces.
- Drone photography coupled with structure for motion analysis can be used to provide bounds on ice thickness and ice volume in small steep rivers, while Borehole-jack (BHJ) measurements provide a method for rapidly obtaining distributed in-situ anchor ice and level ice strengths.
- River slope, rate of change of river slope and width can be used to predict anchor ice dam locations in small steep rivers. Large boulder density however has little predictive power.

Chapter 7

Future work

The strength and thickness of ice in small steep rivers is complex and has a sensitive dependency on a myriad of factors. The river bathymetry, discharge variations, snow fall, air temperature, insolation and many other factors have a part to play. Even with a fully specified static ice cover it is difficult to predict the properties of ice floes as they flow down a river in an ice run. Furthermore , even if the properties of ice floes in the ice run is known, it is still difficult to predict how these ice floes will interact with structures and impart forces. Reliably predicting ice forces on structures in small steep rivers is a difficult undertaking. However, despite the theoretical complexities inherent in relating bathymetry and meteorological variables to ice forces, the principal problem facing improving understanding of river ice forces is not theoretical but empirical. It is a sad truth that very little river ice data from small steep rivers exist, much of it described in this thesis. Without data, theories cannot be falsified, unexpected relationships will not be found and progress in the field will be stifled. With this in mind, these priorities are suggested for future work:

- Adoption of standardized methods of ice strength measurement would be a great benefit to the field. This would enable data from different research teams to be reasonably compared. While there has been initiatives to develop testing standards (see for example Schwarz et al., 1981 Schwarz et al., 1981) take-up remains patchy resulting in difficulties comparing data from different research groups.
- Further data collection in small steep rivers would enable the creation of parameter distributions and statistical evaluation of expressions. This would also allow for testing the model in different rivers.
- More in-situ measurements of ice forces on bridges would be helpful for cross referencing with forces predicted by standards. Specifically maintaining and improving upon the load panel developed as part of this PhD would be worthwhile.
- Ice force codes have narrow geographical applicability. Currently the only way of extending the applicability of a code to a new region is the collection of substantial amounts of ice force data. The development of a

method for extending and verifying the geographical applicability of ice force codes based on meteorological, climatological and geographical data would be of great benefit. This is especially important because climate change likely will render previous data unrepresentative for future ice runs.

- At present ice force codes contradict each other and provide poor guidance. Harmonization and improved guidance is necessary.
- Currently no robust quantitative method exists for predicting which failure mechanism will dominate in each interaction. The best current methods are purely empirical and compare only two failure mechanisms, crushing and bending. Developing such a method would be of great benefit.
- A great many ice force equations exist, they should be systematically compared to a large, consistent, and applicable set of field data. Equations that provide the worst predictions should be rejected.
- It is necessary to reach a consensus on the quantitative effect of scale and aspect ratio.
- Clarification on the difference between crushing failure and shear failure is necessary.
- Some of these recommendations are large in scope and partially addressed in ISO 19906. Therefore recommending ISO 19906 for use in rivers and addressing gaps in ISO 19906 which relate to ice action on bridges in rivers is likely the least laborious and highest impact way of improving ice force predictions in small steep rivers.

Bibliography

NTB. (2018). Vegdirektoratet har snart sjekket alle Norges 17.500 broer. https://www.tu.no/artikler/vegdirektoratet-har-snart-sjekket-alle-norges-17-500-broer/443780

Rødtang, E., Alfredsen, K. & Høyland, K. (2023). Estimating ice forces on a bridge pier using field observations and a deformation model. *Canadian Journal of Civil Engineering*. https://doi.org/10.1139/cjce-2023-0029

Ghobrial, T. R. & Loewen, M. R. (2021). Continuous in situ measurements of anchor ice formation, growth, and release. *Cryosphere*, *15*(1), 49–67. https://doi.org/10.5194/tc-15-49-2021

Osterkamp, T. & Gosink, J. (1983). Frazil ice formation and ice cover development in interior alaska streams. *Cold Regions Science and Technology*, *8*(1), 43–56. https://doi.org/https://doi.org/10.1016/0165-232X(83)90016-2

Shen, H. H., Ackley, S. F. & Yuan, Y. (2004). Limiting diameter of pancake ice. *Journal of Geophysical Research: Oceans*, *109*(12), 1–13. https://doi.org/10.1029/2003JC002123

Pariset, E., Hausser, R. & Gagnon, A. (1966). Formation of ice covers and ice jams in rivers. *Journal of the Hydraulics Division*, *92*(6), 1–24.

Wazney, L., Clark, S. P. & Wall, A. J. (2018). Field monitoring of secondary consolidation events and ice cover progression during freeze-up on the lower dauphin river, manitoba. *Cold Regions Science and Technology*, *148*, 159–171. https://doi.org/https://doi.org/10.1016/j.coldregions.2018.01.014

Dubé, M., Turcotte, B. & Morse, B. (2014). Inner structure of anchor ice and ice dams in steep channels. *Cold Regions Science and Technology*, *106-107*, 194–206. https://doi.org/https://doi.org/10.1016/j.coldregions.2014.06.013

Turcotte, B., Morse, B. & Anctil, F. (2011). Steep channels freezeup processes. *CRIPE*, 85–101.

Nafziger, J., She, Y. & Hicks, F. (2016). Celerities of waves and ice runs from ice jam releases. *Cold Regions Science and Technology*, *123*, 71–80. https://doi.org/https://doi.org/10.1016/j.coldregions.2015.11.014

Madaeni, F., Lhissou, R., Chokmani, K., Raymond, S. & Gauthier, Y. (2020). Cold Regions Science and Technology Ice jam formation , breakup and

prediction methods based on hydroclimatic data using arti fi cial intelligence : A review. *Cold Regions Science and Technology*, *174*(January), 103032. https://doi.org/10.1016/j.coldregions.2020.103032

Beltaos, S. (2008). *River Ice Breakup* (1st). Water Resources Publications.

Ashton, G. D. (n.d.). Water Resources Publications.

Palmer, A., Dempsey, J. & Masterson, D. (2009). A revised ice pressure-area curve and a fracture mechanics explanation. *Cold Regions Science and Technology*, *56*(2-3), 73–76. https://doi.org/10.1016/j.coldregions.2008.11.009

Stickler, M., Alfredsen, K. T., Linnansaari, T. & Fjeldstad, H.-P. (2010). The influence of dynamic ice formation on hydraulic heterogeneity in steep streams. *River Research and Applications*, *26*(9), 1187–1197. https://doi.org/10.1002/rra.1331

Heggen, S. & Alfredsen, K. (2013). Ice Breakup in Small Norwegian Streams. *Proceedings of the 17th Workshop on River Ice*, (June), 18 pages.

The Norwegian Water Resources and Energy Directorate. (n.d.). nevina.nve.no

Kallelid, M. S. (2018). *A Study of the Strength and the Physical Properties of Glacier-ice Runways* (Master Thesis). NTNU. http://hdl.handle.net/11250/2574921

Schulson, E. & Duval., P. (2009). *Creep and fracture of ice* (Vol. 57). Cambridge University Press. https://doi.org/10.3189/S0022143000206254

Shkhinek, K., Jilenkov, A., Smirnov, V. & Thomas, G. (2010). Analysis of borehole jack records. *20th IAHR International Symposium on Ice*.

Nord, T. S., Oiseth, O. & Lourens, E. M. (2016). Ice force identification on the Nordströmsgrund lighthouse. *Computers and Structures*, *169*, 24–39. https://doi.org/10.1016/j.compstruc.2016.02.016

Hellgren, R., Malm, R., Fransson, L., Johansson, F., Nordström, E. & Westberg Wilde, M. (2020). Measurement of ice pressure on a concrete dam with a prototype ice load panel. *Cold Regions Science and Technology*, *170*(July 2019), 102923. https://doi.org/10.1016/j.coldregions.2019.102923

Shrestha, N. & Brown, T. G. (2018). 20 years of monitoring of ice action on the Confederation Bridge piers. *Cold Regions Science and Technology*, *151*(March), 208–236. https://doi.org/10.1016/j.coldregions.2018.03.025

Gow, A. J. (1986). Optical Characterization Of Sea Ice Structure Using Polarized Light Techniques (M. A. Blizard, Ed.). *264*, 264. https://doi.org/10.1117/12.964241

Knapik, J. J. & Hamlet, M. P. (1996). Influence of Boot-Sock Systems on Frequency and Severity of Foot Blisters. *161*(October).

Korzhavin. (1971). *Action of Ice on Engineering Structures* (2002nd ed.). Books for Business.

Ralston, T. D. (1980). Plastic Limit Analysis of Sheet Ice Loads on Conical Structures. *Physics and mechanics of ice* (pp. 289–308). Springer Berlin Heidelberg. https://doi.org/10.1007/978-3-642-81434-1_21

ISO 19906. (2019). *ISO/FDIS 19906:2019(E)* (tech. rep.). The Onternational Organization for Standardization.

SNiP. (2004). *SNiP code 2.06.04.82*
See Sandwell (Tseng).

standards association, C. (2019). *CSA S6:19 Canadian Highway Bridge Design Code*. CSA group.

Eurocode, F. (2017). *Finnish Eurocode - Bridges*. Liikenneviraston.

Vägverket. (1987). *Istryck mot bropelare* (Vol. 43). Serviceavdelining Väg- och Brokonstruktion
isränna, strömfåra, stoppklackar,sötvatten, rännor, stjälpning vectorial addition of forces when forces incident at an angle.

Turcotte, B., Nafziger, J., Clark, S., Beltaos, S., Jasek, M., Lind, L. & Stander, E. (2017). Monitoring river ice processes : Sharing experience to improve successful research programs. *Proceedings of the 19th Workshop on the Hydraulics of Ice Covered Rivers Whitehorse, YK, Canada*, (July). http://cripe.ca/docs/proceedings/19/Turcotte-et-al-2017b.pdf

Alfredsen, K., Haas, C., Tuhtan, J. A. & Zinke, P. (2018). Brief Communication: Mapping river ice using drones and structure from motion. *Cryosphere*, *12*(2), 627–633. https://doi.org/10.5194/tc-12-627-2018

Stott, E., Williams, R. D. & Hoey, T. B. (2020). Ground control point distribution for accurate kilometre-scale topographic mapping using an rtk-gnss unmanned aerial vehicle and sfm photogrammetry. *Drones*, *4*(3), 1–21. https://doi.org/10.3390/drones4030055

Maddock, I. & Lynch, J. (2020). Assessing the accuracy of river channel bathymetry measurement using an RTK rotary-winged Unmanned Aerial Vehicle (UAV) with varying Ground Control Point (GCP) number and placement. *EGU General Assembly 2020*. https://doi.org/https://doi.org/10.5194/egusphere-egu2020-1534

Mandlburger, G., Pfennigbauer, M., Schwarz, R., Flöry, S. & Nussbaumer, L. (2020). Concept and performance evaluation of a Novel UAV-Borne Topo-Bathymetric LiDAR sensor. *Remote Sensing*, *12*(6). https://doi.org/10.3390/rs12060986

Alfredsen, K. & Juarez, A. (2020). Modelling stranded river ice using lidar and drone-base models. *IAHR International Symposium on Ice*.

Husson, E., Ecke, F. & Reese, H. (2016). Comparison of manual mapping and automated object-based image analysis of non-submerged aquatic vegetation from very-high-resolution UAS images. *Remote Sensing*, *8*(9), 1–18. https://doi.org/10.3390/rs8090724

Schwarz, J., Frederking, R., Gavrillo, V., Petrov, I., Hirayama, K.-I., Mellor, M., Tryde, P. & Vaudrey, K. (1981). Standardized testing methods for measuring mechanical properties of ice. *Cold Regions Science and Technology*,

4, 245–253. https://doi.org/https://doi.org/10.1016/0165-232X(81)90007-0

Paper I

Cold Regions Science and Technology 209 (2023) 103809

Contents lists available at ScienceDirect

Cold Regions Science and Technology

journal homepage: www.elsevier.com/locate/coldregions

Review of river ice force calculation methods

Einar Rødtang *, Knut Alfredsen, Knut Høyland, Leif Lia

IBM – Depaprtment of Civil and Environmental Engineering, Norwegian University of Science and Technology, S.P. Andersens Vei 5, 7491 Trondheim, Norway

ARTICLE INFO

Keywords:
River ice
Ice forces
Review of codes
Steep rivers
Small rivers

ABSTRACT

This paper constitutes a review and evaluation of current analytical methods for determining quasi-static ice forces on bridge piers in rivers. Both peer-reviewed and grey literature is evaluated. The aim is to evaluate the applicability of these methods for the calculation of forces on bridge piers in small steep rivers. Limit stress equations will be considered, while thorough consideration of limit force and limit momentum equations are beyond the scope of this review. Disagreement between investigators and scope for further inquiries are highlighted.

1. Introduction

Structures across and along rivers with winter ice cover can experience high loads from ice. In particular, ice runs can cause critical ice actions and structures need to be designed to withstand these in order to ensure safety and reliability. This paper provides an overview of the widely different methods that have been used to estimate these forces. An ice run in a river is defined as a sudden transport of large amounts of ice. There are two main types of ice runs: thermal and mechanical. Thermal ice runs occur when the ice cover thaws and weakens such that the current can fracture and transport the ice. Thermal ice runs tend to have thinner and lower strength ice, and therefore generally apply small forces on infrastructure. Mechanical ice runs occur when a competent (I.e., at full mechanical strength) ice cover breaks apart due to changes in water level or external forces, such as wind. Once broken the current transports the ice. Mechanical ice runs can contain thick, strong ice and can therefore apply significant forces to structures (Beltaos, 2008).

Infrastructure should be safe for people, safe for the environment and have a reasonable cost. Accurately estimating ice forces on river piers is important since overestimation causes significant building costs, while underestimation entails a risk of structural failure, which is costly and a risk to users. However, accurate estimation of ice forces is a difficult problem due to the variability of ice properties and hydraulic conditions. This variability gives rise to a plethora of phenomena and failure mechanisms, which complicates the development of a single analytical framework for ice force prediction. Empirical methods are therefore often relied upon for design. Empirical methods however are not better than the data they are based on and little river ice data and even less ice force data are available. Although some work has been done to collate data in systematic databases, most notably by Kellner et al. (2019), it is still the case that most collected ice data, be it fracture, ice action or ice properties data are spread across the literature and in closed databases. Empirical methods therefore may have limited general applicability. Old regional empirical relations must be considered with suspicion as climate change has caused and continues to cause shifts in ice run timing and severity (Agafonova and Vasilenko, 2020; Rokaya et al., 2018). The U.S.S.R.-SN-77/66 Code (used to estimate design ice action on bridge piers) relies on regional climate coefficients that at the time of writing are over 50 years old. While U.S.S.R.-SN-77/66 Code has been phased out in Russia in favour of the more modern SNiP 2.06.04–82 Code, much of the same data still underpin the two. Other empirical relations have implicit regional factors since their coefficients are based on data collected in very few locations. These relations should only be used if it can be shown that the new location in which they are being applied is analogous to the data set that the empirical relationship is based on.

Calculating the ice force exerted by a previous ice run and calculating the most likely ice force exerted by a future ice run are two different problems the latter is more difficult but in general much more useful. Another challenge is to find the design ice action, that is, the force corresponding to a design return period. Where the design return period is the average expected time until the next ice force sufficiently large to induce failure of a structure. This is perhaps the most important problem to solve as the design ice action governs the cost of structures and their probability of failure. Every river has a probability distribution and correlation matrix associated with ice load calculation parameters. Ideally the full probability and correlation matrix with statistical

* Corresponding author.
E-mail address: einar.a.rodtang@ntnu.no (E. Rødtang).

https://doi.org/10.1016/j.coldregions.2023.103809
Received 4 February 2022; Received in revised form 22 December 2022; Accepted 21 February 2023
Available online 27 February 2023

methods would be used to derive the relationship between forces and return periods. In general, however, neither the individual probabilities nor the correlations between them are known. Therefore, relationships employing various degrees of simplification must be used instead. No matter which relationship is used, being clear on what each of the parameters are and what the equation claims to be able to calculate is vital. Similar-looking equations may calculate different statistics, such as upper bounds, lower bounds, best estimates, or design values. They may only apply to specific geometries, ice conditions or locations. They may also have very different parameter definitions. Misunderstanding an equation can therefore result in vastly overpredicting or underpredicting forces.

Most of the research on ice loads has been carried out offshore and in larger modestly sloped rivers. Evaluating the applicability of these results on small steep rivers is therefore important. Small steep rivers is here defined as rivers with gradients in excess of 0.5% and mean winter discharge of $<10\ m^3/s$, representative examples of such rivers include the Sokna river in Norway, the Catamaran brook in Canada or the Montmorency watershed in Canada (Stickler et al., 2010; Turcotte et al., 2013). A lot of work has been done reviewing and comparing codes for predicting ice forces on marine structures (Frederking, 2012; Sandwell Engineering Inc, 1998). Here the ISO19906 is often considered the state of the art (ISO 19906, 2019). However, little work has been done to evaluate the applicability of these standards on the design of river infrastructure. The applicability of these marine equations in steep rivers cannot be assumed for several reasons. First, there is negligible salinity in river ice and, since salinity is known to have a large impact on ice structure and strength, a lot of ice strength data is therefore not applicable to river ice. Furthermore, sea ice and river ice experience different driving forces. Finally, river structures are usually smaller than marine structures, which affects size-effects.

In lakes and low gradient rivers ice covers can generally be approximated as level ice. In steep rivers level ice is a poor approximation due to turbulent surface waters, ice free rapids generating suspended ice particles (frazil) and frazil depositing on the riverbed (anchor ice formation).Ice thickness and strength will vary substantially throughout these rivers (Dubé et al., 2014; Turcotte et al., 2013). There are currently no straightforward and accurate ways of predicting ice thickness and ice strength in these rivers. This is true even though some computational schemes have had some success (Carson et al., 2011; Hopkins and Daly, 2003; Timalsina et al., 2013). While the relationship between ice thickness and strength is not precisely known, anchor ice dams constitute some of the thickest ice in these rivers. However, anchor ice dams are also known to be porous and weaker than thinner level ice sections (John, 2021). Which ice thickness and ice strength combinations would result in the highest ice forces on a structure is not clear. When designing river infrastructure one must step through an entire ice season with reasonable estimates for parameters and then repeat that for any number of seasons in a Monte Carlo procedure, however lack of knowledge of physically possible combinations of ice thickness, ice strength and other parameters reduce the possible accuracy of this approach. During an ice run, floes will break up due to interactions with the banks and riverbed, as well as other floes. The narrower width, higher steepness, and more complex paths of small steep rivers are expected to exacerbate this effect. Thus, even with a complete areal specification of ice thickness and ice strength, it is still not clear what the ice strength and ice thickness combinations of the floes interacting with the structure will be. Large aspect ratio relationships are inapplicable to the generally slender structures that narrow rivers contain. The ice field fetch of small rivers is small; therefore, wind can be assumed to be negligible as a driving force. The steepness on the other hand causes floe momentum to be much more important. Small river size leads to loss of cohesion for ice ridges transported downstream. It is therefore unlikely that Croasdale's methods for estimating forces from ice ridges impacting marine structures is applicable to structures in steep rivers (Croasdale et al., 2018a, 2018b).

Climate change will have diverse effects on ice runs, including changes in ice growth and higher incidence of midwinter mechanical ice runs. River-ice phenomena will therefore continue to be an important consideration even in a warming climate (Beltaos and Prowse, 2009).

The primary aim of this paper is to catalogue the most important simple analytical equations for the prediction of quasi-static ice forces on structures in small steep rivers. Their respective applicability and merits are then discussed and recommendations for their use attempted. Finally, suggestions for further research are outlined.

2. Theory

2.1. River ice growth

It is instructive to highlight the main mechanisms for river ice growth as these relate to the thickness and strength of ice. As water cools below 0 °C frazil needles start to form. These coalesce and freeze together to form slush ice. Under this layer of slush ice, columnar ice will grow downwards. Ice generally grows either from riverbanks as border ice, upstream from a bridging point through accumulation of slush and floes transported by the river. As forces in the streamwise direction increases, shoving and consolidation may play an important part in the evolution of the ice cover. If snow depresses the ice cover or the stage increases, then the snow on top of the ice cover may get soaked. If this soaked snow freezes, this is called snow ice. Suspended frazil particles that impact the riverbed sometimes stays there and forms anchor ice (Turcotte et al., 2011). These ice types have different strength characteristics, and throughout the river there will be significant spatial variation in strength (Prowse and Demuth, 1993). Cold columnar ice is generally considered the strongest ice type, however slush ice and particularly snow ice retain their strength much better throughout the melting process (Beltaos, 2008, p. 87; Prowse and Demuth, 1993). Anchor ice is generally assumed to be weak, although less is known about how ice strength varies when anchor ice coalesces into anchor ice dams.

2.2. Limiting mechanisms and failure modes

When ice floes impact a structure, the forces measured on the structure is limited by one of 3 different limiting mechanisms: limit momentum, limit force and limit stress. If restricted by limit momentum the floe does not have enough kinetic energy for significant fracture to occur and peak force measured on the structure is closely tied to how much kinetic energy the floe has. If restricted by limit force, the floe does not have sufficient external driving forces for the floe to not be arrested and the force measured at the structure is closely correlated with the external driving force. In the limit stress condition, the strength of the ice is closely correlated with the measured force on the structure, while the kinetic energy and external driving force is uncorrelated with the force measured on the structure. Limit stress often results in the highest forces and is therefore usually used for design purposes. When observing a fracture, the event can be classified according to various failure modes, briefly summarized in Table 1. While these failure modes are relatively easy to distinguish it can be difficult to predict a priori which will occur in a given situation. This often makes it difficult to apply the appropriate theoretical model (Ashton, 1986, p. 135). The strategy for predicting which failure modes are relevant is usually some combination of qualitative reasoning and choosing the possible failure mode that results in the lowest forces. Crushing failure results in the highest forces. However, crushing failure is often chosen whenever it is thought possible, since it is the most conservative option.

2.3. General relationships between variables and forces

2.3.1. Key parameters

Ice force is a function of several different parameters such as Ice

Table 1
Failure mode descriptions.

Failure mode	Failure mode description	References
Crushing	A complete disintegration of the ice.	Ashton, 1986, p. 135
Shear	Flaking of the ice along failure planes at angles near 45° upwards or downwards.	Ashton, 1986, p. 135
Buckling	The formation of one or more cracks at some distance from the structure by a combination of bending and compression.	Ashton, 1986, p. 135
Cleavage	Ice sheet cracking horizontally.	Hirayama et al., 1975
Splitting	Ice sheet cracking vertically.	Vazic et al., 2020
Bending	The structure deflects the ice vertically, inducing bending failure.	Keijdener et al., 2018
Mixed	A mixture of failure mechanisms.	

thickness, ice strength, structure width, structure shape, structure angle, aspect ratio, floe width, indentation rate, pier rigidity and water depth. With these parameters the horizontal ice force on a structure can be expressed with the following general equation:

$$F_H = f\left(h, \sigma, b, m, \alpha, \frac{h}{b}, B, x, I, z, \ldots\right) \quad (1)$$

Parameters are fully specified in Appendix A: Nomenclature. The effect of each of these parameters is discussed in the following sections. Note that this list is non-exhaustive, it is always possible to account for more phenomena and parameters can always be factorised into more fundamental parameters.

2.3.2. Ice thickness

There is general agreement that ice force increases with ice thickness all else held equal (Johnston et al., 1999; Schwarz, 1970). In many of the older formulas the force increases linearly with ice thickness with no dependence between ice thickness and ice pressure. The small-scale laboratory experiments of Frederking and Gold support this, but they used a narrow range of ice thicknesses (50 mm – 82 mm), where most samples ($n_{50} = 22$ of $n_{tot} = 37$) had an ice thickness of 50 mm. (Frederking and Gold, 1975). The Arctic Offshore Structures standard (ISO 19906, 2019) suggest that ice force is proportional to $h^{0.86}$. This means that the average ice pressure decreases with increasing ice thickness and this indicates a "size-effect" and seems to apply for wide structures. The Frederking and Gold paper uses the phrase "Examination of the plotted data indicates" rather than use a statistical test to support their conclusions. This approach is by no means unique to Frederking and Gold, a lack of rigorous statistical treatment of the data is ubiquitous in the field and helps explain many contradictory results. The so called "size-effect" is one of the fields fiercest controversies, and a range of papers have been published that discuss this phenomenon (Kim and Schulson, 2015; Palmer et al., 2009; Timco and Sudom, 2013; Zou et al., 1996). In practice, the trend of increasing force with increasing ice thickness is limited by grounding, both by limiting ice thickness and by diverting force chains to the ground. It must be noted that the structure and strength of ice varies widely over cross sections and between samples, i.e., sometimes thin competent ice exerts higher forces than thick rotten ice.

2.3.3. Ice strength

For all the mechanisms discussed in this paper, ice force increases with increasing ice strength. It is however possible for an increase in ice strength to cause a drop in ice force if this increase causes a change in failure mechanism. For example, a drop in temperature increases ice strength, while also making ice more brittle. This may cause the failure mechanism to change from crushing to splitting or to another localized failure mechanism. Crushing generally implies higher forces than localized failure mechanisms, hence a reduction in force is observed.

2.3.4. Pier shape

The shape of the pier has a significant effect on the maximum forces realised. Angling the cutting face of the pier with respect to the horizontal leads to a substantial decrease in the horizontal force component on the pier. However, excessively steep ice aprons (with angles >75–80° relative to the horizontal) do not give the expected effect and therefore should not be used in applications where ice forces are a concern (Korzhavin, 1971, p. 298). A few relationships describe how horizontal and vertical forces experienced by sloping structures vary with the slope angle, notably Korzhavin's, Zylev's and the frictional formulation:

Korzhavin's relation between vertical and horizontal ice forces (Korzhavin, 1971)

$$F_H = F_V tan(\beta) \quad (2)$$

Zylev's relation between vertical and horizontal ice forces (Korzhavin, 1971)

$$F_H = 1.1 F_V tan(\beta) \quad (3)$$

Frictional relation between vertical and horizontal ice forces ice (Ashton, 1986, p. 147)

$$F_H = \left(\frac{sin\beta + \mu_{i,p} cos\beta}{cos\beta - \mu_{i,p} sin\beta}\right) F_V \quad (4)$$

Where F_V is vertical ice force and β is the pier slope angle as seen from the side, measured between the horizontal and the pier slope and $\mu_{i,p}$ is ice – pier coefficient of friction. In the case of disintegration from shearing or bending B.V. Zylev suggests that $F_{V(max)}$ takes a value given by *Eq. 2* (Korzhavin, 1971).

A pier's taper (the angle of a wedge in the horizontal plane) has a substantial effect on maximum forces. For a vertical cutting face, if the angle is reduced from 120° to 60° the following reductions in force can be expected:

- If cutting through a large floe: A 1.33 times reduction.
- If stopping a floe: A 2.00 times reduction.
- If splitting a flow: A 2.10 times reduction.

Blunt cutting faces of piers are therefore not recommended for rivers with severe ice loads (Korzhavin, 1971, p. 298). Kim et al. found that forces increase with increasing curvature, but that the scale-effect exponent in the Sanderson curve (Sanderson, 1988) is independent of curvature (Kim and Schulson, 2014).

2.3.5. Pier width

Frederking and Gold (1975) showed in laboratory experiments that the maximum pressure realised during indentation of columnar grained ice plates decreases with indentor width according to $P \propto b^{-0.4}$ where P is pressure and b is indentor width. Frederking and Gold (1975) arrived at their expression using indentation width in the range 13 mm–150 mm and ice thicknesses in the range 38 mm–98 mm. Korzhavin showed a similar relationship with a different exponent: $P \propto b^{-0.33}$. Korzhavin's experiments used pier widths in the range 70 mm–300 mm. Korzhavin argues that ice thickness did not matter for the experiments due to uniform loading and confinement, they don't state the ice thicknesses used (Korzhavin, 1971, p. 71). Notably, Frederking and Gold (1975) explain this discrepancy as being due to the experiments being conducted at different temperatures with different indentation rates.

2.3.6. Aspect ratio

There is considerable disagreement in the literature about the effect of structure width over ice thickness aspect ratio $\left(\frac{b}{h}\right)$. See section 5.1.3.

2.3.7. Floe width

According to Korzhavin's work, crushing ice force against piers increases with the ratio of floe width to pier width up to a maximum controlled by limit stress (Korzhavin, 1971). In other words, the author holds that the width of the floe only influences ice forces for the limit force or limit momentum condition. Afanasev's formula for crushing forces (*Eq. 9*) does not make reference to floe width. For small rivers the floe width to pier width ratio will frequently be beneath 2.5 and can thus influence the realised force. For small rivers we therefore recommend using Korzhavin's formula in preference to Afanasev's formula if possible. For marine pack ice the current consensus is that the thickness averaged pressure in the pack ice decreases with increasing floe width. The magnitude of the decrease, however, is debated (Charlebois et al., 2018), how this averaged pressure in the pack ice relates the force seen by the structures isn't clear either.

2.3.8. Indentation rate

Using −10 °C laboratory indentation experiments, Frederking and Gold showed that ice pressure increases with indentation rate according to: $P \propto v^{0.35}$ where P is ice pressure and v is indentation rate. Their experiments tested 3 indentation rates in the range:$8.3 \times 10^{-8} - 33.3 \times 10^{-8} \frac{m}{s}$, where most experiments were carried out at $8.3 \times 10^{-8} \frac{m}{s}$ (Frederking and Gold, 1975). Experiments by Qi et al. using −0.1 °C lake ice found that at strain rates lower than 10 s^{-1} splitting was the dominant failure mechanism, while above 10 s^{-1} crushing was the dominant failure mechanism (Qi et al., 2017). However, these results are likely to vary depending on the temperature, structure and orientation of the ice studied.

In Croasdale et al. (1977) the field experiments do not show dependences between ice forces and strain rate over the range 7.5×10^{-5} to 4.4×10^{-3} s^{-1}, whereas the laboratory experiments do show a dependence between strain rate and ice strength in the same range. (Qi et al., 2017) later determined that over strain rates of 10^{-1} to 10^{2} s^{-1}, the uniaxial compressive strength of ice increases by a factor of 10. At higher strain rates, the failure mechanism changes from shear to crushing (Qi et al., 2017). Furthermore, Traetteberg et al. have experimentally shown that apparent modulus (that is, the Young's modulus after a set amount of time has passed) increases with increasing indentation rate (Traetteberg et al., 1975).

2.3.9. Pier deformation

In general, the deformation of the pier need only be considered on piers of slight rigidity. For large piers and floes the deformation of the pier can safely be neglected (Korzhavin, 1971). For less rigid structures, ice induced vibration effects may have to be considered. A detailed account of vibration effects is beyond the scope of this paper; for further information refer to Browne, Nord or Palmer (Browne et al., 2013; Nord et al., 2015; Palmer et al., 2010).

2.3.10. Water depth

Lemström et al., 2020 have shown through finite-element modelling of a two-dimensional sloping structure that – because of rubble pile up – peak ice load should increase with decreasing water depth, and that the force in general should be applied lower on the structure as depth decreases. This is limited by grounding. Grounding chance increases with increasing depth/ice thickness ratio, and this trend is stronger for thicker ice than for thinner ice (Lemström et al., 2020).

3. Methods

A lot of the work conducted on river ice has not been published and peer-reviewed in English. This paper therefore uses both the available peer-reviewed literature as well as conference proceedings, handbooks, reports and codes. Sources were gathered through a scholarly search engines, Mendeley suggestions, library searches and suggestions from fellow researchers. The compiled ice force calculation methods were then classified and compared. Each equation's theoretical soundness and consistency with existent research has furthermore been evaluated. For the systematic search, first the most relevant journals were identified from experience. Then the title of every paper published in those journals were read and their possible relevance to this review was determined. This resulted in a short-list of papers as described in Table 2. These papers abstracts and conclusions were then read and considered. The papers were then read and evaluated in varying depth depending on how relevant and important for the objectives of this paper reading that paper revealed it to be. (See Tables 3 and 4.)

4. Results and discussion

Ice force calculation methods can be broadly classified in the following way:

This paper will primarily classify methods according to failure mechanism. Pier geometry and theoretical basis will be discussed. Limit stress equations will be considered, while thorough consideration of limit force and limit momentum equations are beyond the scope of this review. Modes of application other than solid sheet and ice rubble drift are also beyond the scope of this review. Equations that can only be solved through numerical methods, such as Wang's bending failure equations are also considered beyond the scope of this paper.

4.1. Ice force equations: crushing

All subsequent equations have been rewritten to ensure parameter consistency and form for ease of comparison. See references for the original equations.

4.1.1. Korzhavin's equation for crushing ice failure (Korzhavin, 1971, p. 118)

$$F_H = \frac{Imkbh\sigma_c}{\sqrt[3]{\frac{v_0}{v}}} \tag{5}$$

Where I is an indentation coefficient with a value depending only on the floe to pier width ratio B/b. m is a pier shape coefficient varying between 1 for a flat faced pier to approximately 0.8 for a 60° wedge. k is a contact coefficient determined by flow velocity and indentor width. k decreases with increasing floe velocity and indentor size. v is the floe velocity, $v_0 = 1\, m/s$ is a reference floe velocity, σ_c is the uni-axial compressive strength of ice (at v_0) and here has a common linear relationship with F_H.

Eq. 5 aims to predict the most probable action, that is, the most likely peak force of a given ice pier interaction satisfying the parameters of the equation. *Eq. 5* is a limit stress equation that assumes crushing failure upon a vertical structure and considers the effects of floe-pier width

Table 2
Journals searched.

Key journals	Level of search	Number of papers retrieved
POAC	Read all titles of conference proceedings 1971–2017	133
IAHR	Read all titles of conference proceedings 1970–2020	119
Cold regions science and technology	Read all titles Vol 1–176	76
OTC Arctic technology	Read all titles of conference proceedings 2011–2018	22
CRIPE	Read all titles 1st-20th Workshop	5
Canadian journal of civil engineering	Searched for all articles containing "Ice" Read all these titles Vol 1–48	12
Cold regions engineering	Read all titles Vol 1–35	13

Table 3
Pier ice force calculation methods classification.

Failure mechanism	Theoretical basis	Mode of application	Pier geometry	Limit mechanism
• Shear • Cleavage • Crushing • Buckling • Splitting • Bending	• Empirical methods • Elastic methods • Plastic methods • Momentum methods • Fracture mechanics methods	• Solid sheet drift • Ice rubble drift • Ice sheet stoppage • Thermal expansion • Vertical buoyant force • Icing deadload	• Cylindrical • Triangular • Sloped • Vertical	• Limit stress • Limit force • Limit momentum

Table 4
River ice force codes.

Code authority	Equation	Eq. no	Source
Istryck mot bropelare (Swedish practice)	$F_h = \frac{i_2(L_1+L_2)}{2}$ $F_h = C_A\sigma_c bh$ $F_h = C_A C_W C_S \sigma_c bh$	36 37 38	Vägverket, 1987
Norwegian code/ ISO19906	$F_h = Ch\left(\frac{b}{h}\right)^{-0.16}\left(\frac{h}{h_1}\right)^n$	39	*Håndbok N400 - Bruprosjektering*, 2015, p. 71
Reglur um hönnun brúa (Icelandic practice)	$F_h = \frac{i_2(L_1+L_2)}{2}$ $F_h = C_A C_W C_S \sigma_c bh$ $F = Ch\left(\frac{b}{h}\right)^{-0.16}\left(\frac{h}{h_1}\right)^n$	40 41 42	Hafliðason et al., 2018
SNiP 2.06.04–82 (Russian practice)	$F_h = mk_b k_v bh\sigma_c$	43	Frederking, 2012
CSA-S6:19 Canadian Highway Bridge Design Code	$F_c = \left(\sqrt{5\frac{h}{b}+1}\right)\sigma_c bh$ $F_b = \frac{1}{2}tan(105-\beta)\sigma_c h^2$ $F_{bc} = \left[\frac{\frac{1}{2}tan(105-\beta)+\sqrt{66}}{72}\right]\sigma_c b^2$	44 45 46	Canadian standards association, 2019, pp. 152–156
Finnish Eurocode	$F_h = \sigma bh$	47	*Finnish Eurocode - Bridges*, 2017

ratio, strainrate and pier shape as well as ice thickness, pier width and ice strength. The equation however does not consider the effect of scale, friction, and the aspect ratio (b/h_i).

Korzhavin notably does not provide values for k for indentor widths outside the range of 3-10 m. This makes the equation not directly applicable to most bridge piers in small rivers, as these commonly are smaller than 3 m. Likewise k is only specified for floe velocities in the range 0.5–2.0 m/s. In small steep rivers the floe velocity can be outside this range. For compressive strengths Korzhavin recommends values of 0.5 MPa in the northern Soviet Union and Siberia, and 0.3 MPa for the European sector of the Soviet Union. For other areas one would have to argue correspondence of areas or use local measurements to determine suitable values of compressive ice strength. Korzhavin does however provide guidance on how to determine whether floes contain sufficient kinetic energy for F_H not to be restricted by driving forces (Korzhavin, 1971, p. 126):

$$KE < \frac{0.6F_H b}{tan\left(\frac{\alpha}{2}\right)} \tag{6}$$

$$\Omega < \frac{16mkb^2\sigma_c}{v^2 tan\left(\frac{\alpha}{2}\right)} \tag{7}$$

Here KE is the minimum kinetic energy of a floe required for the peak force not to be restricted by driving forces and Ω is the corresponding floe area. Consider as an example a 3 m wide, wedge shaped pier with wedge angle 60° incident upon an ice floe moving at a velocity of 2 m/s with a compressive strength of 0.5Mpa.

$$\Omega < \frac{16*\left(0.85\sqrt{sin(60)}\right)0.5*3^2*0.5*10^6}{2^2 tan\left(\frac{60}{2}\right)} \approx 12km^2 \tag{8}$$

Even this relatively weak ice floe moving at a relatively high speed requires a size of several square kilometres to guarantee forces that are not being controlled by driving forces. If this holds, then that would imply that that for small rivers peak forces will more often be controlled by limit momentum or limit force than by limit stress. Hence *Eq. 5* will often overestimate forces in small rivers. *Eq. 5* has been validated against small scale laboratory tests (Korzhavin, 1971, p. 121). These tests ($n = 814$) resulted in an average deviation of 7.3%. However, the small scale of the tests (b = 2.5 cm, h = 7.5 cm) leaves the equations treatment of size-effect unvalidated. Furthermore, friction, indentation rate and aspect ratio were fixed. The underlying papers and data developing this equation are unavailable in English so further comment upon this empirical basis is difficult. Croasdale et al. (1977) carried out 5 tests (b = 75 cm, h = 77 cm – 84 cm) on lake ice in the field and compared the results to the theoretical predictions made by *Eq. 5*. Here predicted forces ranged from 0.75 times to 2.5 times the measured value. Korzhavin's equation overestimated forces in 4 out of 5 of these tests, though this seems a slim basis on which to base, say, a 50-year load.

4.1.2. Afanasev's crushing formula (Ashton, 1986, p. 137)

$$\begin{gathered} F_H = mf_{h_b} bh\sigma_c \\ f_{h_b} = \sqrt{\left(5\frac{h}{b}+1\right)}\ for\ 1 < \frac{h}{b} \\ f_{h_b} = \frac{4\left(1-\frac{h}{b}\right)+\sqrt{6}\left(\frac{h}{b}-0.1\right)}{1-0.1}\ for\ 0.1 < \frac{h}{b} < 1\ (interpolation) \\ f_{h_b} = 4\ for\ \frac{h}{b} = 0.1 \end{gathered} \tag{9}$$

Where f_{h_b} is an aspect ratio function that only depends on the aspect ratio b/h. The remaining parameters are defined as for *Eq. 5*. Afanasev's crushing formula aims to predict the most probable ice action. This equation applies to vertical piers of a given shape factor. It assumes a limit stress condition and a crushing mechanism. *Eq. 9* accounts for aspect ratio, shape, width, ice thickness and ice crushing strength. It does not explicitly consider the strain rate, friction, incomplete contact or size-effect. Notably Afanasev's formula is based on model tests using saline ice, not freshwater ice. Saline ice is a composite material with a solid ice matrix containing liquid and gas inclusions. Freshwater ice on the other hand tends to have simpler structure. Freshwater ice is generally stronger than saline ice; it might be possible to approximately capture this difference by varying the ice strength parameter. Parameters not explicitly handled by the expression, however, may also be impacted; changing Young's modulus, density and toughness for instance may modify functional relationships and change fracture mechanism.

4.2. Ice force equations: Shear

4.2.1. Croasdale, Morgenstern, Nuttall flat indentor formulae (Croasdale et al., 1977)

Rough indentor

$$F_H = \left(sec\theta_s cosec\theta_s + \frac{h}{b}\frac{tan\theta_s cosec\theta_s}{4} + \frac{cot\theta_s}{2} \right) bh\sigma_c \tag{10}$$

Smooth indentor

$$F_H = \frac{bh\sigma_c}{cos\theta_s}\left(\frac{h}{4b} + \frac{1}{2sin\theta_s} \right) \tag{11}$$

Where θ_s is the shear plane angle (see Fig. 1). *Eq. 10* and *Eq. 11* are theoretical expressions based on the upper bound theorem of plasticity, and thus provide upper bounds for forces developed during shear failure. The equation assumes a vertical flat indentor incident upon an unconfined large ice field, subject to a Tresca yield criterion. The failure is assumed to be a limit stress shear failure.

The shear plane angle that occurs in practice is the one that satisfies $\frac{\partial(F_H)}{\partial\theta_s} = 0$ as this minimizes energy dissipation. Carrying out this optimization for a range of b/h yields the upper bound curves in Fig. 2.

Eq. 10 does have the advantage of having an explicit dependence on aspect ratio, however it does not account for the size-effect. Also, since it does not explicitly handle how to determine ice strength, it implicitly encapsulates all dependence on strain rate and temperature into the parameter σ_c. This is a recurrent issue with several equations. *Eq. 10* does simplify in useful ways given some assumptions:

$F_H = bh\sigma_c$ *if* $b \gg h$

$F_H = 2.57bh\sigma_c$ *if* $b \ll h$

(Croasdale et al., 1977) compared *Eq. 10* against full scale field tests using a hydraulic ram inserted in a hole cut in columnar lake ice (27 tests with b = 75 cm and h = 18 cm–99 cm). Ice is reported to have failed in limit stress shear failure. Croasdale found that the theory on average predicted 20% higher forces than the field data. Furthermore, *Eq. 10* was conservative in 5 out of 6 field sites. The authors suspect that this disparity and variability may be due to a volumetric size effect on the ice strength parameter that is not taken into account, and further notes that small scale laboratory crush tests give ice strengths that are too high compared to field tests. They do not recommend unqualified use of *Eq. 10* for design purposes. The equation is however ultimately based on field data at a scale comparable to a bridge pier, hence some cautious use of this approach is acceptable.

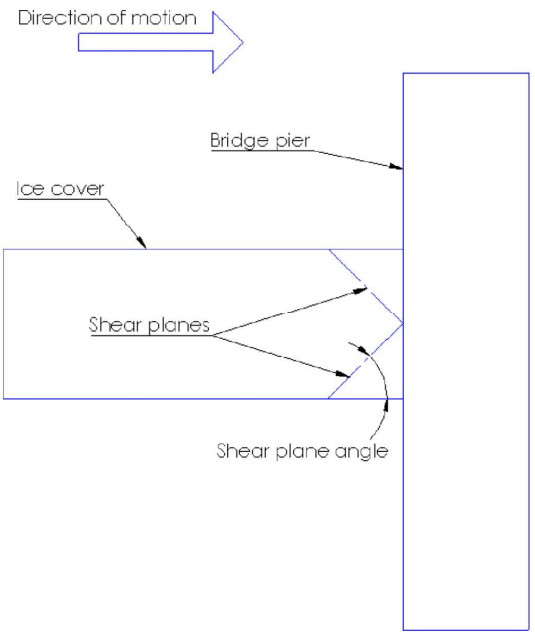

Fig. 1. Shear plane angle, wedges defined by shear plane angle are extruded up and down respectively.

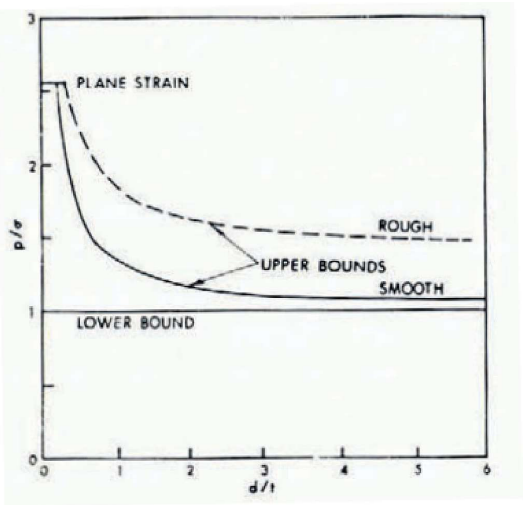

Fig. 2. Croasdale.Morgenstern and Nuttall plane strain upper bounds (Croasdale et al., 1977).
d/t is b/h in this papers nomenclature.
p/σ is $\frac{F_H}{bh\sigma_c}$ in this papers nomenclature.

4.3. Ice force equations: Cleavage

4.3.1. Cleavage power law formulae (Schwarz et al., 1974)

$$F_H = C_p b^{0.5} h^{1.1} \sigma_c \tag{12}$$

Where, C_p is an empirical coefficient. This equation predicts the most probable ice action, assumes limit stress and cleavage failure (That is fracture parallel to the ice cover) and only applies to vertical structures. C_p varies depending on the shape of the structure. Schwarz et al. (1974) provide a good example of how poorly defined the concept of ice strength is in the ice mechanics community, as they, claim that ice strength varies with the inclination and the geometry of the structure with which the ice is incident, thus treating ice strength as more than a material property. Schwarz's power law formula is based on scaled down laboratory experiments. The authors argue size-effects are avoided by controlling the ratio of ice crystal to pier size, notably this implies that in circumstances where the pier size over ice crystal size ratio is substantially below 25 Schwarz's equation may become inapplicable. Schwarz's equation is only valid for aspect ratios satisfying b/h $\leq$ 12 as it was found that above this critical value buckling, rather than cleavage occurred. Buckling was found to be associated with a substantial reduction in forces. Schwarz only carried out experiments with piers up to 60 cm wide. Size-effects other than those precipitated by the ice crystal size ratio may come into effect at larger scales. These include porosity, statistical and confinement driven size-effects. While *Eq. 12* does not provide a factor for the degree of contact, Schwarz et al. (1974)

does point out that in the case of the pile frozen in place forces increase by about 50%. *Eq. 12* does not explicitly consider the effects of strain rate, but Schwarz argue that, by using the maximum ice strength corresponding to the critical strain rate, one obtains the peak force of any ice cleavage event. Notably *Eq. 12* predicts that increasing structure width is accompanied by an increase in forces and a reduction in pressure.

4.3.2. Stress intensity factor formulae (Matsushita et al., 2001)

$$F_H = \frac{K_{IC} \cdot hb}{s\sqrt{\pi l_c}} \tag{13}$$

Where K_{IC} is the stress intensity factor of the ice, S a shape factor, l_c crack length, assumed equal to the grain size of the columnar ice crystals.

Stress intensity factor methods are theoretically distinct from strength-based methods and require different measurements to be made. Kamio et al. has recorded statistical distributions of K_{IC} and l_c for sea ice (Kamio et al., 2003). Various other investigations of the K_{IC} of ice have also been conducted, both for saline and freshwater ice (Liu and Miller, 1979; Shen and Lin, 1988; Urabe et al., 1980). In 2005, Epifanov published a paper with river ice K_{IC} values, but without statistical distributions and small steep river considerations (Epifanov and Yur'ev, 2006).

4.4. Ice force equations: Splitting

4.4.1. Korzhavins equations for splitting of small floes by vertical pier (Korzhavin, 1971)

Splitting on the side:

$$F_H = 2\sigma_s B h \tan\left(\frac{\alpha}{2}\right) \tag{14}$$

Partial splitting:

$$F_H = 2\sigma_s h S \sin(\alpha) \tag{15}$$

Splitting across:

$$F_H = n\sigma_t L h \tag{16}$$

Where σ_s is the ice shear strength, α is the pier wedge angle, that is, the angle of a wedge-shaped pier in plan, S is the crack length, L is the floe length and n is a function of the pier wedge angle. These equations predict the most probable action and assume a splitting failure of small ice floes incident upon a vertical wedge. *Eq. 14* applies when the crack splits the floe in two by propagating sideways compared to the flow direction. *Eq. 15* applies when the floe is only partially split and remains in one piece. *Eq. 16* applies when the floe is split in two, the crack propagating from the pier to the side of the floe opposite to the pier. *Eq. 14* and *Eq. 16* are limit stress equations. The crack length S has a dependence on the initial and final velocity of the floe. *Eq. 15* is therefore a limit momentum equation. The derivation of the equations are further based upon the following assumptions:

- The floe has a known kinetic energy which is primarily expended by splitting the floe.
- Shear stresses play a significant role in the splitting of blunter piers.
- Tensile stresses play a significant role in the splitting of sharper piers.
- Splitting only occurs before the wedge has fully penetrated the floe.
- Force on pier is always less during splitting than when a pier cuts into a large floe.

Theoretically Korzhavin's splitting equations are fundamentally derived by equating kinetic energy to the work required to split the floe, where the work calculation is based on either the tensile strength or the shear strength of the floe as well as rudimentary geometric considerations. (Korzhavin, 1971) does provide a comparison between theoretical and experimental results. However, scale is not specified so how the results generalize is difficult to evaluate. In addition to the equations for the prediction of force Korzhavin also provides equations for predicting whether splitting will take place as well as equations for predicting the splitting angle:

$$KE < 0.6 F_H d \tag{17}$$

$$If\ splitting\ on\ side\ \gamma = 90 - \frac{\alpha}{4} \tag{18}$$

$$If\ partial\ splitting\ \gamma = 90 - \frac{\alpha}{2} \tag{19}$$

$$If\ splitting\ across\ \gamma = \frac{\alpha}{2} \tag{20}$$

Where γ is the angle of the crack to the wedge central axis and d is the wedge length.

4.4.2. The Komarovskiy splitting equation (Korzhavin, 1971, p. 138)

$$F_H = \frac{\sigma_t (L - x) h}{\sin\alpha\cos\alpha} \tag{21}$$

Where σ_t is the tensile strength of ice and x is length of indentation into the ice sheet. Similar to Korzhavin's splitting equations, Komarovskiy's splitting equation is a limit stress splitting equation that predicts the most probable ice force, where x = 0 gives the peak ice force. Korzhavin criticises Komarovskiy's equation for the assumptions of uniform distribution of tensile stress along the section and the inevitability of total splitting of the floe into two parts, and does therefore not recommend this equation for application, and while this equation was in use for the design of bridge-piers in the 1920s it has since fallen out of use (Korzhavin, 1971, p. 138).

4.5. Ice force equations: Bending

Bending failure usually occurs for sloping structures. All the following equations assume sloping structures.

4.5.1. Simple 2D theory (Croasdale, 1980)(Ashton, 1986, p. 146)

$$F_H = b\left[\sigma_f \left(\frac{\rho_w g h^5}{E}\right)^{\frac{1}{4}} C_1 + Z h \rho_i g C_2\right] \tag{22}$$

Where σ_f is the flexural strength of ice, ρ_w is the density of water, g is the gravitational constant, E is the Youngs modulus of ice, C_1 is a function of slope angle and friction coefficient, Z is the height reached by ice on the slope, ρ_i is the density of ice and C_2 is also a function of slope angle and friction coefficient. The equation predicts the most probable action. The derivation of the simple 2D (Two-dimensional) theory assumes a 2D slope of α horizontally impacted by a semi-infinite ice sheet of thickness h, resting on an elastic foundation driven by an unlimited driving force and failing through bending. The ice sheet is assumed to experience local crushing upon impact with the slope and thereafter the ice gets pushed up the slope. The equation is derived using elastic beam theory. The ice sheet sees a horizontal reaction, vertical reaction, gravity and buoyancy force, the slope sees a normal force and a friction force. The horizontal force is subsequently neglected, the steeper the structure the more unrealistic this assumption becomes. The unlimited driving force assumption is reasonable so long as the driving force is sufficient to cause the ice to fail, if the driving force is less than this the driving force controls the force experienced by the structure.

For very wide structures the 2D approximation may be permissible, for narrow structures it breaks down primarily due to two reasons: The ice failure zone is wider than the structure and the ice may be deflected to the side of the structure rather than being forced up along the slope. The deflection issue is more severe for conical structures rather than flat

faced structures. Furthermore, the equation does not consider the effect of rubble accumulation.

The equation has two terms, the first representing the force required to break the ice sheet, the second representing the force required to push the broken ice up the slope. Investigating the terms of the equation we see that the breaking component scales faster than the lifting component ($F_{breaking} \sim h^{\frac{5}{4}}$ *vs* $F_{lifting} \sim h$). Breaking force scales linearly with ice flexural strength as expected. And interestingly the breaking force decreases with increasing Young's modulus $\left(F_{breaking} \sim E^{-\frac{1}{4}}\right)$. Both ice forces increase with friction and slope and become relatively more important at high slope and high friction. Furthermore the equation predicts that the lifting force component will exceed the breaking component, while this may hold true for wide structures, it will not hold true for narrow structures (Ashton, 1986, pp. 146–150).

While interesting from a theoretical point of view this equation is inapplicable to the narrow structures most commonly encountered in small steep rivers. Croasdale 1994 describes an extension of the simple 2D theory taking into account 3D effects and rubble accumulation, this result is further refined in Croasdale 2016 (Croasdale et al., 2016; Croasdale and Cammaert, 1994), which in turn formed the basis of the ISO19906 standard (ISO 19906, 2019).

4.5.2. Nevel equation (Nevel et al., 1977)

$$F_H = \frac{1}{6} b_0 \sigma_f h^2 \left[1.05 + 2.00\left(\frac{a}{l_W}\right) + 0.5\left(\frac{a}{l_W}\right)^3 \right] \tag{23}$$

Where b_0 is a constant defining the width of an ice wedge, a is the distance from the tip of the wedge over which it is loaded and l_W is the characteristic length of an ice wedge. The Nevel equation is a most probable action equation that assumes limit stress and bending failure. The Nevel equation considers the situation of ice incident upon a conical structure. It predicts the force necessary to break a series of wedges formed by radial cracking due to the ice moving against the structure. The derivation of *Eq. 23* is based on elastic plate theory. Notably *Eq. 23* predicts that the ice force scales with ice thickness squared, and indeed so do the other sloping structure equations considered. This predicts a transition from bending failure to a failure mechanism that scales with just thickness at high thicknesses. The equation does not consider the aspect ratio effect, it also does not account for the size-effect. Nevel 1972 does compare the equation to lab experiments of a corner loaded ice square, however it is unknown whether the Nevel equation has been validated against field data. The paper further notes that for most cones 6 wedges form, thus implicitly suggesting a standard value for the wedge defining constant b_0.

4.5.3. Ralston 3D result (Ralston, 1980)

$$F_H = A_4 \left[A_1 \sigma h^2 + A_2 \varrho_W g h D^2 + A_3 \varrho_W g h \left(D^2 - D_T^2\right) \right] \tag{24}$$

$$F_V = B_1 F_H + B_2 \varrho_W g h \left(D^2 - D_T^2\right) \tag{25}$$

Where A_1 and A_2 are coefficients dependent on $\frac{\rho_w g D^2}{\sigma h}$. A_3, A_4, B_1 and B_2 are coefficients dependent on cone angle β and coefficient of friction $\mu_{i,p}$. D_T is cone top diameter and D is waterline diameter. *Eq. 24* and *Eq. 25* are most probable action equations that assumes limit stress and bending failure. They apply to ice incident upon conically shaped structures.

The Ralston equations account for both ride up forces and breaking forces. Notably *Eq. 24* predicts an increase in the relative importance of ride up forces vs breaking forces with increasing structure width. Furthermore *Eq. 24* derivation is insensitive to the exact bending failure criterion used. *Eq. 24* has an interesting dependency on the non-dimensional weight strength ratio $\frac{\rho_w g D^2}{\sigma h}$. The Ralston equation is a comparatively complex equation and the while the parameters A_1, A_2, A_3, A_4, B_1 *and* B_2 are defined in (Ralston, 1977) through plots, analytical expressions are not provided, deducing how the predicted force scales with the various parameter combinations is therefore not immediately obvious. The equation does not directly use the aspect ratio, rather it uses the ratio $\frac{D^2}{h}$.

The derivation of *Eq. 24* is based on plastic limit analysis. The author is not aware of any empirical validation of *Eq. 24*. These equations form the basis of the plastic methods for cones described in ISO19906 (ISO 19906, 2019). It must be pointed out that Ralstons work was intended for offshore structures, not bridge piers therefore extra care must be taken when considering its applicability to bridge piers in rivers.

4.5.4. Edwards and Croasdale - empirical model (Ashton, 1986, p. 155)

$$F_H = 1.6\sigma_f h^2 + 6.0\rho_i g D h^2 \tag{26}$$

The Edwards and Croasdale empirical model is a most probable action formula, and assumes limit stress bending failure. It applies to 45° cones. The model is a two-term model. Edwards and Croasdale suggest that the first term represents the ice breaking component, and the second term represents the ice clearing component of the total ice force. The empirical basis for this equation are scale model tests carried out on 45° angle cones of sizes up to 1 m in diameter with ice up to 7 cm thick. This is quite thin ice; therefore, this model cannot be claimed to account for size-effects. Original paper is unavailable, so spread of data and closeness of fit cannot be evaluated. Furthermore Edwards and Croasdales work was intended to explain the behaviour of offshore structures not bridge piers in rivers, therefore caution should be exercised when using this equation for bridge piers in rivers.(Ashton, 1986, p. 155).

4.5.5. Afanasev's - elastic plate model (Ashton, 1986, p. 155)

$$F_H = \frac{\sigma h^2 S_x \tan(\beta)}{1.93 l_p} \tag{27}$$

Where S_x is the circumferential crack length given by:

$$S_x = 0.88D + \frac{\pi}{4} l_p$$

and l_p is the characteristic ice plate length given by:

$$l_p = \left[\frac{E h^3}{12\rho_w g (1-\nu)^2} \right]^{0.25}$$

ν is the Poisson ratio of ice.

Afanasev's elastic plate model is a limit stress model based on empirical data and elastic plate theory. It predicts the most probable ice action, assumes bending failure and is only strictly applicable to conical structures.

The model is empirically based on lab experiments conducted with cone diameters up to 28 cm and ice thickness's up to 3.5 cm. These are small scale tests and therefore do not verify the extent to which *Eq. 27* accounts for size-effects. Edwards and Croasdale empirical equation notably is based on higher ice thickness data and predicts a somewhat weaker dependence on ice thickness ($F \sim h^2$ *vs* $F \sim const^* h^{\frac{8}{3}} + const^* h^2$). It should be noted that Afanasev's elastic plate model is very similar to the first term in the ISO model, which is too be expected since both are based on based on the theory of a plate on an elastic foundation. The equation does not account for the aspect ratio effect or strain rate effect.

4.5.6. Tryde, 1977 Empirical model for a narrow sloping wedge (Tryde, 1977)

$$F_H = C_F \sigma_c h b \tag{28}$$

$$C_F = \frac{5.2\sqrt{\frac{\sigma_f}{\sigma_c}}}{\sqrt{C}} \tag{29}$$

$$C = 0.16\left(\frac{E}{\varrho v^2 sin\left(\frac{\alpha}{2}\right)}\right)^{\frac{1}{4}} C_\alpha C_\beta^2 C_\gamma^2 \tag{30}$$

$$C_\alpha = 1 - \mu_{i,p}\frac{tan(\beta)}{sin\left(\frac{\alpha}{2}\right)} \tag{31}$$

$$C_\beta = \mu_{i,p} + \frac{tan(\beta)}{sin\left(\frac{\alpha}{2}\right)} \tag{32}$$

$$C_\gamma = 6\left(\frac{h}{b}cos\left(\frac{\alpha}{2}\right) + \frac{C_\alpha}{C_\beta}\right) \tag{33}$$

Where $\mu_{i,p}$ is the ice-pier coefficient of friction and C_F is referred to as the reduction coefficient. β is the inclination of the face of the wedge to the horizontal and α is the included angle at the point of the wedge in the horizontal plane. *Eq. 28* Is a most probable action equation, it assumes limit stress bending failure and applies to sloping wedges. *Eq. 28* does not account for ride-up forces and assumes effective clearing of ice. Furthermore, shear strength is assumed to equal 50% of compressive strength. And while Tryde does account for aspect ratio effects, size-effects are not taken into account. Nor is the effect of strain rate explicitly accounted for. *Eq. 28* is notably a lot more sensitive to Young's modulus than most other bending failure equations.

(Tryde, 1977) does include a comparison of *Eq. 28* to empirical data. However, the range of this empirical data is not specified, no statistical tests are carried out and the only representation of this data are derivative parameters plotted against each other on log-log scales. Therefore, this data is not useful for supporting *Eq. 28*. Furthermore *Eq. 28* is strangely complex for an empirical equation with relatively few basic parameters.

4.5.7. The ISO elastic-brittle sloping structure solution (Croasdale et al., 2016)

$$F_{II} = [H_B + H_P + H_R + H_L + H_T]I_P \tag{34}$$

Where, H_B is the horizontal component of the force to break the ice, H_R is the horizontal component of the force to push the broken ice blocks up the slope, H_P is the force to push the oncoming ice through any ice rubble on top of the ice sheet, H_L is the horizontal component of the force required to lift the ice rubble prior to breaking the ice sheet, H_T is the horizontal component of the force to turn the ice blocks at the top of the slope as they meet the vertical shaft, I_P is the correction for the effect of in plane compression in the ice sheet due to F_H. There is an equation for calculating each of these terms. For the full specification of *Eq. 34* see (Croasdale et al., 2016; ISO 19906, 2019).

Eq. 34 adds up a lot of mechanisms and assume maximum contribution of each of them, and as such is a design formula, it assumes limit stress bending failure, and applies to sloping wedges. The equation is based on elastic-brittle theory. *Eq. 34* is verified against the large full-scale confederation bridge dataset and has achieved an average deviation from that empirical data of 5% and a standard deviation of 23%. The small average deviation does however come with a large caveat: The model has several calibration factors and was calibrated against the same data set that it was tested against. Therefore, it is unclear how well the model will do on other bridges in general and on bridges without large datasets specifically. The model has 21 parameters, this means that without extensive data and guidance, the model can be tuned to give whatever answer is convenient. These parameters can be broadly classified into 5 groups, structural properties, ice-structure properties, level ice properties, ice rubble geometrical properties and ice rubble geometrical properties. That the equation requires the specification of the rubble pile geometry is problematic since these parameters cannot be measured before the bridge in question is built. It is possible that the values observed at Confederation can be used more generally, this however must be investigated further. While 21 is a lot of parameters, some have a relatively small effect on the final force over their range of possible values: Ice density, water density, the gravitational constant, the poisson ratio of ice, ice-ice friction, porosity, friction angle, Young's modulus and rubble height all have small effects on the calculated force. The structure's slope, ice-structure friction, ice thickness, ice rubble cohesion and ice rubble angle of repose all have a big effect on the calculated force. The bending strength and width of the structure has some effect on the calculated force. Note that rubble pile cohesion and angle of repose have both a big effect and cannot be measured at the location before the structure is built.

That being said, the ISO-elastic brittle sloping structure solution is the most theoretically complete closed form analytical equation available for describing these kinds of ice structure interactions. It accounts for a wider range of phenomena than any other equivalent expression available. Further theoretical improvements however are still very much possible. The equation has a discontinuity at the point where 2*waterline diameter = Distance to first circumferential crack. The equation does have some trouble dealing with variable amounts of ice rubble. How to determine friction coefficients under realistic interface conditions is an open question, and it is not clear whether static or dynamic friction is more suitable. Predicting ice strength and ice thickness is still hard. How ride up height is determined by clearing and flexural strength is unclear. The validity of the in-plane compression correction factor is unclear.

4.6. Ice force equations: multiple failure mechanisms

4.6.1. Ashton quick force (Ashton, 1986, p. 160)

$$F = K\sigma_c bh \tag{35}$$

Where K is a function of all other relevant variables. For vertical structures K is uniquely given by the aspect ratio $\frac{h}{b}$:

	Slender vertical			Wide or wedge shaped	
h/b	0.5	1	10	<10	>10
K	3	2.5	1	1	0.8

For sloping structures K is given by Fig. 3. K values below 0.2 should not be used.

The shape of the curve in Fig. 3 is explained as an increasing

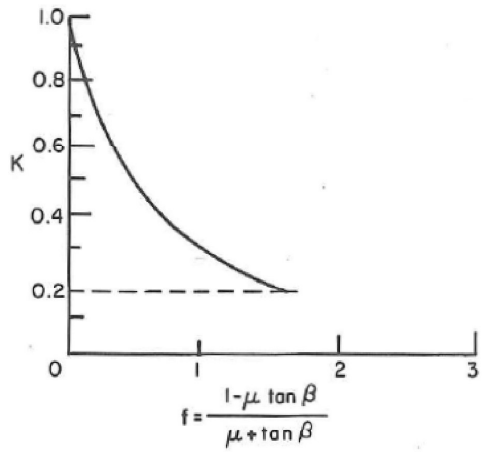

Fig. 3. Force coefficient K. μ is slope friction and β is slope angle.

tendency towards bending failure rather than crushing failure. For sloping wedges Ashton suggest using Tryde's empirical model with $5.2\sqrt[3]{\frac{\sigma_f}{\sigma_c}} = 3.5$ I.e letting $K = C_F = \frac{3.5}{\sqrt{C}}$. For further details on Tryde's empirical model see section 4.5.6. Ashton stresses that this equation should only be used for first pass, order of magnitude estimation. Lower forces are expected for floes with low kinetic energy or small size. For vertical structures the equation assumes limit stress crushing failure.

4.7. Ice force codes

4.7.1. Current practice, ice force codes and standards for quasi-static ice forces on bridges

It is instructive to review the current standards and best practices for determining design quasi-static ice loads on bridge piers.

4.7.2. The Swedish standard

The Swedish standard provides specifications for three cases: Ice rubble drifting against pier with adjacent piers of arbitrary geometry (*Eq. 36*). Ice floes drifting against vertical pier (*Eq. 37*). Ice floes drifting against wedged and sloping pier (*Eq. 38*). Whereof *Eq. 37* is a special case of *Eq. 38*. The ice rubble equation *Eq. 36* effectively only has two parameters. The average distance from the pier under consideration to its adjacent piers $\left(\frac{L_1+L_2}{2}\right)$ and an ice force per unit length of bridge (i_2) varying between 10kN/m to 30kN/m. No further guidance is given on how to choose i_2. Effectively this approach assumes that the rubble ice force scales linearly with bridge span. This assumption must necessarily become increasingly false as the span width increases and rubble density decreases. The wider the span and the sparser the rubble the less likely the central rubble pieces of a span are to transmit any force at all to the piers. However, if this equation is conservative for narrow spans and dense rubble packs it will also be conservative for wider bridge spans and sparser rubble. The standard also suggests using *Eq. 36* for drifting solid ice covers. Solid ice cover ice force can more reasonably be assumed to vary linearly with span.

Eq. 38 is a simple equation providing shape factors and a linear dependence on compressive ice strength, ice width and structure width. The equation therefore does not consider any size-effects. Three values are suggested for the compressive strength, one for regulated rivers, one for more substantial ice runs and one for saltwater ice. C_A is a coefficient depending solely on the $\frac{b}{h}$ aspect ratio. C_W is a coefficient depending solely wedge angle. C_S is a coefficient depending solely on slope angle. The standard provides tabulated values of these coefficients.

4.7.3. The Norwegian and Icelandic bridge codes

The Norwegian and Icelandic bridge codes specify *Eq. 39*, which is effectively the old ISO equation for determining ice forces on offshore structures. The newer ISO equations adds an empirical factor:

$$f_{AR} = e^{\frac{b}{3h}}\sqrt{1+5\frac{h}{b}} \tag{48}$$

The addition of this factor by ISO is supported by observations on relatively narrow lighthouse structures (~2 m). ISO argues that the f_{AR} can be ignored for structures with aspect ratios (D/h) >5. Most bridges, especially ones in smaller rivers, will when meeting a design ice event have aspect ratios much <5. Therefore, the Norwegian and Icelandic standards would likely be improved by the addition of the f_{AR} term. The empirical basis for the ISO equation is data from the Okhotsk sea, Caspian sea, Baltic Sea, Bohai Sea, Beaufort and Cook inlet. C in the ISO equation is a regional ice strength coefficient, empirically determined using data from the mentioned areas. ISO suggests C = 1.8 MPa for temperate areas and this is the value used in the Norwegian and Icelandic practice. ISO does contain guidance suggesting a C value of 1.8, 2.4 or 2.8 depending how arctic an area is. This C value has a return period of 100 years, assuming 24 ice interaction events per year. The Norwegian and Icelandic practice has no further guidance on how to adjust the C value to suit local conditions. The most recent version of the ISO standard at the time of writing however has been updated to include such guidance. Updating the Norwegian and Icelandic practice to reflect this advance would be beneficial.

The Icelandic practice is similar to the Swedish practice for ice floes and ice rubble. For solid ice covers the Icelandic practice uses the offshore ISO approach. Both the Norwegian and the Icelandic practice use the same equation for calculating ice thickness based on freezing degree hours (FDH), with units *hours*Celsius*:

$$h = \frac{\sqrt{FDH}}{175} \tag{49}$$

However, the Norwegian practice suggests using the 10-year return period FDH for temporary constructions and the 100-year return period FDH for permanent constructions. While the Icelandic practice is to take the average of the 100- and 10-year return period FDH for all constructions. It should be noted that the ISO approach, and hence the Norwegian and Icelandic approaches are based on full scale date from many regions around the world and hence these methods should be given more weight than others. With the caveat that methods based on local data may be given precedence if applied where the underlying data was collected from.

4.7.4. Russian practice - SNiP 2.06.04–82

The Russian standard provides a more in-depth treatment of ice force prediction than other Standards. Notably the Russian standard specifies characteristic ice strengths and thicknesses depending on the region of Russia. Furthermore, the Russian standard specifies a method for calculating bulk ice strength depending on the uniaxial compressive strength of ice layers. Furthermore, the standard also makes some considerations based on ice temperature. As such the Russian standard provides a more clearly defined procedure for finding ice strength than most other standards. Care must be taken however in comparing the Russian standard to the other standards because its equations have a built-in safety factor while the other standards calculate a characteristic force.

4.7.5. Canadian standard CSA S6:19

The Canadian standard has two fairly standard relationships for predicting ice force. A crushing force equation scaling with ice thickness and a bending force equation scaling with ice thickness squared. Choice of ice strength is broadly left down to engineering judgement. The novel development in CSA S6:19 is the transition force equation, which provides a smooth transition between crushing mechanism and bending mechanism. This equation is defined by the average of the calculated bending and crushing force at an aspect ratio of 6 (Source: Private communication with Robert Frederking). A key advantage of this standard compared to the others is that it has a clearly defined easy to apply method for varying force depending on likely failure mechanism.

4.7.6. Finnish practice

The Finnish practice is by far the simplest one of those considered. Ice force equals a fixed ice strength * ice thickness * structure width. While it is easy to criticize this procedure, it is nonetheless very simple to apply, and may be a justifiable approach in regions with minor ice force problems.

5. Comparative analysis

5.1. Functional relationship comparisons

5.1.1. Ice thickness

Fig. 4 considers forces realised upon a 3.05 m wide pier of various geometries. Note that "Korzhavin design force" and "Korzhavin crushing" are the same equation, except Korzhavin design force has more

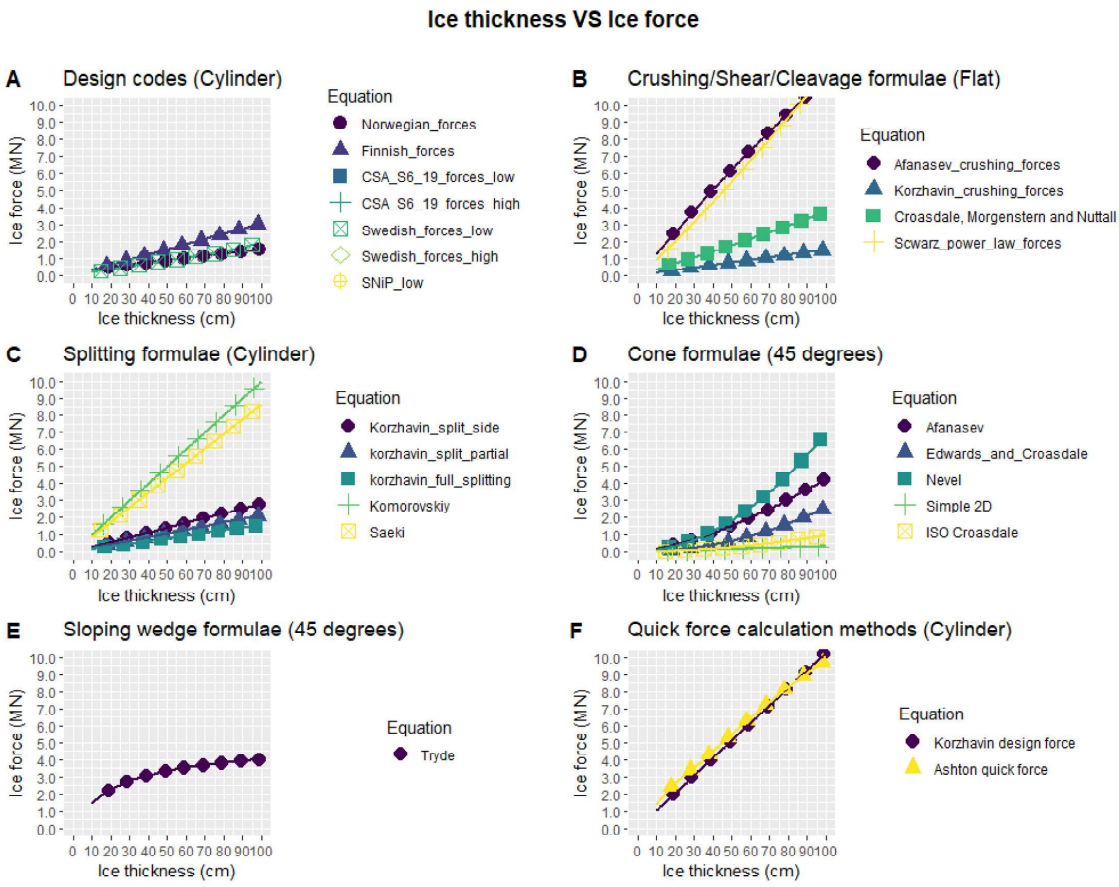

Fig. 4. Ice thickness Vs. ice force functional comparison for a 3.05 m wide pier of various geometries. For full specification of parameters see Appendix B:Parameter specification for Fig. 4 and Fig. 5.

parameters fixed according to Korzhavin's recommendations.

The most notable takeaway from the design codes plot is that there is substantial disagreement between the different codes. The upper bound of what the SNiP standard can predict is so high that it would dwarf the rest of the plot were it included. Furthermore, within standards there is substantial scope for choosing ice strengths. And depending on which ice strength is chosen the resultant force may vary widely. Furthermore, the different standards use various empirical parameters that can vary substantially from location to location. The transferability of standards between locations should therefore be treated with care.

Ice thickness and ice strength are frequently treated as independent. This however is rarely true. Ice usually grows thicker throughout the winter season, however towards the end of the winter season (when the ice is at its thickest) insolation can significantly weaken the ice cover. Bulatov reports that an ice cover can lose significant strength due to solar insolation, before ice thickness reducing significantly (Ashton, 1985). Hence treating ice thickness and ice strength as independent will result in forces being overestimated. The details of the temporal correlation of ice thickness and ice strength will vary depending on location.

There is good agreement among the cone bending failure formulae that ice force scales with h^2 for narrow cones. For wider cones the clearing and ride up forces are significant and these scale with h but these are seldom seen in small rivers. The ice force on conical, or sloping structures depends on two different physical processes, ice breaking and ice accumulation. The ice breaking component can mostly be treated as an elastic plate on an elastic foundation and which scales with $\sim\sigma_f h^{1.25}E^{-0.2}w$. Whereas the pile-up and accumulation component scales with $\sim\rho g h^2 w$, hence the scaling of the force with ice thickness will be in between $h^{1.25}$ and h^2, depending on how much ice accumulates. For vertical structures most equations agree that ice force scales, or scales approximately, with h. The magnitude of predicted forces however can vary by an order of magnitude between different equations, depending on exact choice of parameters.

5.1.2. *Ice strength*

"Ice strength" in the ice mechanics community is an ill-defined concept. Depending on the equation ice strength is defined in a great variety of ways. Bending, uniaxial compression, tensile and shear strength are of course different. However even when two equations refer to say uniaxial compressive strength, it cannot be assumed that these two strengths are comparable variables. One may be referring to the strength obtained when crushing small cubic samples, the other to the strength obtained when crushing large rectangular column samples. Furthermore, the samples may be confined or unconfined. The tests may be carried out at different temperatures, with differing salinities and at different strain rates. All these variables are known to affect strength.

This goes a long way to explain why different standards and equations for the calculation of ice forces all specify such variable ranges of ice strength. Any attempt to compare equations by plotting ice strength vs ice force, must therefore be treated with suspicion. None the less, some useful observations can be made about Fig. 5. (See Fig. 6.)

There is broad agreement for most failure mechanisms that the equation should be on the form:

$$F_H = \sigma f(\ldots) \tag{50}$$

This applies to all crushing, shear, cleavage and splitting equations as well as all current standards, with the notable exception of bending equations. Bending failure equations display various functional dependencies:

Simple 2D theory, Edwards and Croasdale, and the ISO bending equation

$$F_H = \sigma_f f_1(\ldots) + f_2(\ldots) \tag{51}$$

Tryde, 1977 empirical model

$$F_H = \sigma_c \sqrt[3]{\frac{\sigma_f}{\sigma_c}} f(\ldots) \tag{52}$$

One notable difference between the *Eq. 51* and *Eq. 52* family of equations is the presence of the crushing strength of ice. Ranta et al.

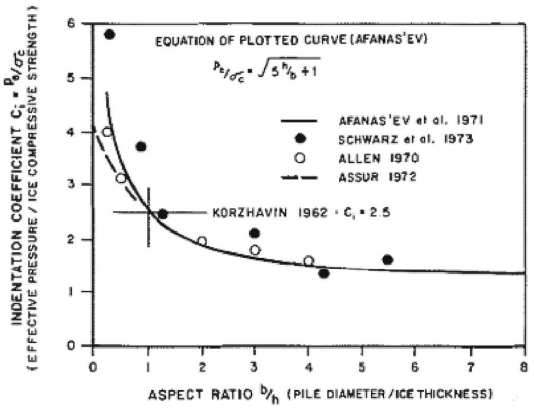

Fig. 6. Indentation coefficient Vs. aspect ratio, vertical piles (Neill, 1976).

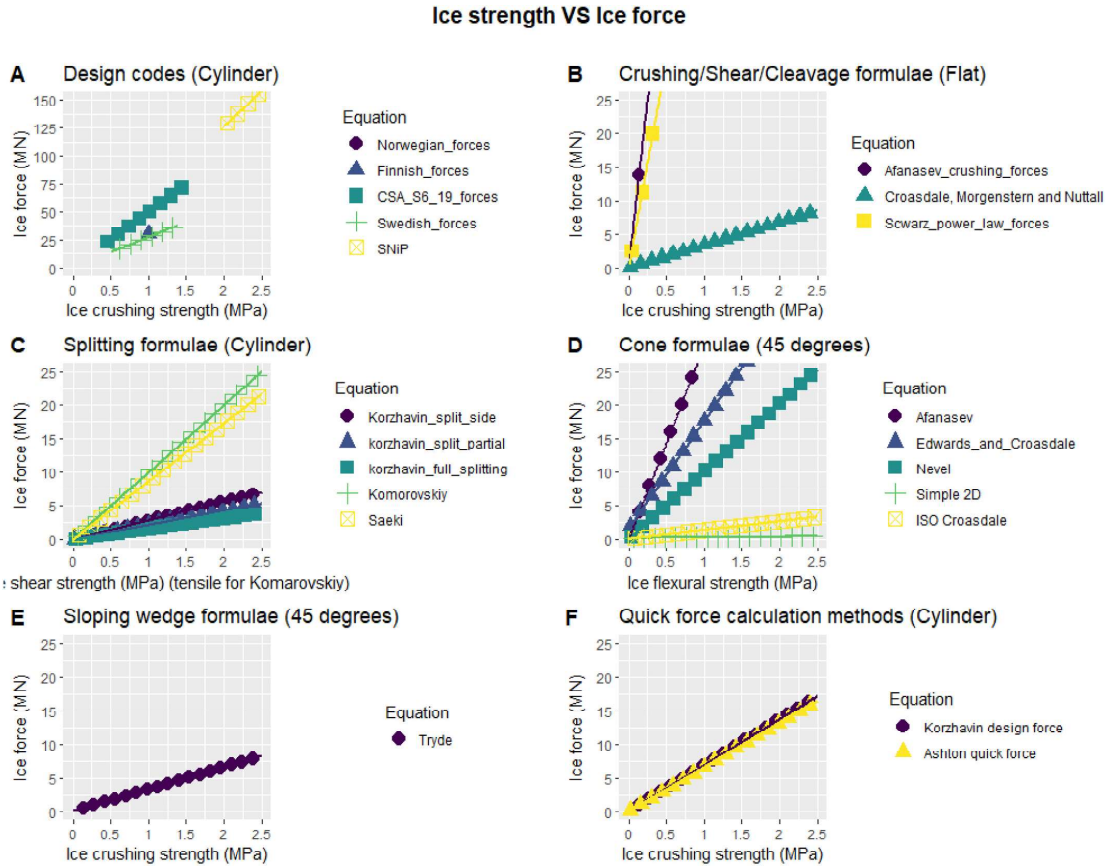

Fig. 5. Ice strength Vs. ice force functional comparison for a 3.05 m wide pier of various geometries. For full specification of parameters see Appendix B:Parameter specification for Fig. 4 and Fig. 5.

found through simulation work that much of the scatter unaccounted for in bending ice calculations stem from neglecting local crushing, suggesting that the inclusion of crushing strength is important even for bending failure (Ranta et al., 2018) While the use of ice strength to predict ice forces seems almost universal, there has been calls to consider the use of the specific energy of mechanical destruction instead (Kim and Tsuprik, 2018). Fig. 5 does show that in practice the Simple 2D and the ISO bending equation vary very little with ice strength, while the Tryde model in practice works out to vary close to linearly with ice strength. As a final note on Fig. 5, Fig. 5A illustrates the range of ice strengths suggested by different standards, this highlights the stark disagreement between the SNiP standards and the other standards.

5.1.3. Aspect ratio

There is considerable disagreement in the literature about the effect of the structure width over ice thickness aspect ratio $\left(\frac{b}{h}\right)$. Afanasev equation for crushing forces suggests $F_H \propto \sqrt{5\frac{h}{b}+1}$ for $\frac{h}{b} > 1$ and $F_H \propto constant$ for $\frac{h}{b} = 0.1$ with linear interpolation in-between. The CSA S6:19 standard uses, for crushing forces, a simplified version of Afanasev where $F_H \propto \sqrt{5\frac{h}{b}+1}$ for all $\frac{h}{b}$. The ISO crushing equation on the other hand uses a different dependence: $F_H \propto \left(\frac{b}{h}\right)^{-0.16}$. Meanwhile the Swedish and Icelandic standards have tabulated values of an aspect ratio coefficient. And finally, Korzhavin's equation (*Eq. 5*) has no dependence between ice force and the ice thickness – structure width aspect ratio. Most bending equations display no dependence between ice force and aspect ratio. This includes Nevel's Equation, Afanasev's elastic plate equation, Edwards and Croasdales's equation, and the Simple 2D equation. Ralston's equation does have a functional dependence on $\frac{b^2}{h}$ however the paper does not provide an analytical expression. Tryde's equation reduces to a proportionality of the form: $F_H \propto \left(\frac{h}{b} constant_1 + constant_2\right)^{-1}$. The ISO Croasdale bending equation displays no direct relationship between ice force and the $\frac{b}{h}$ aspect ratio. The power law equations for shear and cleavage cannot readily be put on the form $F_H \propto f\left(\frac{h}{b}\right) hb$, though they can be put in the form $F_H \propto f\left(\frac{h}{b}\right) f(h) f(b)$. Timco's energy relation, Ashton's quick force equation, the stress intensity formula and all the splitting equations display no relation between ice force and aspect ratio. We can conclude that there is little consensus except for splitting where aspect ratio is acknowledged to have little effect. For crushing the consensus is that increasing aspect ratio either does not affect the force or increases it at a diminishing rate.

6. Conclusions

1. Current ice force calculation methods give forces that differ from each other by an order of magnitude.
2. There is broad agreement that for narrow vertical structures ice force increases linearly with ice thickness and with ice thickness squared for sloping structures.
3. There is broad agreement that ice forces increase linearly with ice strength, except for wider structures where clearing forces can be significant. However, the definition of ice strength varies substantially between authors.

A great deal of data and research has been conducted on river ice in large rivers. Practical and reliable guidelines exist for the construction of infrastructure in large low gradient rivers. Substantially less data has been collected and research conducted on small high gradient rivers, practical and reliable guidelines therefore do not exist for the construction of infrastructure in such rivers.

6.1.1. Recommended ice force equations

Recommended equations depend upon the intended application. However, under no circumstances should an ice force equation be used uncritically and without proper understanding of the equation's limitations. Where the purpose of the calculation is design, the most conservative equation should be used, unless the validity of less conservative equations can be justified.

However, some equations should not be used for small steep rivers at all: The Korzhavin crushing equations is not strictly applicable to small rivers and is therefore not recommended for this purpose. The simple 2D bending equation is not applicable to narrow structures and is therefore not recommended for use in small rivers. The Ralston 3D result lacks empirical basis and is therefore not recommended. Furthermore, analytical expressions for several of its parameters is not available.

Most of the equations considered may be used, but only in specific circumstances. Where bending failure is known to occur, and substantial data exists the ISO elastic-brittle sloping structure solution should be used. Because the ISO elastic-brittle sloping structure solution is recent and developed through the consensus of international experts it should in general be favoured where possible. Where there is a lack of data the large number of parameters that need to be specified the ISO elastic-brittle sloping structure solution must be used with caution. The approach in this case should be to perform sensitivities with ranges of the parameters which may not be known and then the results of this analysis should be weighted up against experience and engineering judgement.

Where minimal resources or ice engineering experience are available simpler approaches can be justified. Both the Afanasev's elastic plate model and Edwards and Croasdales empirical model are applicable to small conical structures. Edwards and Croasdales equation rely upon a wider range of ice thicknesses and should therefore be preferred. However, for thick ice both expressions should be treated with suspicion.

The Russian practice SNiP 2.06.04–84 is underpinned by substantial geographically distributed data and can therefore be safely applied in Russia. However, lack of data and translation means that SNiP cannot easily be applied outside Russia. Furthermore, SNiP may err on the side of being overly conservative.

The CSA S6:19 standard can safely be applied where reliable ice strength data exists. If reliable ice strength data does not exist, the standard is not especially useful since the range of suggested ice strengths is wide.

The ISO crushing equation can be safely applied in region where the C factor has been shown to be acceptable. Although it must be pointed out that the ISO C factors are nominally developed from offshore data and as such their applicability to rivers without modification is debatable for various reasons: Ice runs only happen a few times, if any, in a river per year, as such exposure rates on riverine structures are quite different from exposure rates on offshore structures. ISO specifically highlights that data for narrow structures in thick ice is lacking.

The Finnish standard is very simplistic. This approach can only be used where the ice strength used has been shown to be sufficiently conservative. Primarily useful in regions with relatively modest ice forces.

The Swedish ice rubble equation should only be used for relatively narrow spans, the equation breaks down for wide spans.

The Korzhavin design pressure formula and the Ashton quick force calculation equations in practice give similar results, but Ashton is easier to use. Either are useful for first pass estimation of ice forces.

6.1.2. Roadmap for research required to predict ice forces on bridges in small steep rivers

1. Adoption of standardized methods of ice strength measurement would be a great benefit to the field. This would enable data from different research teams to be reasonably compared. While there has been initiatives to develop testing standards, see for example (Schwarz et al., 1981), take-up remains patchy resulting in difficulties comparing data from different research groups.
2. Further data collection in small steep rivers would enable the creation of parameter distributions and statistical evaluation of expressions.
3. Correlating ice data to hydraulic parameters such as river slope and roughness would greatly improve models based on meteorological data alone.
4. Ice force codes have narrow geographical applicability. Currently the only way of extending the applicability of a code to a new region is the collection of substantial amounts of ice force data. The development of a method for extending and verifying the geographical applicability of ice force codes based on meteorological, climatological and geographical data would be of great benefit. This is especially important because climate change likely will render previous data unrepresentative for future ice runs.
5. At present ice force codes contradict each other and provide poor guidance. Harmonization and improved guidance is necessary.
6. Currently no robust quantitative method exists for predicting which failure mechanism will dominate in each interaction. The best current methods are purely empirical and compare only two failure mechanisms, crushing and bending. Developing such a method would be of great benefit.
7. A great many ice force equations exist, they should be systematically compared to a large, consistent, and applicable set of field data. Equations that provide the worst predictions should be rejected.
8. It is necessary to reach a consensus on the quantitative effect of scale and aspect ratio.
9. Clarification on the difference between crushing failure and shear failure is necessary.
10. Some of these recommendations are large in scope and partially addressed in ISO 19906. Therefore recommending ISO 19906 for use in rivers and addressing gaps in ISO 19906 which relate to ice action on bridges in rivers is likely the least laborious and highest impact way of improving ice force predictions in small steep rivers.

Funding

Norwegian University of Science and Technology (NTNU).

Declaration of Competing Interest

The authors have no conflicts of interest to declare.

Data availability

Data will be made available on request.

Acknowledgements

Hörn Hrafnsdóttir for access to Icelandic standard.

Ekaterina Kim for fruitful discussion and translation of Russian language texts.

The cats Era and Umbriel for moral support.

Amandine Sophie Muller for language advice and proofreading, any errors that remain are my own.

Appendix A. Nomenclature

Table 5
Nomenclature.

Parameter	Parameter definition	Units
F_H	Horizontal ice force	N
θ_s	Shear plane angle to horizontal	Degrees
h	Ice thickness	m
b	Pier width	m
σ_c	Compressive strength of ice	Pa
I	Indentation coefficient	–
m	Shape coefficient	–
k	Contact coefficient	–
x	Strain rate function	–
$f_{\frac{h}{b}}$	Aspect ratio function	–
C_p, α_p, β_p	Empirical power law coefficients	Varies depending on data
K_{IC}	Stress intensity factor	$MPa\sqrt{m}$
s	Shape factor	–
l_c	Crack length	m
B	Floe width	m
σ_s	Shear strength of ice	Pa
α	Pier wedge angle	Degrees
S	Crack length	m
σ_t	Tensile strength of ice	Pa
L	Floe length	m
n	Wedge angle function	–
d	Wedge length	m
v	Floe velocity	$\frac{m}{s}$
Ω	Floe surface area	m^2
P	Nominal pressure F/(bh)	Pa
F_V	Vertical ice force	N
β	Pier slope angle as seen from the side, measured between the horizontaland the pier slope	Degrees
α_2	Site dependent Stefan's law coefficient	

(*continued on next page*)

Table 5 (*continued*)

Parameter	Parameter definition	Units
		$\frac{m}{\sqrt{C\ days}}$
FDD	Accumulated freezing degree days	$C\ Days$
t	Time	s
β_2	Site dependent Stefan's law coefficient	$\frac{m}{s^{\theta}}$ (Varies depending on data)
θ	Site dependent Stefan's law coefficient	–
σ_f	Flexural strength of ice	Pa
ρ_w	Density of water	$\frac{kg}{m^3}$
g	Gravitational constant	$\frac{m}{s^2}$
E	Youngs modulus of ice	Pa
C_1	Function of slope angle and friction coefficient	–
Z	Height reached by ice on the slope	m
ρ_i	Density of ice	$\frac{kg}{m^3}$
C_2	Function of slope angle and friction coefficient	–
a	Distance from the tip of the wedge over which it is loaded	m
l_W	Characteristic length of ice wedge	m
b_0	Ice wedge width defining constant	–
$\mu_{i,\,p}$	Ice – pier coefficient of friction	–
A_1, A_2	Coefficients dependent on $\frac{\rho_w g D^2}{\sigma h}$	–
A_3, A_4, B_1, B_2	Coefficients dependent on cone angle β and coefficient of friction $\mu_{i,\,p}$	–
D_T	Cone top diameter	m
D	Waterline diameter	m
S_x	Circumferential crack length	m
l_p	Ice plate characteristic length	m
ν	Poisson ratio of ice	–
K	Function of all other relevant variables	–
A	Empirical coefficient	$m^{-0.532}\left(kg\frac{m}{s^2}\right)^{0.468}$
KE	Kinetic energy of ice floe	$kg\frac{m^2}{s^2}$
z	Water depth	m

Appendix B. Parameter specification for Fig. 4 and Fig. 5.

Parameter	Value	Unit
Youngs modulus	9,000,000,000	Pa
Pier width	3.05	m
Slope	45	Degrees
Water density	1000	Kg/m^3
Ice density	917	Kg/m^3
Rubble height	3	m
Ice-Ice friction	0.25	–
Ice-structure friction	0.15	–
Poisson ratio	0.33	–
Porosity	0.15	–
Angle of repose	45	Degrees
Friction angle	0	Degrees
Cohesion	5	–
Effective turning width	1	m
Number of wedges	6	–
Location (for codes)	Central Norway	–
Strain rate factor (SNiP)	1	–
Shape factor (SNiP)	0.83	–
C factors (ISO and derivatives)	1,800,000	PA
C_1 (Swedish standard)	1	–
C_3 (Swedish standard)	1	–
Ice thickness (Fig. 5)	1	m
Ice flexural strength (Fig. 4)	690,000	PA
Ice crushing strength (Fig. 4)	1,000,000	PA

Appendix C. Glossary

Table 6
Glossary.

Anchor ice	Ice growing from riverbed
Anchor ice dam	Anchor ice that has grown such that is dams up water upstream.
Aspect ratio	Ratio of ice thickness to structure width
Aufeis	Ice forming through repeated the repeated process of exposed liquid water freezing then being cover with more liquid water
Border ice	Ice adhering too and growing from the riverbank
Buoyant force	Upwards force on submerged objects equal to weight of displaced fluid
Competent ice cover	Ice cover with significant mechanical strength
Correlation matrix	For n random variables, the correlation matrix is a n by n matrix of correlation coefficients describing the correlation between each of the n variables.
Dynamic ice forces	Vibration forces induced in structures due to ice fracture
Elastic methods	Ice force calculation methods assuming fully elastic behaviour until fracture
FDD	Freezing degree days, sum of negative temperatures per day for a given period
Flexural strength	Stress required for ice to fail in bending
Frazil	Small discoid ice crystals formed in supercooled water
Frazil pans	Frazil slush that has frozen together into floating plates
Frazil rafts	Stacked, adhering frazil pans
Frazil slush	Frazil particles that have agglomerated
Frontal progression	Ice cover growing upstream through addition of frazil and frazil pans at the ice front
Hummocky ice cover	Non-flat jumbled ice cover
Hydraulic thickening	Ice cover growing in thickness due to ice upstream of the ice front depositing under the ice cover.
Ice field fetch	Area of ice field over which wind blows
Ice floe	Free floating piece of ice, usually approximately flat
Ice force	Force experienced by a structure due to ice floes pushing against structure
Ice front	Upstream of ice front there is open water, downstream there is bank to bank ice cover
Ice jam	A stationary accumulation of fragmented ice or frazil that restricts flow
Ice rubble drift	Ice floes moving downstream due to current
Ice run	Large amounts of previously stationary ice breaking apart and drifting down a river
Ice sheet stoppage	Ice sheet drift stopping due to impact to structure
Ice strength	Stress required for ice to fail
Indentation coefficient	Coefficient depending on floe to structure width
Level ice	Flat ice field
Limit force	Peak force restricted by the force driving the ice floe
Limit momentum	Peak force restricted by the kinetic energy of ice floe
Limit stress	Peak force restricted by the strength of the ice floe
Mechanical breakup	Global transport of ice down river triggered by a change in discharge or external forces
Momentum methods	Ice force calculation methods based on a momentum balance
Most probable action	Under given circumstances the most likely ice force to be experience by a structure
Plastic methods	Ice force calculation methods using energy required for plastic deformation
Poisson ratio	Negative of the ratio of transverse to axial strain
Polycrystalline	Consisting of multiple crystals
Ride up forces	Force experienced by structure associated with ice accumulating onto the structure, above the water level, due to ice drifting against the structure
Rotten ice cover	Warm ice cover with significant liquid fraction
Shear strength	Stress required for ice to fail in shear
Size-effect	Change in pressure of a floe-structure interaction depending on the physical scale of the interaction
Skim ice	Initial thin and immobile ice cover
Small steep rivers	Rivers sufficiently small for significant anchor ice dam formation
Snow ice	Ice formed from submerged snow
Solid sheet drift	Global motion of an relatively intact ice cover due to external forces such as current of wind
Stefan's law	Law relating ice-cover thickness to temperature history
Supercooling	Lowering temperature below freezing point without freezing taking place due to lack of nucleation site
Thermal breakup	Global transport of ice down the river triggered by ice melting in place
Uniaxial compressive strength	The uniaxial compressive stress required to fail a sample
Upper and lower bound theorem of plasticity	Theorems placing upper and lower bound on force required to fracture a material
Young's modulus	Measure of stiffness, ratio of tensile stress and axial strain

References

Agafonova, S.A., Vasilenko, A.N., 2020. Hazardous ice phenomena in rivers of the Russian arctic zone under current climate conditions and the safety of water use. Geogr. Environ. Sustain. 13, 43–51. https://doi.org/10.24057/2071-9388-2020-12.

Ashton, G.D., 1985. Deterioration of floating ice covers. J. Energy Resour. Technol. Trans. ASME 107, 177–182. https://doi.org/10.1115/1.3231173.

Ashton, G.D., 1986. River Lake Ice Engineering, 1st ed. Water Resources Publications, Chelsea, Michigan, U.S.A.

Beltaos, S., 2008. River Ice Breakup, 1st ed. Water Resources Publications.

Beltaos, S., Prowse, T., 2009. River-ice hydrology in a shrinking cryosphere. Hydrol. Process. 23, 122–144. https://doi.org/10.1002/hyp.7165.

Browne, T., Taylor, R., Jordaan, I., Gürtner, A., 2013. Small-scale ice indentation tests with variable structural compliance. Cold Reg. Sci. Technol. 88, 2–9. https://doi.org/10.1016/j.coldregions.2012.12.006.

Canadian standards association, 2019. CSA S6:19 Canadian Highway Bridge Design Code. CSA group.

Carson, R., Beltaos, S., Groeneveld, J., Healy, D., She, Y., Malenchak, J., Morris, M., Saucet, J.-P., Kolerski, T., Shen, H.T., 2011. Comparative testing of numerical models of river ice jams. Can. J. Civ. Eng. 38, 669–678. https://doi.org/10.1139/l11-036.

Charlebois, L., Frederking, R., Timco, G.W., Watson, D., Richard, M., 2018. Evaluation of pack ice pressure approaches and engineering implications for offshore structure design. Cold Reg. Sci. Technol. 149, 71–82. https://doi.org/10.1016/j.coldregions.2018.01.020.

Croasdale, K.R., 1980. Ice Forces on Fixed, Rigid Structures, CRREL Special Report 80–26 Working Group on Ice Forces on Structures. Hanover, New Hampshire.

Croasdale, K.R., Cammaert, A.B., 1994. An improved method for the calculation of ice loads on sloping structures in first-year ice. Hydrotech. Constr. 28, 174–179. https://doi.org/10.1007/BF01545935.

Croasdale, K.R., Morgenstern, N.R., Nuttall, J.B., 1977. Indentation tests to investigate ice pressures on vertical piers. J. Glaciol. 19, 301–312. https://doi.org/10.1017/S0022143000029361.
Croasdale, K., Brown, T., Wong, C., Shrestha, N., Li, G., Spring, W., Fuglem, M., Thijssen, J., 2016. Improved equations for the actions of thick level ice on sloping platforms. In: Artic Technology Conference. OTC, pp. 1–15. https://doi.org/10.4043/27385-MS.
Croasdale, K., Brown, T., Li, G., Spring, W., Fuglem, M., Thijssen, J., 2018a. The action of short multi-year ridges on upward sloping conical structures. Cold Reg. Sci. Technol. 154, 142–154. https://doi.org/10.1016/j.coldregions.2018.06.013.
Croasdale, K., Brown, T., Li, G., Spring, W., Fuglem, M., Thijssen, J., 2018b. The action of long multi-year ridges on upward sloping conical structures. Cold Reg. Sci. Technol. 154, 166–180. https://doi.org/10.1016/j.coldregions.2018.04.002.
Dubé, M., Turcotte, B., Morse, B., 2014. Inner structure of anchor ice and ice dams in steep channels. Cold Reg. Sci. Technol. 106–107, 194–206. https://doi.org/10.1016/j.coldregions.2014.06.013.
Epifanov, V.P., Yur'ev, R.V., 2006. Fracture viscosity of fresh ice. Dokl. Phys. 51, 28–32. https://doi.org/10.1134/S1028335806010071.
Finnish Eurocode - Bridges, 2017. Eurokoodin soveltamisohje Siltojen Kuormat ja suunnitteluperusteet - NCCI 1. Liikenneviraston, Helsinki.
Frederking, R., 2012. Review of Standards for Ice Forces on Port Structures. In: Cold Regions Engineering 2012. American Society of Civil Engineers, Reston, VA, pp. 725–734. https://doi.org/10.1061/9780784412473.072.
Frederking, R., Gold, L.W., 1975. Experimental study of edge loading of ice plates. In: IAHR Proc. 3rd Int. Symp. Ice Probl, Hanover, New Hampsh, pp. 479–486. https://doi.org/10.1139/t75-053.
Hafliðason, E., Guðmundsson, G.V., Ólafsson, H.S., Sigurðsson, G., 2018. Reglur um hönnun brúa. Vegagerðin.
Håndbok N400 - Bruprosjektering, 2015th ed, 2015. Vegdirektoratet.
Hirayama, K., Schwarz, J., Wu, H.C., 1975. Ice forces on vertical piles. In: IAHR Symp. Ice, pp. 429–445.
Hopkins, M., Daly, S.F., 2003. Recent Advances in Discrete Element Modeling of River Ice. CGU HS Comm. River Ice Process. Environ. - 12th Work. Hydraul. Ice Cover. Rivers.
ISO 19906, 2019. ISO/FDIS 19906:2019(E).
John, J., 2021. Janik John Master Thesis. NTNU.
Johnston, M.E., Timco, G.W., Frederking, R.M.W., 1999. Overview of ice load measurements on bridge piers. In: Proc. 10th Work. Comm. River Ice Process. Environ. (CRIPE), Winnipeg, pp. 290–302.
Kamio, Z., Matsushita, H., Strnadel, B., 2003. Statistical analysis of ice fracture characteristics. Eng. Fract. Mech. 70, 2075–2088. https://doi.org/10.1016/S0013-7944(02)00255-2.
Keijdener, C., Hendrikse, H., Metrikine, A., 2018. The effect of hydrodynamics on the bending failure of level ice. Cold Reg. Sci. Technol. 153, 106–119. https://doi.org/10.1016/j.coldregions.2018.04.019.
Kellner, L., Stender, M., von Bock und Polach, R.U.F., Herrnring, H., Ehlers, S., Hoffmann, N., Høyland, K.V., 2019. Establishing a common database of ice experiments and using machine learning to understand and predict ice behavior. Cold Reg. Sci. Technol. 162, 56–73. https://doi.org/10.1016/j.coldregions.2019.02.007.
Kim, E., Schulson, E.M., 2014. Some secrets of the ice pressure-area curve for the indentation of ice. In: IAHR Int. Symp. Ice. https://doi.org/10.3850/978-981-09-0750-1_1152.
Kim, E., Schulson, E.M., 2015. A phenomenological explanation of the pressure–area relationship for the indentation of ice: two size effects in spherical indentation experiments. Cold Reg. Sci. Technol. 115, 48–55. https://doi.org/10.1016/j.coldregions.2015.03.008.
Kim, E., Tsuprik, V., 2018. Concept of the specific energy of the mechanical destruction of ice versus the 24th IAHR international symposium on ice concept of the specific energy of the mechanical destruction of ice versus the ice pressure-area relationship : review and discussion. In: IAHR Int. Symp. Ice.
Korzhavin, 1971. Action of Ice on Engineering Structures, 2002nd ed. Books for Business.
Lemström, I., Polojärvi, A., Tuhkuri, J., 2020. Numerical experiments on ice-structure interaction in shallow water. Cold Reg. Sci. Technol. 176, 103088 https://doi.org/10.1016/j.coldregions.2020.103088.
Liu, H.W., Miller, K.J., 1979. Fracture Toughness of Fresh-Water Ice. J. Glaciol. 22, 135–143. https://doi.org/10.3189/S0022143000014118.
Matsushita, H., Kamio, Z., Ushikoshi, J., Takeuchi, T., Akagawa, S., Nakazawa, N., Saeki, H., 2001. Failure mode of a sea ice sheet - cleavage cracking. In: Proc. Elev. Int. Offshore Polar Eng. Conf.
Neill, C.R., 1976. Erratum: dynamic ice forces on piers and piles. An assessment of design guidelines in the light of recent research. Can. J. Civ. Eng. 3, 478. https://doi.org/10.1139/l76-053.
Nevel, D., Perham, R., Hogue, G., 1977. Ice forces on vertical piles. In: CRREL Rep., 77–10.
Nord, T.S., Lourens, E.-M., Øiseth, O., Metrikine, A., 2015. Model-based force and state estimation in experimental ice-induced vibrations by means of Kalman filtering. Cold Reg. Sci. Technol. 111, 13–26. https://doi.org/10.1016/j.coldregions.2014.12.003.
Palmer, A.C., Dempsey, J.P., Masterson, D.M., 2009. A revised ice pressure-area curve and a fracture mechanics explanation. Cold Reg. Sci. Technol. 56, 73–76. https://doi.org/10.1016/j.coldregions.2008.11.009.
Palmer, A., Qianjin, Y., Fengwei, G., 2010. Ice-induced vibrations and scaling. Cold Reg. Sci. Technol. 60, 189–192. https://doi.org/10.1016/j.coldregions.2009.11.005.
Prowse, T.D., Demuth, M.N., 1993. Strength variability of major river-ice types. Nord. Hydrol. 24, 169–182. https://doi.org/10.2166/nh.1993.0020.
Qi, C., Lian, J., Ouyang, Q., Zhao, X., 2017. Dynamic compressive strength and failure of natural lake ice under moderate strain rates at near melting point temperature. Lat. Am. J. Solids Struct. 14, 1669–1694. https://doi.org/10.1590/1679-78253907.
Ralston, T.D., 1977. Ice force design considerations for conical offshore structures. In: Proc. 4th Int. Conf. Port Ocean Eng. Under Arct. Cond. (POAC 77), pp. 741–752.
Ralston, T.D., 1980. Plastic limit analysis of sheet ice loads on conical structures. In: Physics and Mechanics of Ice. Springer, Berlin Heidelberg, Berlin, Heidelberg, pp. 289–308. https://doi.org/10.1007/978-3-642-81434-1_21.
Ranta, J., Polojärvi, A., Tuhkuri, J., 2018. Limit mechanisms for ice loads on inclined structures: buckling. Cold Reg. Sci. Technol. 147, 34–44. https://doi.org/10.1016/j.coldregions.2017.12.009.
Rokaya, P., Budhathoki, S., Lindenschmidt, K.E., 2018. Trends in the timing and magnitude of ice-jam floods in Canada. Sci. Rep. 8, 1–9. https://doi.org/10.1038/s41598-018-24057-z.
Sanderson, T.J.O., 1988. Ice Mechanics: Risks to Offshore Structures. Graham & Trotman, London.
Sandwell Engineering Inc, 1998. Comparison of International Codes for Ice Loads on Offshore Structures - PERD/CHC Report 11-20. Vancouver, Canada. https://doi.org/10.4224/12328412.
Schwarz, J., 1970. The pressure of floating ice-fields on piles. Coast. Eng. 484–486.
Schwarz, J., Hirayama, K., Wu, H.C., 1974. Effect of ice thickness on ice forces. In: Offshore Technology Conference. OTC, Dallas, Texas, p. 11. https://doi.org/10.4043/2048-MS.
Schwarz, J., Frederking, R., Gavrillo, V., Petrov, I.G., Hirayama, K.-I., Mellor, M., Tryde, P., Vaudrey, K.D., 1981. Standardized testing methods for measuring mechanical properties of ice. Cold Reg. Sci. Technol. 4, 245–253. https://doi.org/10.1016/0165-232X(81)90007-0.
Shen, W., Lin, S.-Z., 1988. Fracture toughness of Bohai Bay Sea Ice. J. Offshore Mech. Arct. Eng. 110, 409–413. https://doi.org/10.1115/1.3257080.
Stickler, M., Alfredsen, K.T., Linnansaari, T., Fjeldstad, H.-P., 2010. The influence of dynamic ice formation on hydraulic heterogeneity in steep streams. River Res. Appl. 26, 1187–1197. https://doi.org/10.1002/rra.1331.
Timalsina, N.P., Charmasson, J., Alfredsen, K.T., 2013. Simulation of the ice regime in a Norwegian regulated river. Cold Reg. Sci. Technol. 94, 61–73. https://doi.org/10.1016/j.coldregions.2013.06.010.
Timco, G.W., Sudom, D., 2013. Revisiting the Sanderson pressure–area curve: defining parameters that influence ice pressure. Cold Reg. Sci. Technol. 95, 53–66. https://doi.org/10.1016/j.coldregions.2013.08.005.
Traetteberg, A., Gold, L.W., Frederking, R., 1975. The Strain Rate and Temperature Dependence of Young ' S modulus of Ice. IAHR.
Tryde, P., 1977. Ice forces. J. Glaciol. 19, 257–264.
Turcotte, B., Morse, B., Anctil, F., 2011. Steep channels freezeup processes. CRIPE 85–101.
Turcotte, B., Morse, B., Dubé, M., Anctil, F., 2013. Quantifying steep channel freezeup processes. Cold Reg. Sci. Technol. 94, 21–36. https://doi.org/10.1016/j.coldregions.2013.06.003.
Urabe, N., Iwasaki, T., Yoshitake, A., 1980. Fracture toughness of sea ice. Cold Reg. Sci. Technol. 3, 29–37. https://doi.org/10.1016/0165-232X(80)90004-X.
Vägverket, 1987. Istryck mot bropelare. Serviceavdelining Väg- och Brokonstruktion.
Vazic, B., Oterkus, E., Oterkus, S., 2020. In-plane and out-of plane failure of an ice sheet using peridynamics. J. Mech. 36, 265–271. https://doi.org/10.1017/jmech.2019.65.
Zou, B., Xiao, J., Jordaan, I.J., 1996. Ice fracture and spalling in ice-structure interaction. Cold Reg. Sci. Technol. 24, 213–220. https://doi.org/10.1016/0165-232X(95)00009-Z.

Paper II

Cold Regions Science and Technology 215 (2023) 103982

Contents lists available at ScienceDirect

Cold Regions Science and Technology

journal homepage: www.elsevier.com/locate/coldregions

Full length articles

In-situ ice strength distribution of anchor ice dams

Einar Rødtang *, Janik John, Knut Alfredsen, Knut Høyland

Department of Civil and Environmental Engineering, Norwegian University of Science and Technology, 7491 Trondheim, Norway.

ARTICLE INFO

Keywords:
Anchor ice dams
Borehole-jack
River ice
Ice strength
Steep rivers

ABSTRACT

Ice runs and ice jams can cause significant damage to infrastructure and other human interests. Accurate modelling and prediction of these events rely on data and assumptions about river ice properties. This paper seeks to address the lack of data on ice strength distributions and associated properties in small, steep rivers and to obtain a better understanding of those. To this end, an ice data collection campaign was carried out in the Sokna river in central Norway during the 2020–2021 winter field season. The following types of data were collected for anchor ice dams and level ice sections: Borehole Jack (BHJ) in-situ ice strength, ice thickness, ice density, thin section imagery and associated depth measurements. A total of 27 ice cores and 68 thin sections were successfully collected and processed. Furthermore, a survey was carried out recording GPS coordinates of anchor ice dams in the river. Meteorological and hydrological data was also collated, and large boulder location data was obtained through the analysis of aerial photography. Ice strength distributions and trends on how ice strength varies in small, steep rivers were obtained from these data. A binomial generalized linear model for predicting ice dam locations was developed using field measurements and aerial photography data. This model describes how river width, slope and to a lesser degree large boulder density affect ice dam location. Sinuosity was shown to have no effect on ice dam location. This work highlights the significant variation in microstructure and large-scale structure of ice in small, steep rivers.

1. Introduction

Steep rivers form complex heterogenous ice covers during winter in cold sub-arctic environments (Stickler et al., 2010; Turcotte and Morse, 2011). Ice generation in these rivers cause a variety of problems, including adverse effect on hydropower systems (Gebre et al., 2013), ice induced flooding (Turcotte et al., 2017), ecological issues (Huusko et al., 2007; Prowse and Culp, 2003) and damage to bridges, ripraps and other infrastructure (Doyle, 1988). Notably climate change will cause shifts in river ice regimes. Therefore, some areas will experience problems due to river ice, while other areas including some unaccustomed to handling river ice problems, will experience more issues arise (Prowse et al., 2011). In addition to the ice effects in the small rivers themselves, the ice regime of small rivers affects the ice regime of the larger rivers into which they flow. While a large proportion of rivers are relatively small and steep, most of the research has focused on ice problems in modestly sloped large rivers. Nevertheless, progress is being made describing ice properties and processes in small, steep rivers (Dubé et al., 2014; Heggen and Alfredsen, 2013; Timalsina et al., 2013; Turcotte et al., 2013, 2011).

Together with ice thickness, ice strength is the primary variable for predicting quasi-static ice forces on structures (Frederking, 2012). Yet, while some work has been done on the qualitative nature of small, steep rivers e.g. (Nafziger et al., 2017; Stickler et al., 2010), very little research has been done on the strength of their ice cover, with the exception of Prowse and Demuth (1993). Even Prowse and Demuth's study, having been conducted on a relatively large river, only considers the properties of black (large columnar grains with a transparent to translucent appearance) and white (small diameter grains comprised of snow-ice and/or frazil ice) ice, but no anchor ice strength data. This is an issue since a poor understanding of ice strength and thickness variability may lead to over – or under – dimensioning bridges and other infrastructure, which is accompanied respectively by excessive cost or a risk of collapse. This lack of data is partially mitigated by the majority of ice mechanics research which has been conducted on marine ice e.g. (Dempsey, 2000). However, when calculating ice forces in steep rivers, results from marine studies are usually applied with minimal consideration for their relevance. Furthermore, when predicting ice forces against structures, it is usually ideal to use ice thickness and ice strength probability

* Corresponding author.
E-mail addresses: einar.a.rodtang@ntnu.no (E. Rødtang), janik.john@tuhh.de (J. John), knut.alfredsen@ntnu.no (K. Alfredsen), knut.hoyland@ntnu.no (K. Høyland).

https://doi.org/10.1016/j.coldregions.2023.103982
Received 1 September 2022; Received in revised form 3 August 2023; Accepted 9 August 2023
Available online 21 August 2023
0165-232X/

distributions together with deterministic formulae to obtain return periods for different ice forces, and then design structures accordingly. While such data exist for marine structures (Ungerman et al., 2017), to the authors' knowledge, no such distributions exist for small, steep rivers. This means that ice force predictions in small rivers are based on a few measurements of ice thickness and ice strength at best, with little understanding of the variability in these parameters. Ice conditions in small and steep rivers are qualitatively different to those in large rivers with a modest slopes. Small, steep rivers more consistently transport frazil particles close to the riverbed and consequently see a significant proportion of the rivers ice being anchor ice (Dubé et al., 2014)(Rødtang et al., 2021). This anchor ice then coalesces into step-pool structures and anchor ice dams (Stickler et al., 2010). Also, as a consequence of the relative importance of groundwater flows, vegetation shading and radiation absorbed by the riverbed being increased, small rivers experience a different thermal regime compared to large rivers (Turcotte et al., 2013).

At present, the relationship between the anchor ice regime of a river before an ice run and forces on structures in the river during an ice run is not well understood. There are two primary mechanisms through which anchor ice dams can affect forces on structures during an ice run: the anchor ice itself can raft down the river and impact the structure, or the anchor ice dams can affect forces indirectly by influencing the formation of level-ice sections immediately upstream. Level-ice sections form through border ice growth from banks and anchor ice dams. They are comparatively flat and have a primarily columnar microstructure.

These level-ice sections can break and form an ice run that raft down the river and impacts structures (Fig. 1). The relative importance of the forces involved is not known, and strength data on the specific type of river ice environment is needed to determine this. Anchor ice dams can exert forces on structures through other mechanisms, such as by forming on or against structures, potentially followed by uplifting forces. However, these mechanisms are beyond the scope of this paper.

This paper aims to address the deficit in the literature of ice strength measurements in small, steep rivers and to obtain an estimate of ice strength distributions in these rivers based on ice type and location within anchor ice dams. This paper also aims to create a model for the prediction of anchor ice dam locations, in order to improve the understanding of the global variation of ice properties throughout small, steep rivers. Ultimately the goal is to connect the properties of ice in steep rivers with their impact on infrastructure..

2. Study site, climate and hydrology

Sokna is a small, steep river situated approximately 40 km south of the city of Trondheim in central Norway (Fig. 2). In Støren, where it feeds into the Gaula river, Sokna has a catchment of 539 km^2. The river has an average slope of 1.7% and a mean winter flow of 2.5 m^3/s. Ice processes dominate its hydraulics during winter. Anchor ice formation causes significant backwater effects, increasing the wetted area (Fig. 3), water depths and reduces water velocities independently of discharge. Anchor ice build-up enables static surface ice formation due to the reduced velocity in the backwater of each anchor ice dam (Stickler et al., 2010). During winter, the river as a whole tends to primarily display a step-pool structure (Turcotte and Morse, 2013). Increased spring discharge and partial melting and weakening of ice cover usually cause a spring ice run and associated ice jamming to occur, but mid-winter ice runs are also known to occasionally occur.

The river was studied during the 2020–2021 winter field season. Fig. 4 shows the key meteorological variables, spanning from the first freezing day (20th of October) until the day snow was last observed in the catchment (30th of May). Air temperature, precipitation and snowfall were obtained from the Soknedal gauge (SN67280), operated by the Norwegian Meteorological Institute. Discharge data for Sokna was obtained from the Hugdal Bru gauge (122.17.0) in Sokna, which is operated by the Norwegian Waterways Authority (NVE). These data was corrected for ice by the NVE. For further details on these corrections see Alfredsen (2017). Most of the ice dams formed during a cold spell that lasted from the 30th of December to the 20th of January. Taken together the snowfall data and the other meteorological variables suggest snow-assisted anchor ice formation, which is not the case every winter. Around the 20th of February, accumulated freezing degree days levelled out and there was only negligible ice growth after that point. The precipitation spike and increase in discharge on the 23rd of March were associated with an ice run. The data collection was conducted in January and February when the ice conditions were at their most stable, with low winter discharge and temperatures the free-spanning state of the ice cover stayed stable and without thickening during this period.

Fig. 1. Shear wall and stranded ice floes surrounding the piers of Sokna bridge after an ice run at the end of the 2019–2020 winter season.

3. Methods

The aim of the study was to collect data such that the variability of river ice properties in small, steep river relevant to ice force prediction could be better understood. The most important parameters for ice force prediction are ice strength and ice thickness (Rødtang et al., 2023). Therefore, the distribution of in-situ borehole-jack (BHJ) ice strength – I.e., the ice crushing force measured by a BHJ inserted in a borehole in the ice cover – at different locations across and along the river was collected with corresponding thickness measurements. To understand variation in ice type and how this connects to ice strength, ice cores were collected for thin section and density analysis. Collecting ice strength and ice thickness information throughout the entire river was not economically feasible, therefore anchor ice dam GPS locations were recorded to enable extrapolation of results throughout the river. Coupled with remote sensing data this GPS data enabled the calibration of a model for predicting anchor ice dam locations.

3.1. Ice cores

3.1.1. Ice core collection

Three anchor ice dams and two level-ice cross sections were chosen for closer investigation. For each an ice core was extracted every 1 to 2 m depending on practicality. The ice cores were extracted using a Kovacs ice core extraction system and each core had a diameter of 75 mm. Cores were photographed in the field, stored in plastic containers and transported to −20C° freezers for storage. As shown in Fig. 5 it was frequently necessary to remove snow off anchor ice dams for access and to assess safety. Fig. 6 shows ice core extraction in process. A total of 27 ice cores were succesfully collected, constituting a large amount of manual labour frequently undertaken at temperatures in the field of close to −25C°. Cold weather often affected coring efforts for various reasons, including

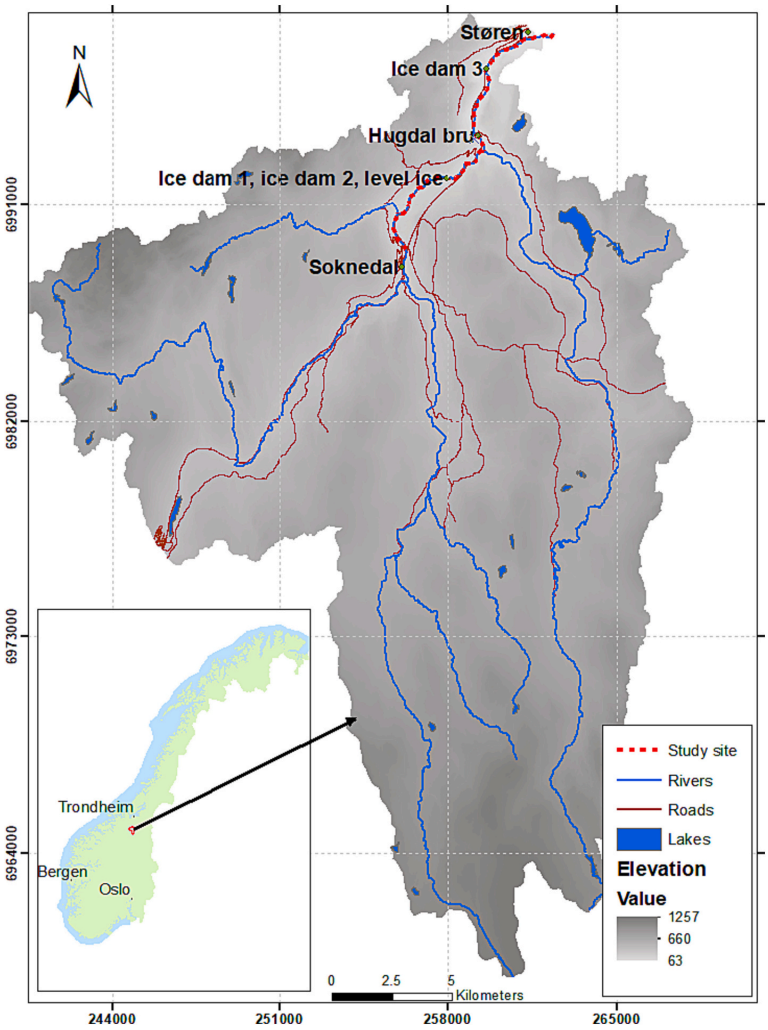

Fig. 2. Sokna catchment including study site locations.

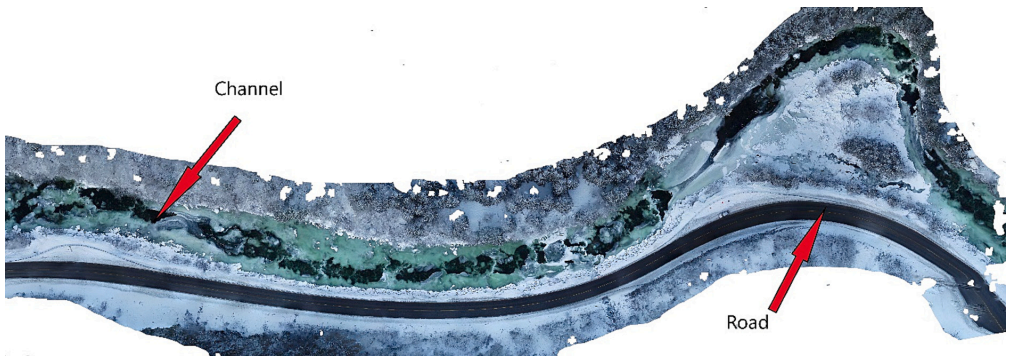

Fig. 3. Orthomosaic of the formation of anchor ice dam 1, anchor ice dam 2 and level ice section taken 2021/01/05. For method of generation of orthomosaic see (Rødtang et al., 2021).

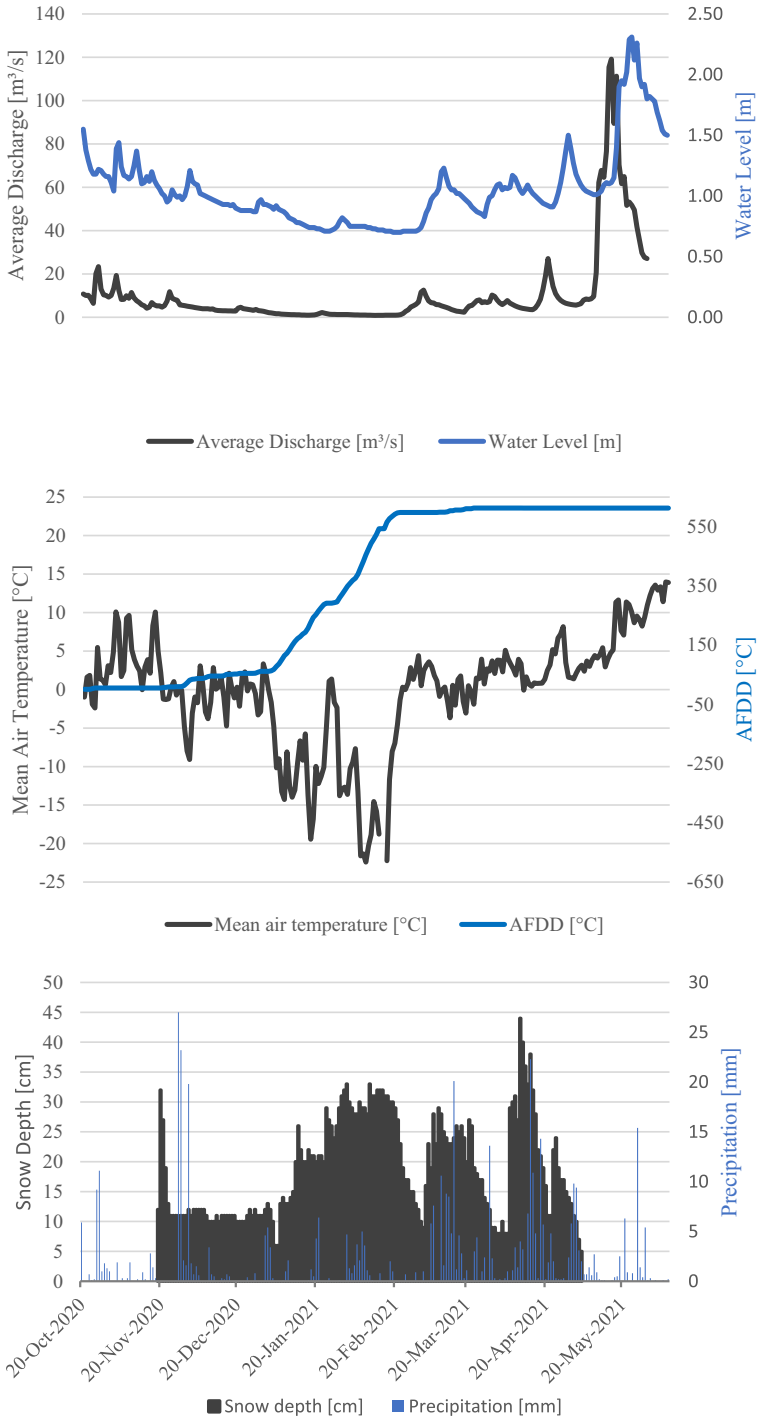

Fig. 4. Environmental and hydrological data for Sokna, winter 2020–2021.

Fig. 5. Einar Rødtang clearing snow off anchor ice dam 1 to allow ice core extraction.

augur blades dulled by ice and rock, frozen batteries, changes in river discharge, vehicle failure, power cut causing frozen samples to thaw, low number of daylight hours, blizzards, loss of dexterity due to the cold and unexpected morphology making further core extraction in a location unfeasible. (See Fig. 7.)

Fig. 6. Ice core extraction in process on anchor ice dam 1.

3.1.2. Ice thickness

Ice thicknesses were collected using a Kovacs ice thickness measurement system. When the ice cover was grounded onto the riverbed a measuring stick was used instead. Ice thickness was measured at every drilled BHJ hole and retrieved ice core. Where there was more complex ice and void (air pocket within emerged anchor ice bodies) layering an attempt was made to subtract voids from the total ice thickness.

3.1.3. Thin section

Ice cores were analysed in a cold room. Each core was visually inspected to determine possible distinct types of ice microstructures. For each identified type a corresponding thin section was prepared. A thin section is made with two horizontal cuts across the ice core using a bandsaw to extract a ~ 20 mm thick sample. This sample is then frozen to a glass plate using distilled water. The other surface is shaved flat using a Leica Microtom and also frozen to a glass plate. Another cut is made between both glass plates using the band saw, splitting the sample in half. The half with the flattened ice face is then shaved down to ~1

Fig. 7. Vegard Hornnes assisting in data collection by recording anchor ice dam location data.

mm if possible (porous structures could seldom reach such a low thickness without destruction) and photographed under polarized light. Thin sections were inspected, observed, and compared, and salient features such as grain size, grain shape (needles, polygons, irregular), void fraction and sharpness of grains were documented. An ANOVA test was carried out to determine whether thin section type can be related to BHJ strength (Ståhle and Wold, 1989).

3.1.4. Density

Density measurements were conducted in a cold room. With 20 mm thick cylindrical samples adjacent to the thin section samples. Two kinds of density measurements were conducted: simple volumetric and buoyancy based. The simple volumetric measurement involved recording the thickness and radius of the samples and then calculating the volume given an assumption of the sample being perfectly cylindrical. Dividing the weight of the sample with this volume gave the simple volumetric density. The buoyancy based measurement was conducted on the same sample afterward by measuring the weight of the sample in air and suspended in paraffin. Paraffin was used instead of water for several reasons: paraffin is lighter than water, liquid water might cause the ice sample to melt, and paraffin does not, over the course of the measurement, interact chemically with the ice to an appreciable degree. With the known density of the paraffin the buoyancy based density can be calculated using Eq. (1) (Pustogvar and Kulyakhtin, 2016).

Eq. 1. Equation for calculating buoyancy based density.

$$\rho = \frac{A}{A-B}(\rho_0 - \rho_L) + \rho_L$$

Where ρ is the calculated sample density, ρ_0 is the density of the liquid used for the measurement, in this case paraffin, and ρ_L is the density of air. A is the weight of the sample in air and B is the weight of the sample in paraffin. Density data was collected to determine the relationship between density, in situ ice strength and ice type. To analyse the data, first an Anderson-Darling test (Anderson and Darling, 1954) was carried out and a Q-Q plot (Marden, 2004) was prepared to determine whether the data was normally distributed. If the data was normally distributed the Pearson correlation formula (Pearson, 1931) was used to determine whether variables were correlated, otherwise the rank-based Spearman correlation formula (Lovie, 1995) was used.

3.2. Ice dams

3.2.1. Anchor ice location data

Anchor ice dam locations were found through manual surveying of the river reach. The location of each observed anchor ice dam was recorded using a RTK GPS (Leica Viva) and later processed in QGIS.

3.2.2. Digital Terrain Model (DTM)

A Digital Terrain Model (DTM) of the study reach was obtained from høydedata (https://hoydedata.no). Specifically, the "NDH Midtre Gauldal 2pkt 2015" dataset was used. This dataset has a resolution of 1 m and was obtained in 2015 using airplane mounted red laser. The DTM uses Euref89 datum, the UTM projection in zone 32, the NN2000 height system and the Href2016A geoid model. Channel slope was derived from this DTM.

3.2.3. Large rock location data (Aerial Photography)

Manual inspection of georeferenced aerial images (www.norgeibilder.no) was done to record large boulders in the surveyed river reach. Each boulder was marked on the image using ArcMap GIS (www.esri.com). These points were then transferred to the digital terrain model (DTM) of the study reach. "Large" is here defined as "boulder that have a diameter greater than 60 - 70 cm and that are partially exposed at a low summer discharge (2.1 m^3/s)".

3.2.4. Ice dam model

To generalize ice strength data from anchor ice dams to the entire river reach (~10 km), it is beneficial to use a statistical model for the distribution of anchor ice dams and level ice sections in the river. A model of the probability of an anchor ice dam in a given river segment was developed. Possible predictor parameters included river slope, width, sinuosity, distance along river and number of large rocks protruding the water surface in the given segment. The studied Sokna River reach was cut into 10 m segments binomially classified as "Ice dam" or "No ice dam". This yielded 1046 data points, whereof 106 were confirmed anchor ice dams. Van Der Ploeg et al. (2014) found that logistic regression models provide good and stable performance for above 20–50 events. A logistic regression technique was therefore chosen as a preferred approach and applying a binomial generalized linear model (BGLM)(Gilmour et al., 1985) was considered reasonable. A correlation matrix was used to eliminate variables without significant predictive power. Model selection was carried out using the Akaike information criterion (Cavanaugh and Neath, 2019) and the selected model performance was evaluated using the ROC curve (Hanley and McNeil, 1982) and "Leave One Out Cross Validation" (LOOCV)(Browne, 2000).

3.3. Ice forces and strength

3.3.1. BHJ

A borehole jack (BHJ) was used for in-situ ice-strength measurements. The design of the BHJ used is described in detail in Kallelid (2018) and is presented in Fig. 8. Briefly, a BHJ is a cylinder that is placed in a circular hole in the ice of a similar diameter to the BHJ, a piston is then pushed out from the BHJ into the ice. This piston breaks the ice and the BHJ measures how much force is exerted on the ice. The BHJ strength (σ_{BHJ}) is the peak measured force divided by piston area.

3.3.2. Ice pressure distributions

Separate histograms for anchor ice dams, level ice sections and stranded ice floes were constructed. Anderson-Darling tests (Anderson and Darling, 1954) and inspection of Q-Q plots (Marden, 2004) were used to determine the most suitable distribution for the data. Scatterplots and correlation tests were used to determine whether and how ice pressure varies with depth, ice type and density.

3.3.3. Ice force multiplied by ice thickness

The thin section analysis and ice core inspection gives an estimate of how much of a given core is of a particular ice type. BHJ measurements were assumed to be taken sufficiently close to ice cores for ice types and thickness to be the similar (while most cores were retrieved <1 m away from a BHJ measurement, this assumption may not always be reasonable). Furthermore it was assumed that ice cores are of homogenous strength characteristics, therefore ice strength could be integrated across the height of the ice core (see Eq. (2)). Note that thickness and strength represent the main input of a wide range of ice-structure line-load estimation equations (Rødtang et al., 2023). Considering the above-mentioned assumptions, the following equation is used to estimate the ice force potential of a given section of the ice cover/anchor ice dam.

Eq. 2. Ice force potential definition.

$$F_{potential} = k \int_0^{h_{total}} \sigma(h)dh$$

Parameter h is ice thickness measured from the top of the ice, h_{total} is the total ice thickness, $\sigma(h)$is BHJ ice strength and k is a constant such that $F_{potential}$equals the maximum force exerted upon a structure by an ice floe with $\int_0^{h_{total}} \sigma(h)dh$ experiencing complete crushing. K can be determined by direct measurement, or estimated with equations described in Rødtang et al. (2023).

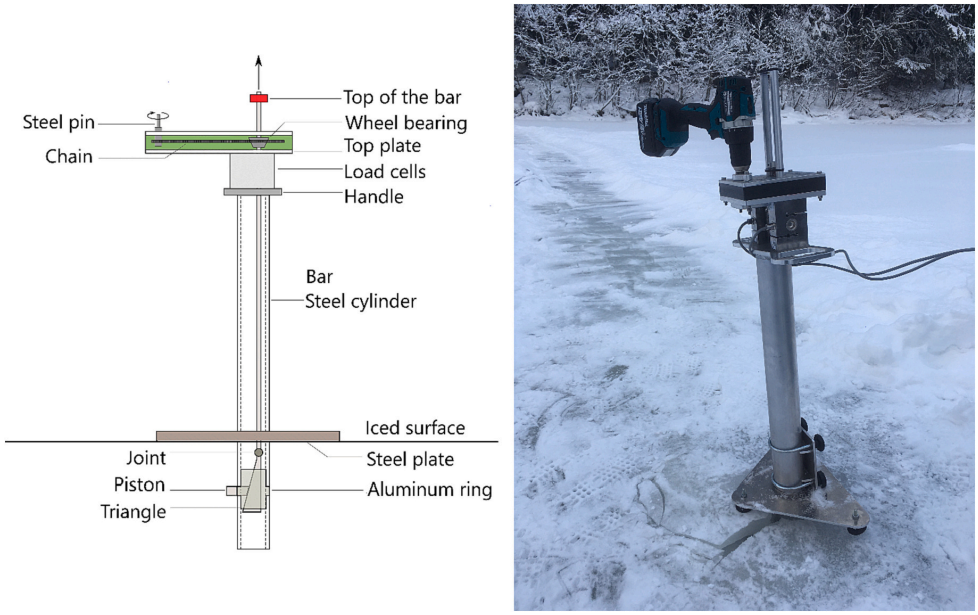

Fig. 8. Schematic of a borehole-jack (BHJ) similar to the one used in this study (Kallelid, 2018).

4. Results

4.1. Ice dam location survey

The relationship between the probability of an anchor ice dam appearing in a river segment and 8 variables was considered. These variables were river width, large boulder density, distance along river, 2 indicators of slope and 3 indicators of sinuosity. Sinuosity was calculated with fixed 140 m Euclidian distance (Sinuosity140), a variable distance selected manually (SinuosityCustom) and sinuosity based on a moving window algorithm (Sinuosity_MovWin). Likewise, slope was calculated over fixed 10 m intervals and with intervals corresponding to Sinuosity_MovWin. In addition, the rate of change of slope and width was also considered. The distributions of these variables can be seen in Fig. 9.

To determine which of these variables have statistically significant differences in means for the ice/no ice dam conditions, an ANOVA analysis was conducted (Ståhle and Wold, 1989).

The *P*-values for each of the variables are recorded in Table 1. Results indicate that all the sinuosity measures and the derivative of width have no significant effect on the probability of finding an anchor ice dam at a point in the river. These variables were therefore excluded from the subsequent analysis.

Results presented in Fig. 10 indicate that width and distance are very highly correlated. To avoid overfitting and to favour predictions purely based on local characteristics of the river, distance was removed from the model in preference to width. Moreover there seems to be no advantage to keeping both the moving window slope and the fixed 10 m increment slope. Therefore only one slope variable is kept in the subsequent analysis, the 10 m slope, which is derived from a less complex algorithm (Eq. (3)).

Eq. 3. Anchor ice dam probability in 10 m segment, with boulder density.

$$P(Icedam) = 1.577 + 0.596s - 0.461\frac{ds}{dx} - 0.205b + 0.054w - 0.046sw + 0.008bw$$

In Eq. (3) P(Icedam) is the probability of finding an anchor ice dam in a given 10 m interval of Sokna, s is the slope of the river calculated over 10 m, $\frac{ds}{dx}$is the rate of change of slope with distance along the river, b is the number of large boulders protruding through the water surface in a 10 m segment at low discharge, and w is the width of the river. To evaluate the model performance, the ROC curve (Hanley and McNeil, 1982) is calculated (Fig. 11).

The area under the ROC curve works out to be 0.733, where 1 corresponds to theoretical ideal and 0.5 corresponds to no better than random. Since the model is tested on the same data set as the one used for empirical calibration, cross validation must be carried out. Leave one out cross validation (LOOCV)(Browne, 2000) gives a prediction error of 0.102. Notably if a simpler model without boulder density is chosen, such as Eq. (4), an area under the curve of 0.719 and a LOOCV prediction error of 0.101 is achieved (I.e., a much simpler model but with only a small drop in performance). This may be because from a sediment transport point of view we expect to find the largest boulders in the steepest sections of the river.

Eq .4. Anchor ice dam probability in 10 m segment, without boulder density.

$$P(Icedam) = 0.9836 - 0.2329s - 0.4493\frac{ds}{dx} + 0.07207w - 0.03172sw$$

The model carries the general limitations of a statistical model as opposed to a physical model. It would be ideal to test it in more field seasons and in other rivers, both similar rivers and additional different ones to determine how widely applicable the equation is and when it needs to be recalibrated.

4.2. Ice dam transects

4.2.1. Density data

Two types of density data were recorded, volumetric and liquid buoyancy based. Fig. 12(A) contains buoyancy based density measurements while Fig. 12(B) contains volumetric density measurements.

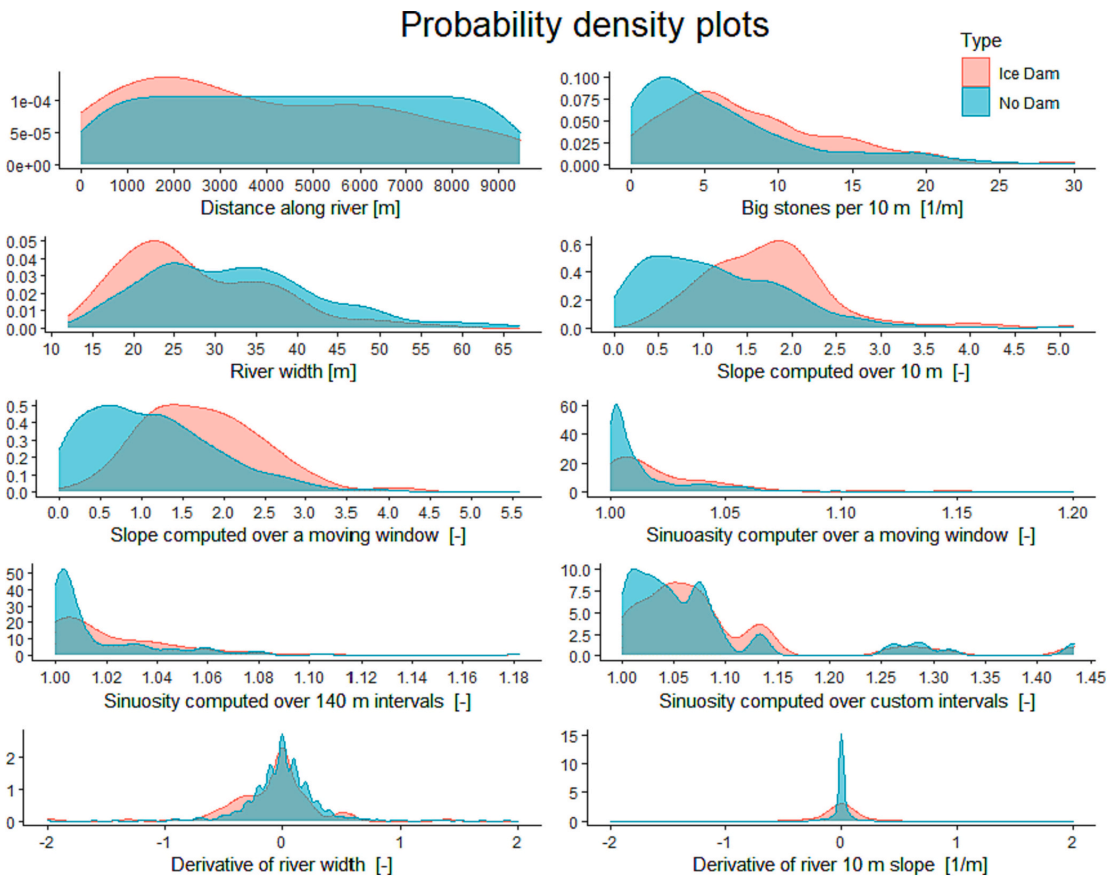

Fig. 9. Probability density plots of 8 variables recorded along a 10,460 m stretch of the Sokna river.

Volumetric density measurements vary significantly more than buoyancy based density measurements. This is because buoyancy based density measurements take into account the volume taken by open voids. Large voids reduce the density measured through volumetric methods. Ice types D, B and E have large void fractions and ice type E has high variability in volumetric density, which indicates that voids are large relative to the measured sample. The number of measurements per ice type is limited and therefore do not justify further analysis. However, from a structural strength point of view, the presence of voids probably represents a weakness, therefore the volumetric density is probably more meaningful.

Table 1
P-values ANOVA test, variable influence on likelihood of finding an anchor ice dam. Bold text implies signficiant at the 1% significance level.

Variable	*P* value	Significant at level
Distance	**0.00613**	**1%**
Boulder density	**0.00359**	**1%**
Width	**1.1e-05**	**0.01%**
Slope (10 m)	**1.86e-12**	**< 0.01%**
Slope (Moving window)	**7.76e-12**	**< 0.01%**
Sinuosity (Moving window)	0.0703	10%
Sinuosity (140 m)	0.0687	10%
Sinuosity (Custom)	0.304	100%
Derivative of width	0.599	100%
Derivative of slope	**0.00117**	**1%**

4.2.2. Thin section data

From 3 anchor ice dams and one level ice transect, 27 ice cores were retrieved and 72 thin sections where prepared. By similarity of microstructure, these were split into the same 6 groups labelled A-F as in the previous section. Table 2 show representative samples from each of these groups, categorized as needle structure (B and D) and non-needle structure (A, C, E and F). Melt damage, variation in thin section thickness and camera settings variation made the classification work more difficult.

Figs. 16–19 in the appendix contains information about the height, location, and microstructure of retrieved ice cores. Ice cores marked black were lost to a faulty freezer. Triangles indicate the location of thin sections. While transitions between zones in these figures is marked as immediate, in reality transitions between zones were more diffuse and varied gradually with height. For the level ice section some obvious simplifications can be made: there is no needle type microstructure, and the larger grained type "A" microstructure tends not to form directly at the surface (white ice).

The dams are less amenable to generalization. They display a tremendous amount of variation within and between anchor ice dams, though the top of the ice dams often contained type "A" microstructure.

4.2.3. Ice strength distributions

Fig. 13 shows the calibrated peak BHJ pressure plotted against the depth across all anchor ice dams measured. Two key observations

Fig. 10. Correlation matrix, anchor ice dam location variables.

should be made about Fig. 13. High BHJ pressures are more common closer to the anchor ice dam crest than lower down, and few measurements were taken between depths of 25 and 45 cm, primarily due large voids being common at those depths. I.e., the average ice strength of an anchor ice dam decreases with thickness. It is uncertain why voids were common at these depths. Checks were carried out confirming that there is no correlation between direction of the BHJ indentor (upstream, downstream, etc) and measured ice strength. Various ice strength distributions can be derived from the data set, those derived from small subsets of the data however have little statistical power. Testing various distributions on all the anchor ice data yields goodness-of-fit criteria presented in Table 3:

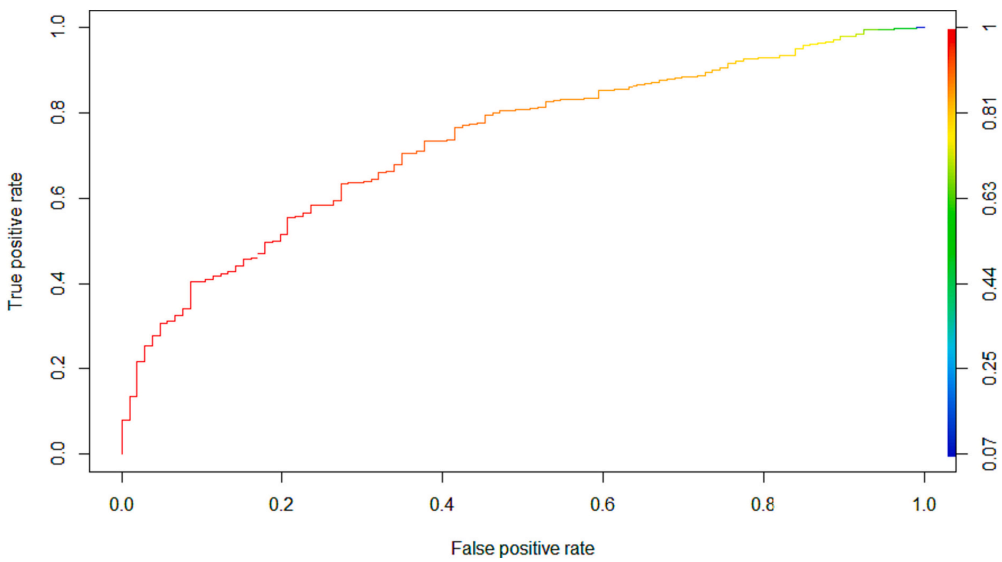

Fig. 11. ROC curve for Eq. (3) applied to the Sokna data set. The colour corresponds to cut-off values. I.e., the probability at which an event is counted as an ice dam.

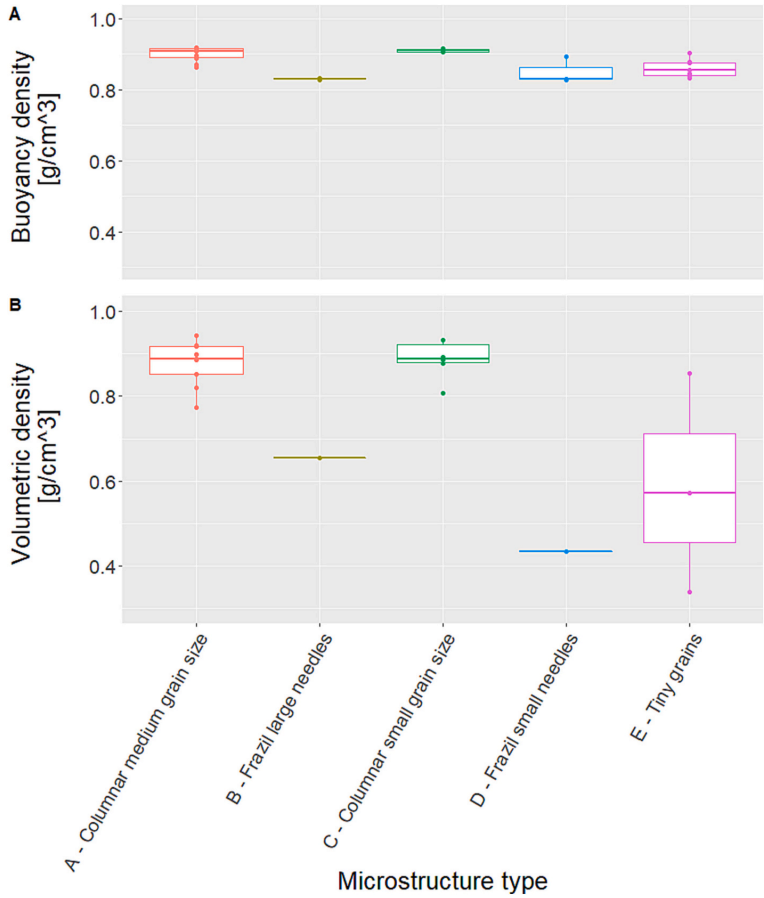

Fig. 12. Volumetric and buoyancy based density dependence on microstructures A, B, C, D and E.

Note that the Gamma, Weibull and Exponential functions have the lowest AiC and BiC (relative measures of model fit). With the rule of thumb that an AiC difference >2 is significant, any of these 3 can be chosen. The exponential distribution however is a one parameter distribution and will therefore be preferred. Fig. 14 shows the Q-Q plot, P—P plot and how the data fits to the theoretical distribution. The Q-Q plot bulges a bit between 15 and 30 MPa. This might suggest some slight left skew or bimodality, but on the whole the distribution tracks the data fairly well. The P—P plot suggests almost a perfect match to the distribution. This gives us confidence that an exponential distribution with a rate parameter of 0.116 (standard deviation 0.01) provides a good representation of the data (Eq. (5)).

Eq. 5. BHJ strength probability distribution.

$$P(\sigma_{BHJ}) \approx 0.12e^{-0.12\sigma_{BHJ}}$$

The distribution associated with Eq. (5) is based on 132 data points.$P(\sigma_{BHJ})$is the probability of a random point in an anchor ice dam giving an in-situ BHJ strength of $\sigma_{BHJ}$when measured. Carrying out the same analysis on level ice sections is hard to justify as there are much fewer datapoints (25).

A subset of the strength measurements in Fig. 13 are represented in Fig. 15, here plotted against the closest observed microstructure. The spread in the observed strengths is likely connected to the high spatial variability of microstructures and difficulty in observing the actual crushed microstructure. Querying the data gives an estimated calibrated ice strength of each ice type as indicated in Table 4.

The data does suggest that columnar ice is stronger than frazil ice in general. There is not enough data for further conclusions. The results can however be used as a rule of thumb when estimating ice strength from observed microstructure until better data is available.

4.2.4. Ice force potential

Carrying out the integral of Eq. (2) gives the ice force potentials in Table 5.

In order to convert ice force potential presented in Table 5 to actual forces, they must be multiplied with the width of the structure, structure shape factors and other theoretical factors. Even without this, however these few results presented in Table 5 are useful for comparison between transects. The average ice force potential of all the ice dams is greater than that of the level ice transect. This would apparently imply that anchor ice dams in small steep rivers would be associated with higher forces applied to river infrastructure compared with that of level ice. However, this discounts the fact that level ice has higher average strength and that anchor ice dams tend to contain weak layers. It could conversely be expected that a channel segment covered with level ice would exert higher forces on a structure than an anchor ice dam, but this is debatable. The size and strength of the ice floes reaching the structure

will depend on several factors, including how far downstream the structure is located and the precise breakup mechanism in addition to whether the ice is from a level ice section or an anchor ice section. A final statistical point, however, does speak in favour of anchor ice dams: the internal structure and thickness of anchor ice dams are highly variable compared to level ice sections. There are many anchor ice dams in a steep rivers and the highest ice force applied on a structure will be dominated by the ice floe with the highest residual ice force potential. The peak surviving ice force potential by level ice sections can be expected to vary relatively little compared to that from anchor ice dams. It can be expected that for brief ice runs residual ice force potential is governed by the mechanical breakup of ice floes. Whereas when ice runs take longer (due to ice jams forming and dissolving) thermal effects may play a role affecting both the strength and size of ice floes. To settle this debate, it will be necessary to obtain a better understanding of how anchor ice dams break apart and if, indeed, ice dams can produce the most resistant ice pieces of an ice run in a steep channel.

5. Discussion

Predicting the formation of anchor ice dams (and other river ice features) has been attempted by Dubé et al. (2015). A global river ice classification model predicting ice cover type (ice shells, suspended ice cover, surface floating ice cover, surface confined ice cover, solid ice,

Table 2
Table of representative microstructures. Number of similar samples collected indicated.

A – Columnar medium grain size
(19 samples)
Ice Dam 2, Core 3, 4 cm from top

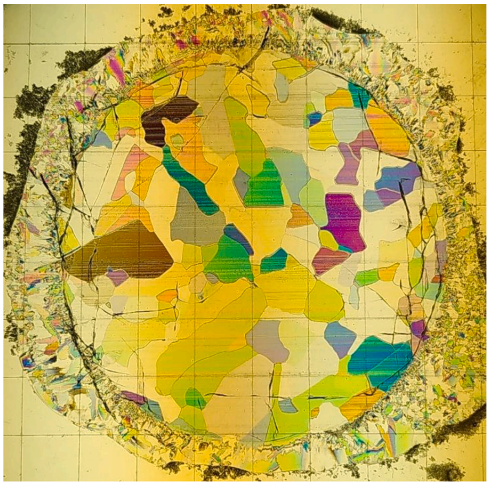

B – Frazil large needles
(11 samples)
Ice Dam 1, Core 8, 17 cm from top

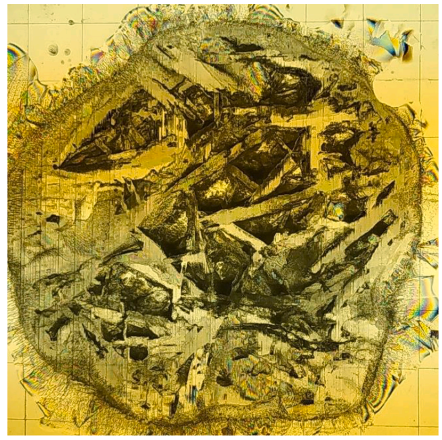

C – Columnar small grain size
(7 samples)
Level ice, Core 1, 30 cm from top

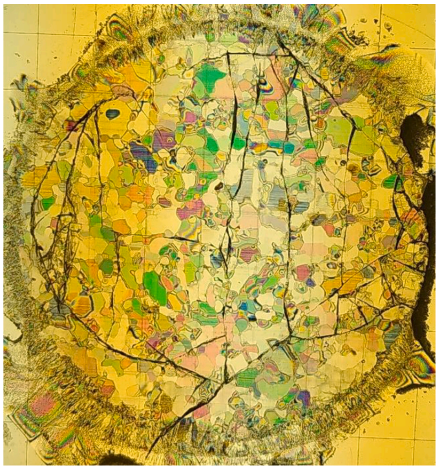

D – Frazil small needles
(8 samples)
Ice Dam 2, Core 5, 60 cm from top

E – Tiny grains
(21 samples)
Ice Dam 1, Core 6, 77 cm from top

F – Large voids and grains
(1 Sample)
Ice Dam 3, Core 1, 8 cm from top

(*continued on next page*)

Table 2 (*continued*)

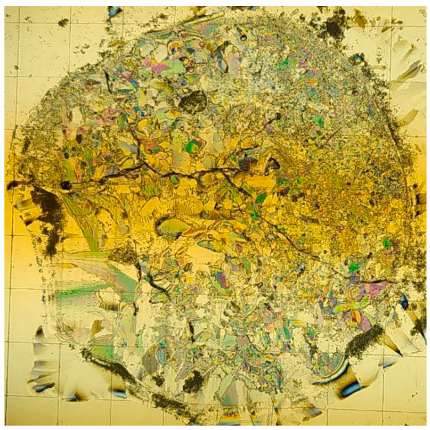

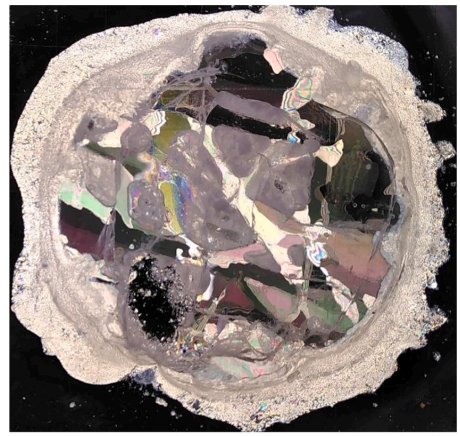

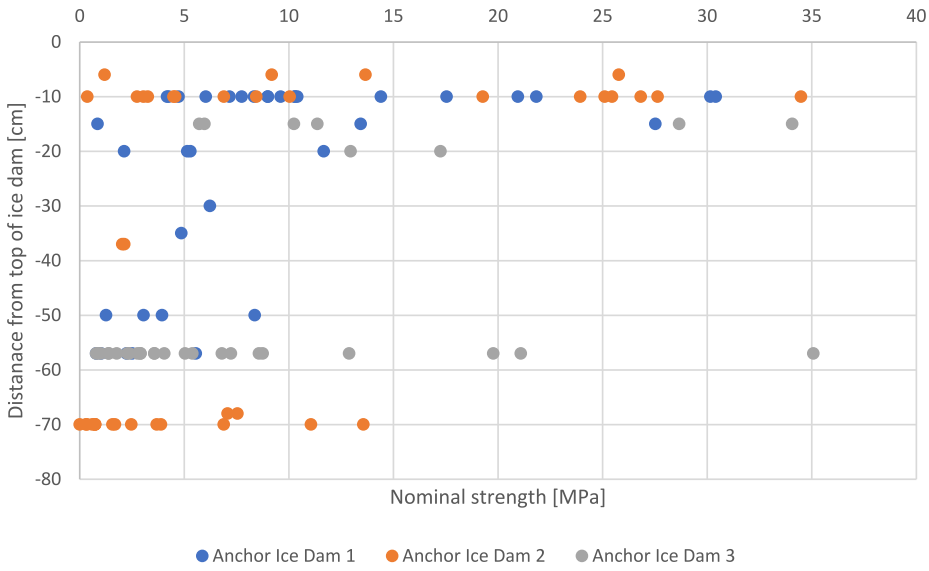

Fig. 13. Calibrated peak BHJ pressure Vs depth across all anchor ice dams measured.

Table 3
Goodness-of-fit criteria for various distributions fitted to all anchor ice dam strength data.

Information Criterion	Gamma	Norm	Weibull	Logistic	Exponential	Log-Normal
Akaike's (AiC)	836.8	941.3	836.9	930.2	835.0	866.9
Bayesian (BiC)	842.7	947.2	842.7	936.0	837.8	872.7

and no ice) and five ice processes (active frazil ice and anchor ice, hanging dams, ice dams, aufeis, and ice jams) was presented by Turcotte and Morse (2013). Input parameters to this model for the Sokna would be cold winter intensity, narrow channel size and steep channel gradient, which results in a suspended ice cover type, typically characterized by anchor ice, ice dams, ice jams and javes. While this model is very useful for a broad classification of the rivers ice regime, it does not give small scale information about the locations of specific ice cover types, ice features, and ice processes.. Models like the one developed in this project can help to fill this gap and would allow the use of anchor ice dam locations for instance in detailed hydraulic models. Notably, the width and slope used In Turcotte and Morse (2013) were also useful anchor ice dam location indicators in the model presented in this work.

Observed ice dam thicknesses of >1.5 m and their resistance to the spring floods back up the suggestions made by Stickler et al. (2010) that seasonal ice formation in steep streams like the Sokna need to be taken into account as a significant driver of in-stream heterogeneity. Stickler et al. (2010) criticized the idea that discharge is the main determinant of in-stream ice structure heterogeneity in steep streams that experience seasonal ice formation. The findings in this paper suggest that ice dam

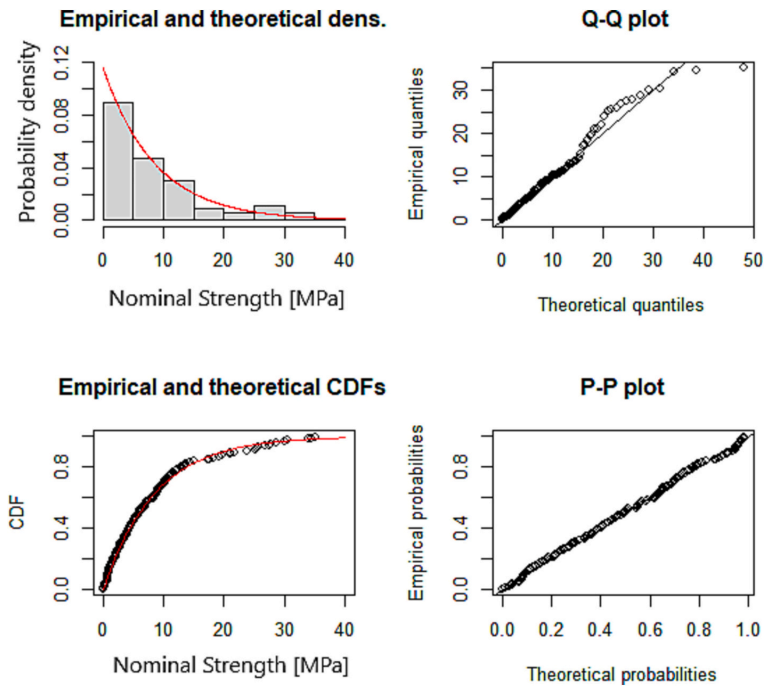

Fig. 14. Anchor ice dam strength data compared to theoretical exponential distribution.

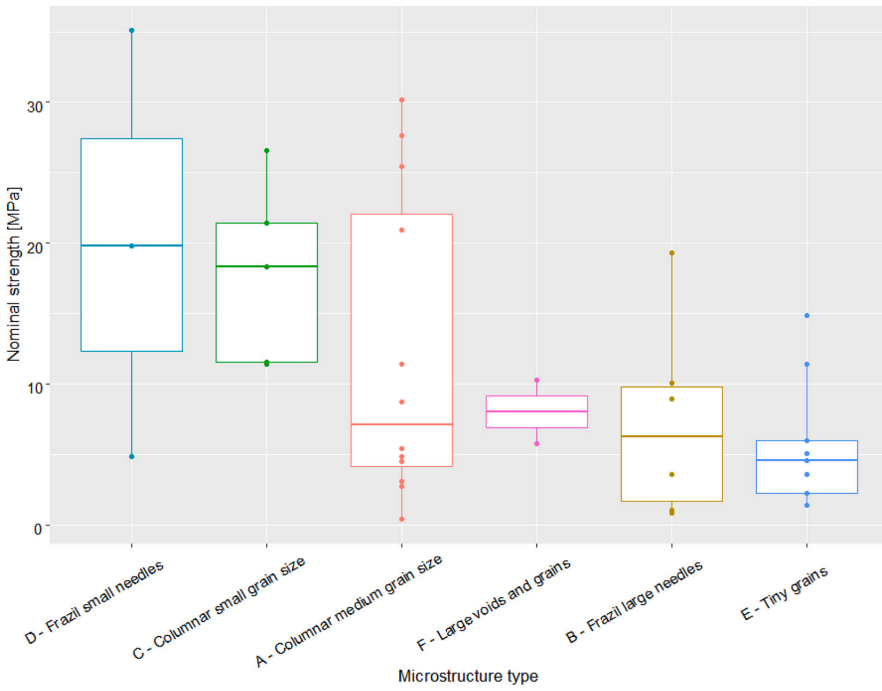

Fig. 15. Thin section microstructure vs closest calibrated BHJ measurement.

Table 4
Average strength of different ice types estimated through averaging the closest BHJ measurements.

Ice type	Nominal strength [MPa]	Min strength [MPa]	Max strength [MPa]	Num. records
A – Columnar medium grain size	12	1	30	12
B – Frazil large needles	7	1	19	6
C – Columnar small grain size	18	11	27	5
D – Frazil small needles	20	5	35	3
E – Tiny grains	6	1	15	9
F – Large voids and grains	8	6	10	2

locations and therefore their effects on hydraulics and habitat can be predicted by knowing just the slope and width for specific river segments. Further developing similar models could be a useful contribution to stream models and assessment tools.

Due to practical limitations different transects were sampled on different days throughout the field season. The ice cover is assumed to change relatively little once the river has frozen over and a significant ice cover thickness has been achieved. This will never be exactly true, however, and variation between transects must be evaluated with this in mind. Furthermore, the ice cover in steep rivers may remain fragile for the entire winter period, which represents an underrated hazard. Most of the data collected for this paper came from a single river. Therefore, care must be taken to generalize the results to other rivers. Moreover, care must be taken when interpreting the meaning of the strength measured by the BHJ. "BHJ" strength does not adhere to the standard definition of uniaxial compressive strength. Nevertheless, findings from this paper should be considered when designing structures in small, steep rivers.

High temperature and radiation often precede ice runs. High temperatures and radiation can reduce ice strength significantly as found by Bulatov (Beltaos, 2008, p. 87). The BHJ measurements in this paper were taken before the ice cover was significantly deteriorated. Therefore, the in-situ BHJ ice strength must be considered an upper limit for pieces of ice in the event of an ice run interacting with a structure. Because of the limited sample size in this study, it is also possible that the maximum ice strength in steep river ice features has yet to be documented.

6. Conclusion

While the structures and properties of ice in small, steep rivers vary significantly, some trends can nonetheless be found. The following conclusions apply to the studied river and may generally apply to steep rivers, however investigations in other rivers are necessary to confirm this.

Where along the length of the river anchor ice dams form, can be modelled with a binomial generalized linear model (BGLM)(Gilmour et al., 1985), giving Eq. (3):

$$P(Icedam) = 1.577 + 0.596s - 0.461\frac{ds}{dx} - 0.205b + 0.054w - 0.046sw + 0.008bw$$

Where slope (s) and width (w) are the most important parameters. (Area under ROC curve 0.718 - > 0.733). Sinuosity was not included in the model due to lack of predictive power. Leave one out cross validation (LOOCV)(Browne, 2000) gives prediction error of approximately 0.1. This model coupled with the observation that anchor ice dams are 2–3 times thicker than level ice sections, implies that anchor ice dams, found at 10% of river segments, still represent 20–30% of the ice in the Sokna river.

Table 5
Ice core force potentials.

Ice core	Ice force potential [MPa m]			
	Level ice	Ice dam 1	Ice dam 2	Ice dam 3
1	8.8	7.8	MD	4.2
2	9.0	MD	7.2	5.5
3	3.6	10.4	9.4	7.9
4	6.1	MD	27.1	18.2
5	5.4	MD	MD	10.1
6	MD	8.4		MD
7	7.6	7.85		12.4
8		7.7		
Average	6.8	8.4	14.6	9.8

Note: Only 5 and 7 cores were retrieved from Ice dam 2 and 3, respectively due to fieldwork constraints.

The in-situ BHJ ice strength in anchor ice dams follow an exponential distribution with parameters given according to according to Eq. (5):

$$P(\sigma_{BHJ}) \approx 0.12e^{-0.12\sigma_{BHJ}}$$

This distribution applies to random points in an anchor ice dam. Nonetheless, there are trends in strength within ice dams: For the Sokna river (which has an average slope of ~1.7%) during the winter 2020–2021, the top 35 cm of ice were generally twice as strong as the 35 cm below. There was no correlation between direction of the BHJ indentor (upstream, downstream, etc) and measured ice strength. Likewise, the date of measurement and distance from the bottom of the ice cover shows no correlation with measured ice strength. The average strength of all measured anchor ice dams is ~8.5 MPa (average strength of surveyed anchor ice dams was in the range of 7.1–10.4 MPa). Level ice sections in the same river had average strength approximately 3 times higher (~23.7 MPa), similar to the strength of post ice run stranded ice floes measured by the main author in the Sona River in Trondelag (a river similar to the Sokna), Norway, during the same winter (~25.6 MPa). Note that the average strength of an anchor ice dam decreases with thickness.

Some limitations of this research include:

- The data was only collected from a single river in a single field season.
- Anchor ice dams are chaotic and hazardous. Systematic data collection was consequently difficult.
- It was not practically possible, due to the different diameters of the BHJ and core retrieval system, to carry out BHJ measurements exactly matching thin sections.
- For some of the microstructures identified in the thin section analysis, only very few samples were retrieved (e.g., class F).

CRediT authorship contribution statement

Einar Rødtang: Conceptualization, Methodology, Software, Validation, Formal analysis, Investigation, Resources, Data curation, Writing – original draft, Writing – review & editing, Visualization, Project administration. **Janik John:** Conceptualization, Methodology, Software, Validation, Formal analysis, Investigation, Data curation, Visualization. **Knut Alfredsen:** Conceptualization, Methodology, Investigation, Resources, Writing – review & editing, Visualization, Supervision, Project administration, Funding acquisition. **Knut Høyland:** Conceptualization, Methodology, Investigation, Resources, Writing – review & editing, Supervision, Project administration, Funding acquisition.

Declaration of Competing Interest

The Author have no conflicts of interest to declare.

Data availability

Data will be made available on request.

Appendix A. River cross sections

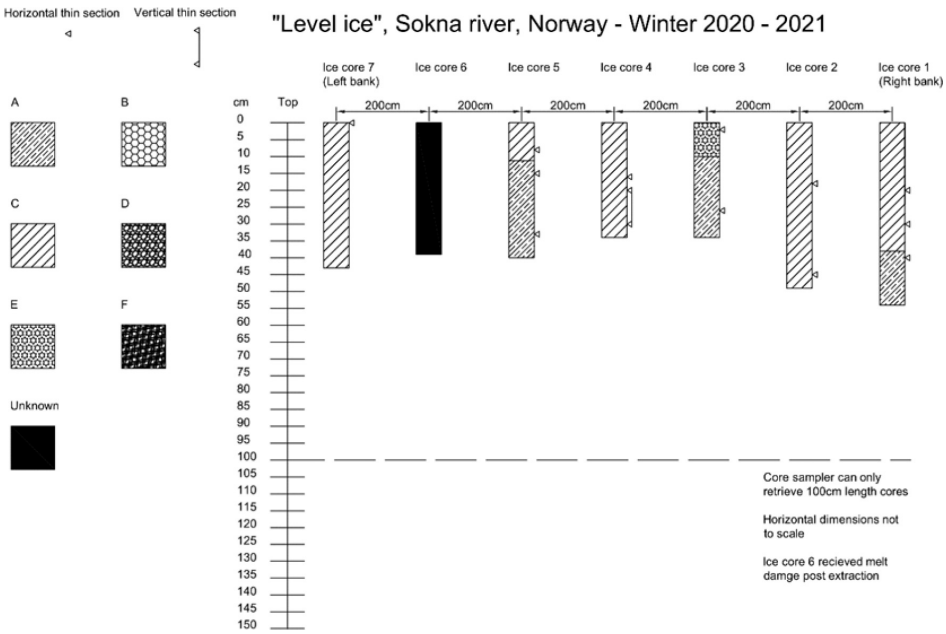

Fig. 16. Level ice river cross-section.

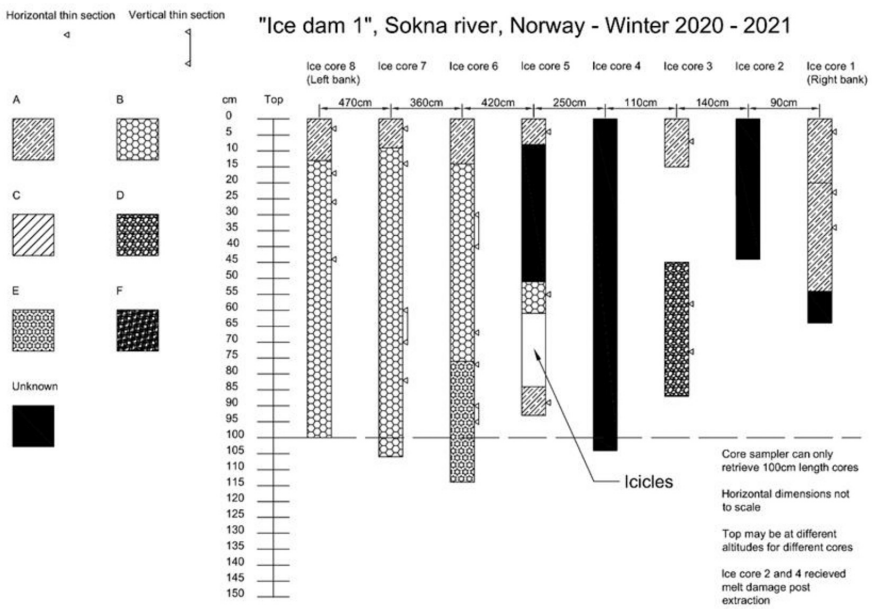

Fig. 17. Ice dam 1 cross section.

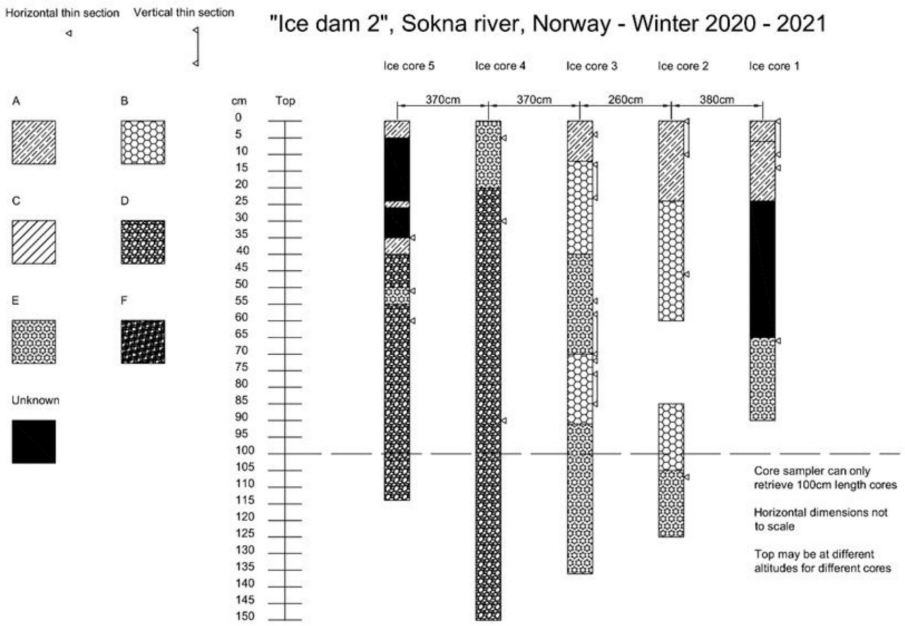

Fig. 18. Ice dam 2 cross-section.

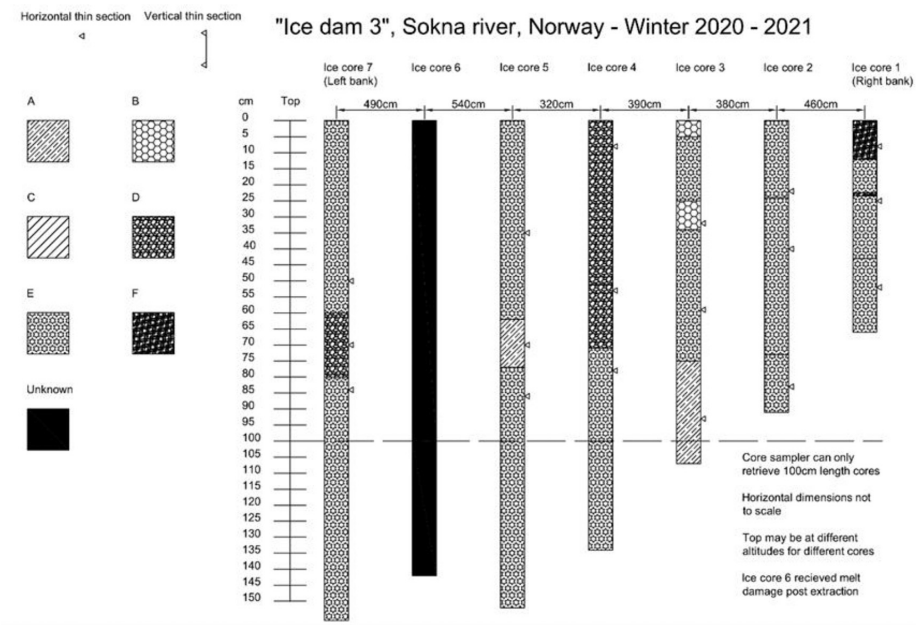

Fig. 19. Ice dam 3 cross-section.

References

Alfredsen, K., 2017. An assessment of ice effects on indices for hydrological alteration in flow regimes. Water. https://doi.org/10.3390/w9120914.

Anderson, T.W., Darling, D.A., 1954. A test of goodness of fit. J. Am. Stat. Assoc. 49, 765–769. https://doi.org/10.1080/01621459.1954.10501232.

Beltaos, S., 2008. River Ice Breakup, 1st ed. Water Resources Publications.

Browne, M.W., 2000. Cross-validation methods. J. Math. Psychol. 44, 108–132. https://doi.org/10.1006/jmps.1999.1279.

Cavanaugh, J.E., Neath, A.A., 2019. The Akaike information criterion: background, derivation, properties, application, interpretation, and refinements. WIREs Comput. Stat. 1–11 https://doi.org/10.1002/wics.1460.

Dempsey, J.P., 2000. Research trends in ice mechanics. Int. J. Solids Struct. 37, 131–153. https://doi.org/10.1016/S0020-7683(99)00084-0.

Doyle, P.F., 1988. Damage resulting from a sudden river ice breakup. Can. J. Civ. Eng. 15, 609–615. https://doi.org/10.1139/l88-082.

Dubé, M., Turcotte, B., Morse, B., 2014. Inner structure of anchor ice and ice dams in steep channels. Cold Reg. Sci. Technol. 106–107, 194–206. https://doi.org/10.1016/j.coldregions.2014.06.013.

Dubé, M., Turcotte, B., Morse, B., 2015. Steep channel freezeup processes: understanding complexity with statistical and physical models 1. Can. J. Civ. Eng. 42, 622–633. https://doi.org/10.1139/cjce-2014-0412.

Frederking, R., 2012. Review of Standards for Ice Forces on Port Structures. In: Cold Regions Engineering 2012. American Society of Civil Engineers, Reston, VA, pp. 725–734. https://doi.org/10.1061/9780784412473.072.

Gebre, S., Alfredsen, K., Lia, L., Tesaker, E., 2013. Review of ice effects on hydropower systems. J. Cold Reg. Eng. 27, 196–222. https://doi.org/10.1061/(ASCE)CR.1943-5495.0000059.

Gilmour, A.R., Anderson, R.D., Rae, A.L., 1985. The analysis of binomial data by a generalized linear mixed model. Biometrika 72, 593–599.

Hanley, A., McNeil, J., 1982. The meaning and use of the area under a Receiver Operating Characteristic (ROC) curve. Diagn. Radiol. 143, 29–36. https://doi.org/10.1148/radiology.143.1.7063747.

Heggen, S., Alfredsen, K., 2013. Ice breakup in small norwegian streams. In: Proc. 17th Work. River Ice, 18 pages.

Huusko, A., Greenberg, L., Stickler, M., Linnansaari, T., Nykänen, M., Vehanen, T., Koljonen, S., Louhi, P., Alfredsen, K., 2007. Life in the ice lane: the winter ecology of stream salmonids. River Res. Appl. 23, 469–491. https://doi.org/10.1002/rra.999.

Kallelid, M.S., 2018. A Study of the Strength and the Physical Properties of Glacier-Ice Runways. NTNU.

Lovie, A.D., 1995. Who discovered Spearman's rank correlation? Br. J. Math. Stat. Psychol. 48, 255–269. https://doi.org/10.1111/j.2044-8317.1995.tb01063.x.

Marden, J.I., 2004. Positions and QQ plots. Stat. Sci. 19, 606–614. https://doi.org/10.1214/088342304000000512.

Nafziger, J., She, Y., Hicks, F., Cunjak, R.A., 2017. Anchor ice formation and release in small regulated and unregulated streams. Cold Reg. Sci. Technol. 141, 66–77. https://doi.org/10.1016/j.coldregions.2017.05.008.

Pearson, E.S., 1931. The test of significance for the correlation coefficient. J. Am. Stat. Assoc. 26, 128–134. https://doi.org/10.1080/01621459.1931.10503208.

Prowse, T.D., Culp, J.M., 2003. Ice breakup: a neglected factor in river ecology. Can. J. Civ. Eng. 30, 128–144. https://doi.org/10.1139/l02-040.

Prowse, T.D., Demuth, M.N., 1993. Strength variability of major river-ice types. Nord. Hydrol. 24, 169–182. https://doi.org/10.2166/nh.1993.0020.

Prowse, T., Alfredsen, K., Beltaos, S., Bonsal, B.R., Bowden, W.B., Duguay, C.R., Korhola, A., McNamara, J., Vincent, W.F., Vuglinsky, V., Walter Anthony, K.M., Weyhenmeyer, G.A., 2011. Effects of changes in arctic lake and river ice. Ambio 40, 63–74. https://doi.org/10.1007/s13280-011-0217-6.

Pustogvar, A., Kulyakhtin, A., 2016. Sea ice density measurements. Methods and uncertainties. Cold Reg. Sci. Technol. 131, 46–52. https://doi.org/10.1016/j.coldregions.2016.09.001.

Rødtang, E., Alfredsen, K., Juárez, A., 2021. Drone surveying of volumetric ice growth in a steep river. Front. Remote Sens. 2, 1–11. https://doi.org/10.3389/frsen.2021.767073.

Rødtang, E., Alfredsen, K., Høyland, K., Lia, L., 2023. Review of river ice force calculation methods. Cold Reg. Sci. Technol. https://doi.org/10.1016/j.coldregions.2023.103809.

Ståhle, L., Wold, S., 1989. Analysis of variance (ANOVA). Chemom. Intell. Lab. Syst. 6, 259–272. https://doi.org/10.1016/0169-7439(89)80095-4.

Stickler, M., Alfredsen, K.T., Linnansaari, T., Fjeldstad, H.-P., 2010. The influence of dynamic ice formation on hydraulic heterogeneity in steep streams. River Res. Appl. 26, 1187–1197. https://doi.org/10.1002/rra.1331.

Timalsina, N.P., Charmasson, J., Alfredsen, K.T., 2013. Simulation of the ice regime in a Norwegian regulated river. Cold Reg. Sci. Technol. 94, 61–73. https://doi.org/10.1016/j.coldregions.2013.06.010.

Turcotte, B., Morse, B., 2011. Ice processes in a steep river basin. Cold Reg. Sci. Technol. 67, 146–156. https://doi.org/10.1016/j.coldregions.2011.04.002.

Turcotte, B., Morse, B., 2013. A global river ice classification model. J. Hydrol. 507, 134–148. https://doi.org/10.1016/j.jhydrol.2013.10.032.

Turcotte, B., Morse, B., Anctil, F., 2011. Steep channels freezeup processes. CRIPE 85–101.

Turcotte, B., Morse, B., Dubé, M., Anctil, F., 2013. Quantifying steep channel freezeup processes. Cold Reg. Sci. Technol. 94, 21–36. https://doi.org/10.1016/j.coldregions.2013.06.003.

Turcotte, B., Alfredsen, K., Beltaos, S., Burrell, B.C., 2017. Ice-related floods and flood delineation along streams and small rivers. In: CGU HS Comm. River Ice Process. Environ. 19th Work. Hydraul. Ice Cover. Rivers, Whitehorse, Yukon, Canada.

Ungerman, M., Tremblay, L.B., Martin, T., Losch, M., 2017. Impact of the ice strength formulation on the performance of a sea ice thickness distribution model in the Arctic. J. Geophys. Res. Ocean. 122, 1–22. https://doi.org/10.1002/2016JC012128. Received.

Van Der Ploeg, T., Austin, P.C., Steyerberg, E.W., 2014. Modern modelling techniques are data hungry: a simulation study for predicting dichotomous endpoints. BMC Med. Res. Methodol. 14, 1–13. https://doi.org/10.1186/1471-2288-14-137.

Paper III

frontiers in Remote Sensing

ORIGINAL RESEARCH
published: 21 December 2021
doi: 10.3389/frsen.2021.767073

Drone Surveying of Volumetric Ice Growth in a Steep River

Einar Rødtang, Knut Alfredsen and Ana Juárez*

Department of Civil and Environmental Engineering, Norwegian University of Science and Technology, Trondheim, Norway

Representative ice thickness data is essential for accurate hydraulic modelling, assessing the potential for ice induced floods, understanding environmental conditions during winter and estimation of ice-run forces. Steep rivers exhibit complex freeze-up behaviour combining formation of columnar ice with successions of anchor ice dams to build a complete ice cover, resulting in an ice cover with complex geometry. For such ice covers traditional single point measurements are unrepresentative. Gathering sufficiently distributed measurements for representativeness is labour intensive and at times impossible with hard to access ice. Structure from Motion (SfM) software and low-cost drones have enabled river ice mapping without the need to directly access the ice, thereby reducing both the workload and the potential danger in accessing the ice. In this paper we show how drone-based photography can be used to efficiently survey river ice and how these photographic surveys can be processed into digital elevation models (DEMs) using Structure from Motion. We also show how DEMs of the riverbed, riverbanks and ice conditions can be used to deduce ice volume and ice thickness distributions. A QGIS plugin has been implemented to automate these tasks. These techniques are demonstrated with a survey of a stretch of the river Sokna in Trøndelag, Norway. The survey was carried out during the winter 2020–2021 at various stages of freeze-up using a simple quadcopter with camera. The 500 m stretch of river studied was estimated to have an ice volume of up to 8.6×10^3 m^3 (This corresponds to an average ice thickness of ~67 cm) during the full ice cover condition of which up to 7.2×10^3 m^3 (This corresponds to an average ice thickness of ~57 cm) could be anchor ice. Ground Control Points were measured with an RTK-GPS and used to determine that the accuracy of these ice surface geometry measurements lie between 0.03 and 0.09 m. The ice thicknesses estimated through the SfM methods are on average 18 cm thicker than the manual measurements. Primarily due to the SfM methods inability to detect suspended ice covers. This paper highlights the need to develop better ways of estimating the volume of air beneath suspended ice covers.

Keywords: ice growth, photogrametry, steep rivers, drone imaging, structure from motion, small river, ice volume, anchor ice

OPEN ACCESS

Edited by:
Matt Westoby,
Northumbria University,
United Kingdom

Reviewed by:
Kieran T. Wood,
University of Bristol, United Kingdom
Yu-Hsuan Tu,
King Abdullah University of Science and Technology, Saudi Arabia

****Correspondence:***
Einar Rødtang
einar.a.rodtang@ntnu.no

Specialty section:
This article was submitted to Unmanned Aerial Systems (UASs and UAVs), a section of the journal Frontiers in Remote Sensing

Received: *30 August 2021*
Accepted: *22 November 2021*
Published: *21 December 2021*

Citation:
Rødtang E, Alfredsen K and Juárez A (2021) Drone Surveying of Volumetric Ice Growth in a Steep River. Front. Remote Sens. 2:767073. doi: 10.3389/frsen.2021.767073

INTRODUCTION

Formation and release of river ice is an important component of river systems in cold climate areas (Bennett and Prowse, 2009). River ice growth and release cause a variety of problems and impact many processes in river systems. Ice jams can cause severe flooding, and ice runs caused by the release of ice jams may cause impact damage and scour of river infrastructure (Beltaos, 1995, 2008). River ice affects the habitats of stream-living and riparian species (e.g., Prowse and Culp, 2003; Huusko et al., 2007; Lind et al., 2014), and poses problems for river infrastructure (e.g., Gebre et al., 2013). The available knowledge on river ice is still developing, and the current body of knowledge is considerably more comprehensive for larger rivers than for smaller streams (Beltaos, 2012). The severity and effects of ice growth and release particularly related to small streams are in practice difficult to predict, in part due to lacking theoretical frameworks related to formation (but see Turcotte et al., 2013) and release of ice and in part due to lacking data. The lack of data is not due to lack of interest, rather it is due to the inherent difficulties of collecting large consistent river ice datasets related to spatial complexity and the potential dangers involved in accessing the river ice especially during the formation and breakup period. A major challenge is to describe the complex geometry and a high spatial and temporal variability of the ice cover. Over a few meters' stretch of river, the author has observed anchor ice dams, level ice, aufeis, hinge cracks, drainage voids, icicles, ice bells, snow, columnar ice, and frazil ice. A full manual characterization of such rich and complex ice utilising traditional mapping tools like total stations or GPS systems is labour intensive and also often impossible due to the potential dangers of traversing the unstable ice (Beltaos, 1995). New methods are therefore needed to create spatially accurate maps of river ice in an efficient way and with minimal needs of accessing the ice cover. Further, accurate mapping of river ice is needed in the process of modelling the ice formation and release processes which are important in predicting the development of ice in the short term [e.g., for ice related flood warnings (Lindenschmidt et al., 2021)] and for modelling ice scenarios for the future. Airplanes and satellite imagery have been used to map and evaluate river ice (Chu and Lindenschmidt, 2016; Kääb et al., 2019). However, the low resolution of the images makes it difficult to use these data for studies of small streams. Furthermore, satellite data introduce issues such as cloud cover and incomplete timeseries that reduces their applicability (Dolan et al., 2019). Imaging from airplanes can also be costly and difficult in narrow river valleys. The advent of unmanned aerial vehicle (hereafter "drone") technology promises to drastically cut the labour costs of carrying out high resolution river surveys (Woodget et al., 2017), and the method can also be applied for river ice (Alfredsen et al., 2018). A combination of improved aerodynamic stability, battery capacity, GPS positioning and image stabilization enables us to use drones to take large numbers of georeferenced images of an ice cover. Structure from motion (SfM) photogrammetry algorithms then allows us to process these pictures and convert them into highly accurate 3D models of the landscape (Smith et al., 2016; Carrivick and Smith, 2019). Some work has been conducted using drones for mapping the cryosphere. Mapping of glaciers and snow in particular has received a lot of attention (Ewertowski et al., 2019; Lamsters et al., 2019; Gaffey and Bhardwaj, 2020). Alfredsen et al. (2018) published the first example of drone imaging of river ice, mapping anchor ice dams and quantifying the size of an ice jam remnant in two Norwegian rivers. Alfredsen and Juarez (2020) used a drone and SfM to map ice jam remnants as a basis for hydraulic modelling of the effect of ice on river hydraulics. Garver, (2019) used drones and SfM to determine the extent and topography of ice jams in Mohawk River, United States. A slightly different application of drone imagery for ice assessment is presented by Ansari et al. (2021) who used the drone images and videos of ice as a basis for training a convolutional neural network to classify ice types. The key challenge in the field of drone imaging ice is currently to move from qualitative results to quantitative results. SfM technology promises to bridge this gap (Westoby et al., 2012; Smith et al., 2016). By comparing 3D models derived from drone images at different times we can make reasonable distributed estimates of ice thickness and volume. These data can then be used to quantify the development of various forms of river ice over a river reach directly from the drone geometries, and to generate data to calibrate and evaluate river ice models. Several hydraulic models that include the effect of ice have been developed including RIVICE (Lindenschmidt, 2017) and River1D (Blackburn and She, 2019). HEC-RAS has also been used to model the effects of ice jams on flow (Beltaos and Tang, 2013). However, lack of data has made it difficult to evaluate and calibrate these models, particularly for small rivers with complex ice conditions.

Ice jams and ice jam residues, however, don't have the suspended ice covers that are observed in pre-breakup steep-rivers, ice jams are significantly rougher, and furthermore previous work does not map pre-breakup ice thickness and temporal variation. In this paper we therefore describe a method that aims at mapping the ice over the season to capture the full formation—release cycle. The objective of this work can be summarized in the following points:

1. Investigate the potential of using a small drone and SfM to map the development of river ice in a small stream from freeze-up to break-up, including the periods at the start and end of the ice season when access to the ice is impossible.
2. Derive the methods to quantify the development of the ice cover by comparing digital elevation models between flights and compare the data from the drone flights with manual ice measurements when access to the ice is possible.
3. Evaluate the methods as a tool for future ice mapping, and identify challenges and needed developments to improve the method.

METHODS AND MATERIALS

Materials

Study Site

Sokna is a small, steep river flowing through a mountainous area in central Norway. Sokna flows into the Gaula river in the town of Støren, approximately 40 km south of the city of Trondheim. See **Figure 1** for catchment location and **Table 1** for river characteristics. The drone flights were undertaken from

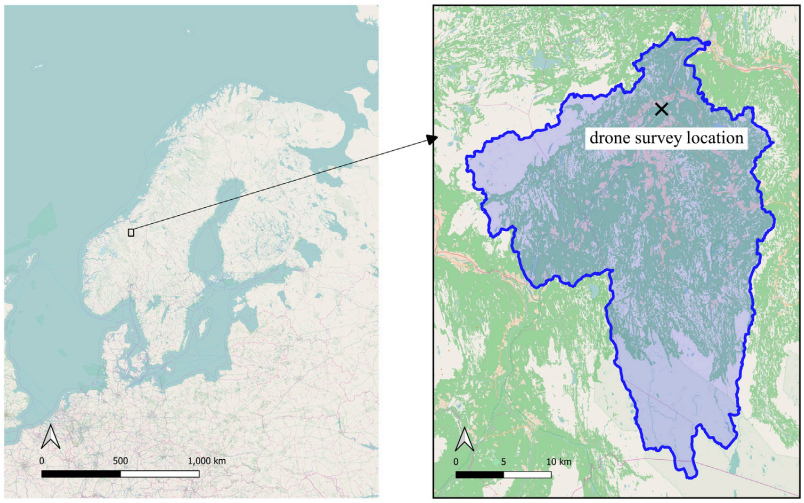

FIGURE 1 | Location of Sokna and its catchment area.

TABLE 1 | Characteristics of the Sokna river (Stickler et al., 2010).

Catchment area	539 km^2
Meters above sea level	160 m
Mean winter flow	2.5 m^3/s
Mean gradient	1.7%

October 2020 until March 2021 on a 500 m stretch of the lower part of the Sokna river close to the northern entrance of Soknedalstunnelen. **Figure 2** shows plots of daily discharge (m^3/s), precipitation (mm), mean temperature (°C), accumulated freezing degree days (°C) and snow depth (cm) for the period between the first freezing day (20th of October) until most snow had melted in the catchment area (30th of May). A relatively mild December with only occasional negative daily mean temperatures was followed by a cold spell starting on 30th of December and extending to 20th of January. This cold spell initiated formation of anchor ice dams within the river, as illustrated in **Figure 3**. Furthermore, it should be noted that ice-dam formation downstream of the Hugdal Bru gauge station caused the water level to rise, which was then detected by the gauge station and falsely recorded as a rise in runoff (increase of ~900% in one week). The precipitation prior to the cold spell (~13.7 mm between 23rd and 26th of December) fell as snow and could not have produced this kind of increase. The decreasing runoff two weeks later indicates that the dam was breached, and its stored water drained.

Overview of Collected Data

The dataset includes drone imagery collected on 11 different days over the 2020–2021 field season. **Table 2** contains the dates and ice conditions of all the drone flights considered in this paper. **Table 3** contains the technical specifications of the pictures taken and the associated camera parameters. Furthermore 50 ice thickness measurements were taken on the 20th of Jan 2021. Locations of these measurements can be seen in **Figure 4**.

Methods

Gathering Drone Imagery

A DJI Phantom 4 RTK drone was used for collecting imagery data. The drone's location is estimated using GPS/GLONASS and corrected using CPOS. The CPOS service consists of real-time correction data received from the Norwegian Mapping Authority (Kartverket) over a 4G internet connection. The CPOS system calculates a virtual reference station (VRS) based on permanent geodetic stations and the user's position. The drone treats data from this VRS as if it was data from a physical base station. A separate base station is therefore not required (Kartverket, 2021). The drone was flown multiple times over the study site throughout the 2020–2021 winter field season. An attempt was made to time the flights such that interesting changes in the ice cover—including no ice, freeze up, stable ice cover and breakup conditions—were captured. Furthermore, an attempt was made at avoiding adverse conditions such as glare, strong wind, fog, darkness, and rain. For each drone flight the drone took off from the same location. Due to the Norwegian drone flight regulations, the drone flight path was manually controlled with the objective of making the images cover the same area at each flight. Pictures were taken such that every picture had a minimum of 30% overlap with the previous picture. The choice of 30% overlap was based on Alfredsen et al. (2018) where ice was mapped over an area similar to the current study. The choice of overlap in the previous work was based on the experience of the drone pilot

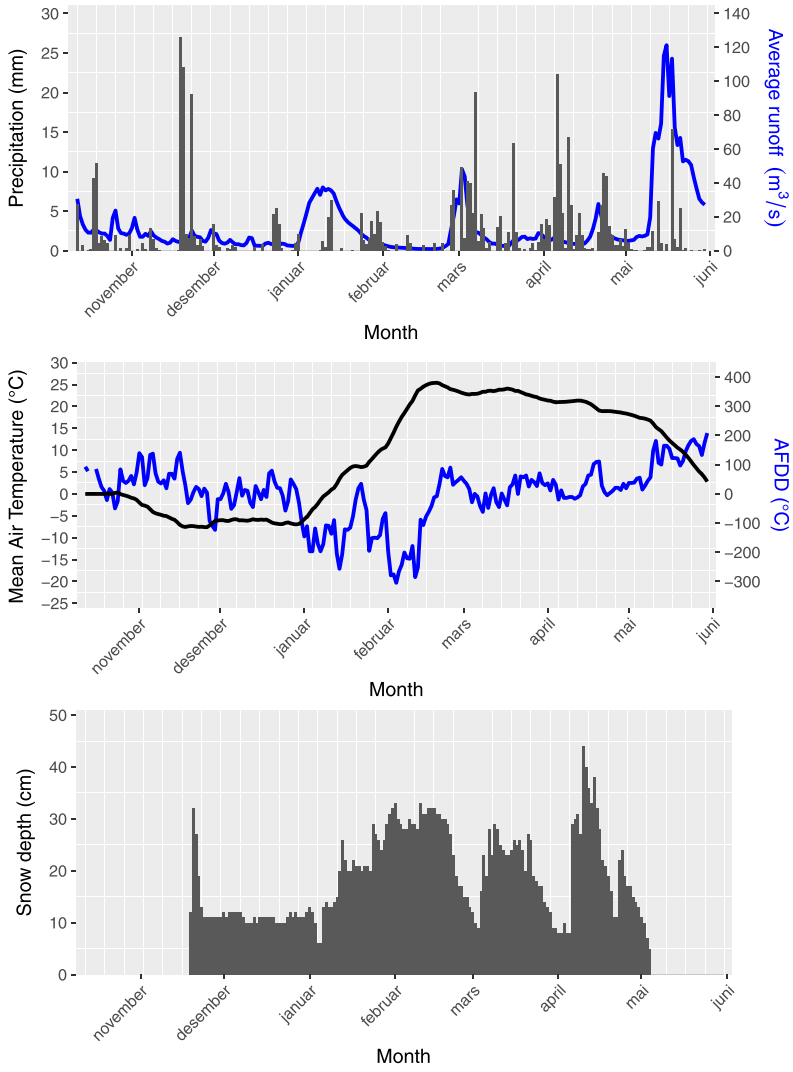

FIGURE 2 | Metrological variables for the season the survey was carried out.

from similar SfM applications. Since the DEM of the ice surface generated by Alfredsen et al. (2018) was shown to be accurate, a similar strategy of a minimum overlap of 30% was adopted also in this project. The ice cover being mostly flat suggests that a relatively low overlap value is acceptable. The flightpath covered the area 3 times each session, once at 20 m altitude with camera pointing straight down, once at 50 m altitude with camera pointing straight down and once at 20 m altitude with camera at a 30° angle to the vertical capturing the sloping riverbank. Pictures were taken using the continuous autofocus setting, for further specification of optical parameters see **Table 3**.

Manual Ice Thickness Measurements

On the 20th of Jan 2021, 50 manual ice thickness measurements were made in the studied area using a Kovacs ice thickness gauge. Each measurement consisted of drilling a hole with an ice auger and then inserting the Kovacs ice thickness gauge. If the ice reached all the way to the riverbed a measuring stick was used instead. Measurement locations were chosen to ensure

FIGURE 3 | Ice Dam 1, Sokna river 5th of January 2021. Ice dam formation in progress. Picture taken at drone survey location.

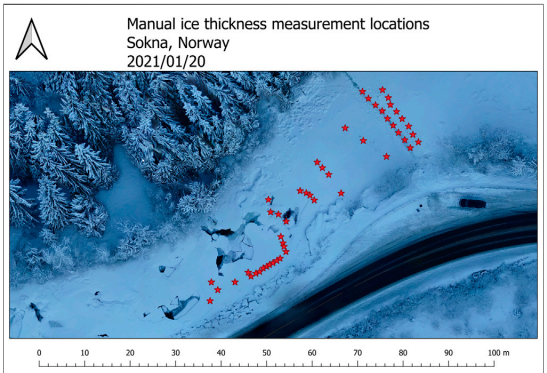

FIGURE 4 | Manual ice thickness measurement locations.

TABLE 2 | Drone flights.

Date	Number of pictures taken	Number of pictures used in model	Note
2020/10/06	257	257	No ice
2020/12/16	121	121	Border ice
2020/12/23	140	139	Border ice
2021/01/05	245	244	Water on top of ice, anchor and border ice
2021/01/11	377	369	Full ice cover, some open leads
2021/01/15	247	247	Full ice cover, some open leads
2021/01/18	220	220	Full ice cover, some open leads
2021/01/27	111	110	Full ice cover
2021/02/28	217	217	Ice melting in progress
2021/03/02	156	156	Meltwater on top of ice
2021/03/12	197	197	Snow on ice remnants

TABLE 3 | Picture parameters and camera information.

Picture parameters	
Resolution	5472 × 3648
Focal length	8.8
F-stop	F/4.5–F/4
ISO	100
Shutter	1/80–1/200
25 mm focal	24
Colours	3 band, unit8
Camera make	DJI
Camera model	FC6310R

measurements from level ice, anchor ice dam crest, downstream of anchor ice dam crest and upstream of ice dam crest. The ice upstream of the anchor ice dam crest in the centre of the river was mostly inaccessible for manual measurement. Much of the ice cover was not manually accessible, measurements were therefore not made in a systematic grid. Major voids in the ice were subtracted from the measured ice thickness using a measuring stick where possible. See **Figure 4** for ice thickness measurement locations.

Photogrammetry

The purpose of the photogrammetry step is to convert raw drone photographs into digital elevation models (DEMs) and orthomosaics. This was achieved using the proprietary software Agisoft Metashape Professional (Agisoft Metashape Professional, 2020). The following procedure—based on the procedure in (Alfredsen et al., 2018)—was adhered to:

1. Estimate image quality and discard images of quality less than 0.7
2. Align photos with accuracy "high", discard any photos with reprojection error above 0.2
3. Build dense cloud with quality "high"
4. Build DEM
5. Build orthomosaic with hole filling enabled

Unless specified all settings were left as default (In Agisoft Metashape v1.7.0 build 11736). Note that camera alignment

optimization based on Ground Control Points (GCPs) was not carried out since we used a drone with an onboard RTK-GPS. The collected GCPs were used to evaluate the accuracy of the positioning of the drone and the model. This procedure was repeated for each dataset, where each dataset consisting of all drone pictures taken of a particular location in a particular day. The output of this procedure was a pair of TIFF raster files—one DEM and one orthomosaic—for each day drone imagery was taken.

QGIS Post-processing

QGIS was used for post-processing the data (QGIS Development Team, 2009). To process the DEM raster output from Agisoft Metashape Professional, the "Ice volume" QGIS plugin was developed using the pythonic QGIS API PyQGIS and the Qt framework for the GUI. The purpose of the "Ice volume" plugin is to process river DEMs to estimate ice volume and ice thickness.

At the time of publication, the plugin takes 3 inputs:

- Path to a folder containing all .tif raster DEMs to be analysed
- Path to a .tif raster DEM with no ice and minimum water level
- Path to a .shp polygon file delineating the riverbank of the river segment

Of these all must be supplied by the user. The no ice and minimum water level raster can be acquired by flying the drone at the same site under low flow conditions with no ice and generating the rasters using SfM similarly to the ice rasters. The rasters must be overlapping and from the same location. The plugin clips all the input DEMs to the shape of the riverbank polygon. The riverbank polygon must be adjusted such that the impact of vegetation on the DEM is minimized. Without post-processing, the DEMs output by Agisoft contain spurious holes and spikes. These holes arise from insufficient number of photos, extreme reflectance values, or other optical disturbances. To remove spurious holes and spikes, Wang and Liu's algorithm (Wang and Liu, 2006) for filling surface depressions is applied twice, once normally and once with an inverted DEM to remove spikes. This algorithm is run with a minimum slope parameter of 0.1. Then the clipped no-ice DEM is subtracted from each clipped DEM, giving difference DEMs. Statistics and transects are then calculated for the difference DEMs. The difference DEMs represent an upper bound on how thick the ice is in any given location. The described photogrammetry workflow applied to a single ~200 picture dataset (covering an area of approximately 400 m × 100 m), run on a Dell Latitude 7,490 laptop with 16 GB of RAM and an Intel i7-8650U CPU completes in about 24 h. Most of this time is spent building the dense cloud. The QGIS post-processing run on the same laptop with the same dataset (+the no-ice basecase) completes in about 15 min.

Snow Adjustment

The drone model cannot easily tell the difference between ice and snow, nor can it easily be used to deduce the snow depth on an ice cover. A local snow depth measurement station, however, is available and its measurements are detailed in **Figure 2**. This snow depth is used to calculate an estimate for the snow depth on the ice cover. We assume that snow depth on ice cover is zero just after freeze-up and is set to zero whenever discharge exceeds freeze-up discharge (when this happens the snow is either flushed away or becomes snow-ice). When discharge is less than the freeze-up discharge, snow depth is assumed to change at the same rate as at the local measurement station. If this algorithm gives negative snow depth, then snow depth is set to zero. From field observations the 10th of January 2021 was set as the freeze-up date. The snow depth on the ice cover is assumed to be of uniform thickness.

RESULTS

DEM Deviation From Control Points

To evaluate the accuracy of the DEM models, control points were recorded for 3 drone flights (2020/10/06, 2021/01/05, 2021/01/11) using a Leica VIVA GS16 RTK GPS system. For the total error the Metashape software was used to compare the model to the manually recorded control points. For these drone flights 10, 4 and 4 control points were recorded respectively, all on the banks of the river. The no-ice condition (2020/10/06) gave an average total error of 0.03 m, with a standard deviation of 0.01 m. (See **Figure 10** for GCP location distribution.) The water on ice condition (2021/01/05) gave an average total error of 0.09 m, with a standard deviation of 0.03 m. The full ice cover condition (2021/01/11) gave an average total error of 0.06 m, which a standard deviation of 0.01 m. To determine altitude errors, the z-coordinate of recorded GPS points were subtracted from the z-coordinate of DEMs at the corresponding x-y coordinate. While for the total error, only control points recorded at crosshairs recognizable in the orthomosaic were used, the altitude error also used points recorded elsewhere (referred to as "other points" in **Table 4**). The water on ice condition (2021/01/05) gave an average altitude error of all GCPs of 0.06 m, with a standard deviation of 0.02 m. GCPs on border ice alone gave an average error of 0.06 m, with a standard deviation of 0.02 m. While points not on the border ice gave an average error of 0.06 m with a standard deviation of 0.02 m, I. e., there is no significant difference in error between border ice GCPs and on land GCPs. A Kendall rank correlation test was carried out to determine whether there is any correlation between distance from the study centre and errors. The test suggests that there is no statistically significant correlation (Kendall correlation coefficient = −0.15, Kendall test statistic = 58, p-value = 0.44). These low errors show that the precision of the RTK drone is sufficient and georeferencing using control points was not considered necessary. Errors are summarized in **Table 4**.

Thickness Deviation From Manual Measurements

To evaluate the performance of the model it is instructive to consider the distribution of errors, i.e., the difference between manual ice thickness measurements and model ice thickness.

TABLE 4 | Model error relative to control points.

Flight	Control points	Other points	Total error	RMS error (m)	Total error	Altitude error	Altitude error
			Mean (m)		Standard deviation (m)	Mean (m)	Standard deviation (m)
2020/10/06	10	0	0.03	0.03	0.01	0.02	0.01
2021/01/05	4	21	0.09	0.09	0.03	0.06	0.02
2021/01/11	4	1	0.06	0.06	0.01	0.01	0.01

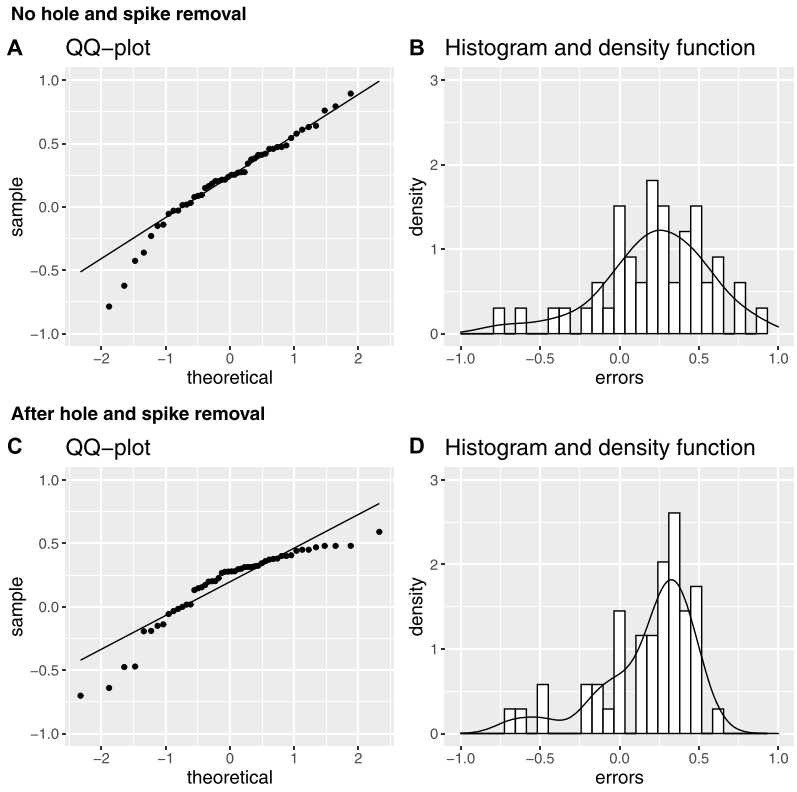

FIGURE 5 | (A) Quantile-quantile plot comparing sample errors and theoretical normal errors without hole and spike removal algorithm applied. **(B)** Distribution of errors (Model ice thickness–real ice thickness) without hole and spike removal algorithm applied. **(C)** Quantile-quantile plot comparing sample errors and theoretical normal errors with hole and spike removal algorithm applied. **(D)** Distribution of errors (Model ice thickness–real ice thickness) with hole and spike removal algorithm applied.

For the model without hole and spike removal the errors have a mean of +21 cm and a standard deviation of 40 cm. **Figure 5B** shows this distribution of errors. An Anderson-Darling test (A = 0.73, p-value = 0.05) suggests that the error distribution is approximately normal. The QQ-plot (**Figure 5A**) suggests the same, with the caveat that the distribution has a long tail of negative errors, this tail also explains why the Anderson-Darling p-value isn't better. Note that negative errors imply that the model predicts thinner ice than the manual measurements while positive errors imply that the model predicts thicker ice, i.e., **Figure 5B** suggests that the model is much more likely to overestimate ice thickness than it is to underestimate it. This is expected as the model does not consider voids or water content below the ice cover. For the model with spike and hole removal the errors have a mean of +18 cm and a standard deviation of 30 cm, i.e., no significant change in the mean, but a useful reduction in standard deviation. An Anderson-Darling test (A = 2.2, p-value < 0.001) suggests that the error distribution is no longer normal (See **Figure 5C,D**).

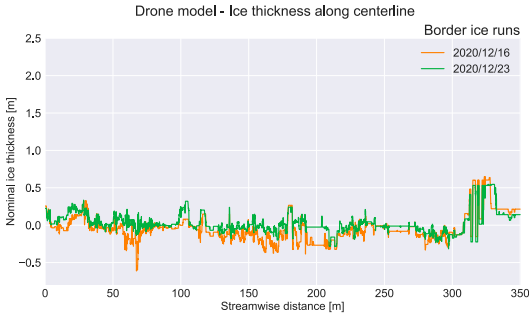

FIGURE 6 | Drone model—Ice thickness along centreline for border ice drone runs.

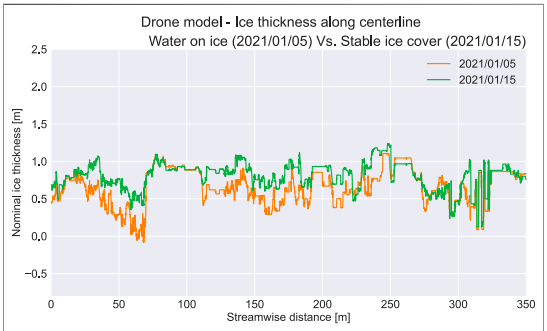

FIGURE 7 | Drone model—Ice thickness along centreline for water on ice drone run.

DEM Temporal Trends

The drone model returns an upper bound on the ice thickness. The model is unable to estimate ice growth under a stable ice cover. This does imply that the drone model's upper bound moves closer to the real ice thickness throughout the season as the ice thickness grows. To consider how the model ice thickness changes over time is still interesting; during freeze-up, when water flows over the ice, the model ice thickness can be expected to be a closer approximation of the true ice thickness. When a stable ice cover has been achieved any changes in ice thickness should be explainable as snow deposition, ice cover collapse or thermal expansion/contraction (or as SfM and GPS inaccuracies). In narrow rivers—such as the one studied—ice-bank adhesion is assumed to be strong enough for height differences due to water pressure to be negligible until break-up. Small changes in the model ice thickness when the ice cover is full and stable gives increased confidence in the model. To record how ice thickness varies with time, we compare ice thickness rasters for all flights. We compare them in two ways; through aggregate statistics and trough ice thickness profile comparisons. **Figure 11** shows how estimated mean and median ice thickness varied during the field season. The key takeaway is that ice thickness increased rapidly in the freeze-up period, then was relatively constant throughout the rest of the season. Note the difference between the mean and the median ice thickness: the median is less affected by outliers than the average is. Ice volume can also be obtained by integrating ice thickness over the raster (this simplifies to raster area x average ice thickness). For the full ice cover condition (2021/01/18), this gives an ice volume of 8.5×10^3 m^3. **Figures 6–9** show how the ice thickness at the river centreline varied through the field season. **Figure 6** corresponds to drone runs where there is only border ice. Here the average centreline ice thickness hovers around zero. This is as expected since there is little ice at the centre of the river. Deviations from this are primarily errors caused by variable water level and water level opacity. The 2021/03/12 drone run in **Figure 9** sometimes dips below zero thickness for the same reason. **Figure 7**, corresponds to the freeze-up water-on-ice condition vs. the subsequent stable ice cover condition. The difference between these two conditions shows that the drone is good at imaging anchor ice, as opposed to the water surface

FIGURE 8 | Drone model—Ice thickness along centreline for full ice cover drone runs.

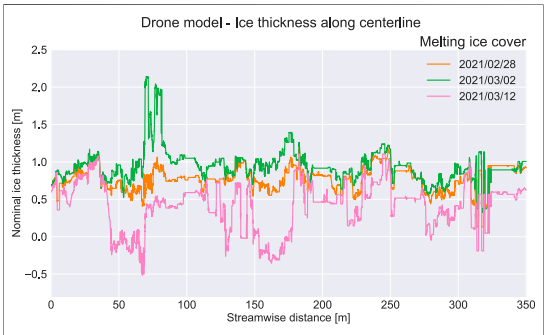

FIGURE 9 | Drone model—Ice thickness along centreline for melting ice cover drone runs.

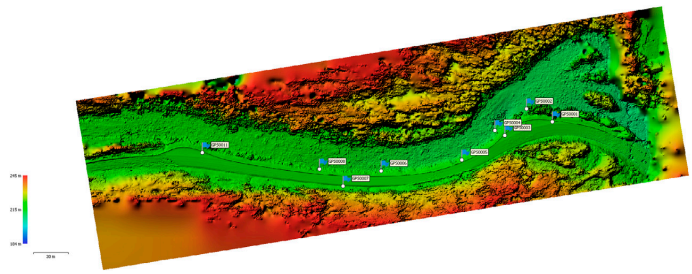

FIGURE 10 | 2020/10/06 No-ice DEM with ground control points (GCPs).

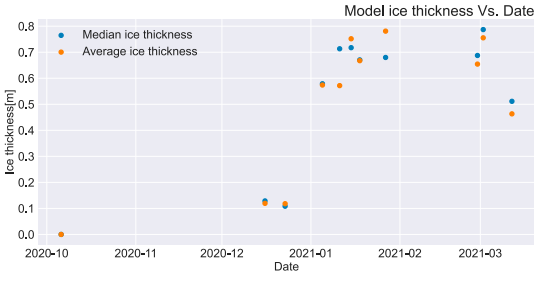

FIGURE 11 | Average and median ice thickness as derived from the drone DEM model.

in this water on ice condition. The 2021/01/05 drone run therefore provides an estimate of anchor ice thickness at this time, and by extension an estimate of anchor ice volume for later runs 7.2 m^3× 103 m^3. In the water on ice condition, the anchor ice has not yet been fully obscured by level ice growth and is still visible through the relatively shallow water. Once the level ice has fully covered the river and the water level has dropped there will be a void in-between the underside of the level ice cover and the water/anchor-ice below. The narrow width of the river, as well as structural support from ice dam crests, mean that these suspended level ice covers and associated voids will not frequently collapse. Therefore, the water-on-ice estimate of anchor ice volume is expected to be closer to the real ice volume than equivalent estimates for full ice cover conditions. Full ice cover conditions are prone to large voids not captured by the drone imagery. **Figure 8** corresponds to stable ice cover drone runs. As seen in the average/median ice thickness figure (**Figure 11**), the ice average thickness stays within an approximately 10 cm range throughout this part of the season.

DISCUSSION

A small unmanned aerial vehicle was used in combination with Structure from Motion photogrammetry to build digital elevation models of river ice during the winter season in a small stream. The use of the UAV allowed us to map the extent and estimate the volume of ice during the winter, also during conditions where traditional mapping strategies requiring access to the ice surface (Turcotte et al., 2017) would be impossible. An important feature of this method is the ability to map anchor ice dams (Turcotte and Morse, 2011), which is controlling the ice formation and hydraulic conditions in small streams like Sokna (Stickler et al., 2010). The RTK drone proved to produce accurate data and compared to ground control points measured with RTK GPS the errors were within a few centimeters. The RMS errors from this study (here they round to the same as the mean errors) are of a similar magnitude to those quoted by Alfredsen et al. (2018), who found RMS errors in the range 0.06–0.106 m. When Stott et al. (2020) mapped a small ice-free river in Scotland using comparable equipment to this study they also achieved similar RMS errors (0.066–0.072 m). Depending on lighting conditions, clarity, and depth of the water, the no-ice DEM may either represent the water surface or the riverbed. The lower the water level in the raw data for the no-ice DEM the harder this type of error is to identify by inspection as the error is small. Conversely, the deeper the water, the easier the error is to identify by inspection, but the error, however, can be much more severe. These types of errors can in principle be removed by manually eliminating the problematic areas from the analysis, however this is prone to human error and bias. The no-ice DEM should therefore ideally either be obtained through visual photography by a drone at discharges corresponding to water depth of less than 1 m (Maddock and Lynch, 2020) or optimally be obtained through lidar scanning at an appropriate wavelength for penetrating the water (Mandlburger et al., 2020). The latter method was used by Alfredsen and Juarez (2020) to integrate ice jam remnants in the river bathymetry, and hence numerically assess the impact of ice on flow patterns. Steep rivers also have an extra source of error compared to low-gradient rivers; they have higher turbulence (Wohl and Thompson, 2000), and highly turbulent water will often be captured in the DEM as solid. Furthermore, small steep rivers have rapid local changes in the water surface therefore two pictures of the same area taken in close succession may

disagree on whether the water surface or the riverbed should be included in the DEM. Small steep rivers do have some advantages over big low gradient rivers: in a small river a higher percentage of the volume under the upper surface of the ice cover is ice, therefore the models' upper bound is closer to the real value than if the same method had been applied to a big river. This makes it easier to justify using the estimates derived from the drone method for engineering purposes. If used for engineering purposes, the data should be treated as an upper bound and care should be taken not to add excessive safety factors on top of that. It should also be kept in mind that manual methods for ice thickness measurement that work well on big rivers are often inapplicable to small steep rivers. The short spans and high ice-bank adhesion in small rivers also make air-filled voids common and freeboard-based calculations unfeasible. The DEMs were cut to the riverbank, as this reduces it to the area of interest, hence removing any potential issues associated with the accuracy at the edge of the DEM, such as tall trees blocking line of sight. Vegetation overhang was a significant source of error in the first pass model. Depending on snow fall and foliage, overhanging trees will show up in the DEM as different elevations unrelated to the underlying ice thickness. These errors were however drastically reduced in the final model by inspecting the orthomosaic and cutting away any overhanging vegetation in the no-ice DEM. It is possible that some errors due to overhanging vegetation persists in later DEMs, as snow can cause vegetation to shift to new places. For DEMs of modest extent, manual inspection and removal of vegetation is likely less labour intensive and less error prone than automatic classification of the point cloud. For larger DEMs and larger data sets, automatic surface classification should be considered (Husson et al., 2016). The difference between manual ice thickness measurements and the drone model ice thickness estimates being reasonably well described by a normal or modified normal distribution suggests that it is possible to calibrate the drone model with manual measurements. I.e., use a few manual measurements to determine the mean error, then subtract that from the drone model. The drone model would then represent a best estimate of the ice thickness, rather than a conservative estimate.

CONCLUSION

This study was motivated by the difficulty of obtaining distributed ice thickness data in steep rivers through manual measurement. The aim of this work was to investigate the possibility of using a small drone and SfM to map the spatial and temporal distribution of ice thickness in a steep river and hence develop and evaluate a method for quantifying ice thickness distributions. The main methods used in this work were: 11 flights with a DJI Phantom 4 RTK drone at different dates for collecting imagery data, GCP points and manual thickness measurements for verification, SfM image processing using Agisoft to obtain DEMs, and a novel PyQGIS plugin for postprocessing DEMs to obtain temporal trends and quantitative statistics. This paper shows that it is possible to use a small drone and SfM to map the development of river ice in a small stream from freeze-up to break-up, including periods at the start and end where access is impossible. The work hence allows larger and more complete river ice data sets to be collected, enabling previously unfeasible analysis. High accuracy measurements of large areas of anchor ice during freeze-up is a particularly novel contribution of this paper. A model—implemented as an open source QGIS plugin—was derived for quantifying the development of ice cover by comparing digital elevation models between flights. This model showed acceptable performance for estimating ice thickness upper bounds when compared to manual measurements. The principal challenge to further develop this model includes developing better ways of estimating volume of air beneath suspended ice covers.

DATA AVAILABILITY STATEMENT

Raw drone footage, environmental data, GCP coordinates and the code version current at the time of publication is available at: https://doi.org/10.5281/zenodo.5674844. For an up to date full specification of the Qgis plugin and to download it for your own use visit: https://github.com/ERodtang/ice_volume. Any other data that support the findings of this study are available from the corresponding author, ER, upon reasonable request.

AUTHOR CONTRIBUTIONS

ER conducted most of the data collection, analysis and writing in this paper. KA supervised and provided comments on the document, discussions on the topic and help with Agisoft data processing. AJ assisted with data collection and processing of data in Agisoft. All authors contributed to the final version of the manuscript.

FUNDING

ER was funded by a strategic scholarship from the Norwegian University of Science and Technology (NTNU).

ACKNOWLEDGMENTS

The authors would like to thank Vegard Hornnes and Janik John for assistance with fieldwork.

REFERENCES

Alfredsen, K., Haas, C., Tuhtan, J. A., and Zinke, P. (2018). Brief Communication: Mapping River Ice Using Drones and Structure from Motion. *The Cryosphere* 12 (2), 627–633. doi:10.5194/tc-12-627-2018

Alfredsen, K., and Juarez, A. (2020). "Modelling Stranded River Ice Using LiDar and Drone-Base Models," in The 25th IAHR International Symposium on Ice, Trondheim, November 23–25, 2020.

Ansari, S., Rennie, C. D., Clark, S. P., and Seidou, O. (2021). IceMaskNet: River Ice Detection and Characterization Using Deep Learning Algorithms Applied to Aerial Photography. *Cold Regions Sci. Tech.* 189 (May 2020), 103324. doi:10.1016/j.coldregions.2021.103324

Beltaos, S. (2012). Canadian Geophysical Union Hydrology Section Committee on River Ice Processes and the Environment: Brief History. *J. Cold Reg. Eng.* 26 (3), 71–78. doi:10.1061/(asce)cr.1943-5495.0000046

Beltaos, S. (2008). *River Ice Breakup*. 1st ed. Colorado: Water Resources Publications.

Beltaos, S. (1995). *River Ice Jams*. 1st ed. Colorado: Water Resources Publications.

Beltaos, S., and Tang, P. (2013). "Applying HEC-RAS to Simulate River Ice Jams: Snags and Practical Hints," in CGU HS Committee on River Ice Processes and the Environment, 17th Workshop on River Ice, 415–430.

Bennett, K. E., and Prowse, T. D. (2009). Northern Hemisphere Geography of Ice-Covered Rivers. *Hydrol. Process.* 24, 235. doi:10.1002/hyp.7561

Blackburn, J., and She, Y. (2019). A Comprehensive Public-Domain River Ice Process Model and its Application to a Complex Natural River. *Cold Regions Sci. Technology.* 163 (April), 44–58. doi:10.1016/j.coldregions.2019.04.010

Carrivick, J. L., and Smith, M. W. (2019). Fluvial and Aquatic Applications of Structure From Motion Photogrammetry and Unmanned Aerial Vehicle/Drone Technology. *WIREs Water.* 6 (1), 1–17. doi:10.1002/wat2.1328

Chu, T., and Lindenschmidt, K.-E. (2016). Integration of Space-Borne and Air-Borne Data in Monitoring River Ice Processes in the Slave River, Canada. *Remote Sensing Environ.* 181, 65–81. doi:10.1016/j.rse.2016.03.041

Dolan, W., Yang, X., Zhang, S., and Pavelsky, T. (2019). *Working towards Optical Remote Sensing of Pan-Arctic River and lake Ice*. Ottawa, Ontario: CRIPE.

Ewertowski, M. W., Tomczyk, A. M., Evans, D. J. A., Roberts, D. H., and Ewertowski, W. (2019). Operational Framework for Rapid, Very-High Resolution Mapping of Glacial Geomorphology Using Low-Cost Unmanned Aerial Vehicles and Structure-From-Motion Approach. *Remote Sensing.* 11 (1), 65. doi:10.3390/rs11010065

Garver, J. I. (2019). "The 2019 Mid-winter Ice Jam Event on the Lower Mohawk River, New York," in Conference: Mohawk Watershed Symposium, Schenectady, NY, March 22, 2019, 22–27.

Gaffey, C., and Bhardwaj, A. (2020). Applications of Unmanned Aerial Vehicles in Cryosphere: Latest Advances and Prospects. *Remote Sensing.* 12 (6), 948. doi:10.3390/rs12060948

Gebre, S., Alfredsen, K., Lia, L., Stickler, M., and Tesaker, E. (2013). Review of Ice Effects on Hydropower Systems. *J. Cold Reg. Eng.* 27 (4), 196–222. doi:10.1061/(ASCE)CR.1943-5495.0000059

Husson, E., Ecke, F., and Reese, H. (2016). Comparison of Manual Mapping and Automated Object-Based Image Analysis of Non-submerged Aquatic Vegetation from Very-High-Resolution UAS Images. *Remote Sensing* 8 (9), 724. doi:10.3390/rs8090724

Huusko, A., Greenberg, L., Stickler, M., Linnansaari, T., Nykänen, M., Vehanen, T., et al. (2007). Life in the Ice Lane: the winter Ecology of Stream Salmonids. *River Res. Applic.* 23 (5), 469–491. doi:10.1002/rra.999

Kartverket (2021). Guide to CPOS | Kartverket.No. Available at: https://www.kartverket.no/en/on-land/posisjon/guide-to-cpos (Accessed November 12, 2021).

Kääb, A., Altena, B., and Mascaro, J. (2019). River-ice and Water Velocities Using the Planet Optical Cubesat Constellation. *Hydrol. Earth Syst. Sci.* 23 (10), 4233–4247. doi:10.5194/hess-23-4233-2019

Lamsters, K., Karušs, J., Krievāns, M., and Ješkins, J. (2019). Application of Unmanned Aerial Vehicles for Glacier Research in the Arctic and Antarctic. *Etr.* 1, 131–135. doi:10.17770/etr2019vol1.4130

Lindenschmidt, K.-E. (2017). RIVICE-A Non-proprietary, Open-Source, One-Dimensional River-Ice Model. *Water.* 9 (5), 314. doi:10.3390/w9050314

Lind, L., Nilsson, C., Polvi, L. E., and Weber, C. (2014). The Role of Ice Dynamics in Shaping Vegetation in Flowing Waters. *Biol. Rev.* 89 (4), 791–804. doi:10.1111/brv.12077

Lindenschmidt, K., Brown, D., and Hahlweg, R. (2021). "Preparing Ice-Jam Flood Outlooks for the Lower Reach of the Red River," in 21st Workshop on the Hydraulics of Ice Covered Rivers, Saskatoon, Saskatchewan, August 29–September 1, 2021. Available at: http://cripe.ca/publications/proceedings/21.

Maddock, I., and Lynch, J. (2020). Assessing the Accuracy of River Channel Bathymetry Measurements Using an RTK Rotary-Winged Unmanned Aerial Vehicle (UAV) with Varying Ground Control Point (GCP) Number and Placement. *EGU Gen. Assembly*. Online, EGU2020–1534. doi:10.5194/egusphere-egu2020-1534

Mandlburger, G., Pfennigbauer, M., Schwarz, R., Flöry, S., and Nussbaumer, L. (2020). Concept and Performance Evaluation of a Novel UAV-Borne Topo-Bathymetric LiDAR Sensor. *Remote Sensing* 12 (6), 986. doi:10.3390/rs12060986

Prowse, T. D., and Culp, J. M. (2003). Ice Breakup: A Neglected Factor in River Ecology. *Can. J. Civ. Eng.* 30 (1), 128–144. doi:10.1139/l02-040

Smith, M. W., Carrivick, J. L., and Quincey, D. J. (2016). Structure from Motion Photogrammetry in Physical Geography. *Prog. Phys. Geogr. Earth Environ.* 40, 247–275. doi:10.1177/0309133315615805

Stickler, M., Alfredsen, K. T., Linnansaari, T., and Fjeldstad, H.-P. (2010). The Influence of Dynamic Ice Formation on Hydraulic Heterogeneity in Steep Streams. *River Res. Applic.* 26 (9), 1187–1197. doi:10.1002/rra.1331

Stott, E., Williams, R. D., and Hoey, T. B. (2020). Ground Control point Distribution for Accurate Kilometre-Scale Topographic Mapping Using an Rtk-Gnss Unmanned Aerial Vehicle and Sfm Photogrammetry. *Drones* 4 (3), 55–21. doi:10.3390/drones4030055

Turcotte, B., Morse, B., Dubé, M., and Anctil, F. (2013). Quantifying Steep Channel Freezeup Processes. *Cold Regions Sci. Tech.* 94, 21–36. doi:10.1016/j.coldregions.2013.06.003

Turcotte, B., and Morse, B. (2011). Ice Processes in a Steep River basin. *Cold Regions Sci. Tech.* 67 (3), 146–156. doi:10.1016/j.coldregions.2011.04.002

Turcotte, B., Nafziger, J., Clark, S., Beltaos, S., Jasek, M., Lind, L., et al. (2017). "Monitoring River Ice Processes : Sharing Experience to Improve Successful Research Programs," in Proceedings of the 19th Workshop on the Hydraulics of Ice Covered Rivers, Whitehorse, YK, Canada, July 10–12, 2017. Available at: http://cripe.ca/docs/proceedings/19/Turcotte-et-al-2017b.pdf.

Wang, L., and Liu, H. (2006). An Efficient Method for Identifying and Filling Surface Depressions in Digital Elevation Models for Hydrologic Analysis and Modelling. *Int. J. Geographical Inf. Sci.* 20 (2), 193–213. doi:10.1080/13658810500433453

Westoby, M. J., Brasington, J., Glasser, N. F., Hambrey, M. J., and Reynolds, J. M. (2012). 'Structure-from-Motion' Photogrammetry: A Low-Cost, Effective Tool for Geoscience Applications. *Geomorphology* 179, 300–314. doi:10.1016/j.geomorph.2012.08.021

Wohl, E. E., and Thompson, D. M. (2000). Velocity Characteristics along a Small Step-Pool Channel. *Earth Surf. Process. Landforms* 25 (4), 353–367. doi:10.1002/(sici)1096-9837(200004)25:4<353:aid-esp59>3.0.co;2-5

Woodget, A. S., Austrums, R., Maddock, I. P., and Habit, E. (2017). Drones and Digital Photogrammetry: from Classifications to Continuums for Monitoring River Habitat and Hydromorphology. *WIREs Water* 4 (4), 1–20. doi:10.1002/wat2.1222

Conflict of Interest: The authors declare that the research was conducted in the absence of any commercial or financial relationships that could be construed as a potential conflict of interest.

Chapter 8

Acknowledgements

Thank you to my cats Era and Umbriel, you made it all worth it. Thank you to Amandine Sophie Muller for your moral support. Thank you to Janik John for your invaluable field work assistance and good cheer. Thank you to my supervisors for your endless patience and belief in me.

Without you this PhD would never have been written.

ISBN 978-82-326-7564-7 (printed ver.)
ISBN 978-82-326-7563-0 (electronic ver.)
ISSN 1503-8181 (printed ver.)
ISSN 2703-8084 (online ver.)

NTNU

Norwegian University of
Science and Technology